Copyright Warning & Restrictions

The copyright law of the United States (Title 17, United States Code) governs the making of photocopies or other reproductions of copyrighted material.

Under certain conditions specified in the law, libraries and archives are authorized to furnish a photocopy or other reproduction. One of these specified conditions is that the photocopy or reproduction is not to be "used for any purpose other than private study, scholarship, or research." If a, user makes a request for, or later uses, a photocopy or reproduction for purposes in excess of "fair use" that user may be liable for copyright infringement,

This institution reserves the right to refuse to accept a copying order if, in its judgment, fulfillment of the order would involve violation of copyright law.

Please Note: The author retains the copyright while the New Jersey Institute of Technology reserves the right to distribute this thesis or dissertation

Printing note: If you do not wish to print this page, then select "Pages from: first page # to: last page #" on the print dialog screen

ABSTRACT

BILINEAR TIME-FREQUENCY REPRESENTATIONS OF HEART RATE VARIABILITY AND RESPIRATION DURING STRESS

by
Rindala Saliba

Recently, joint time-frequency signal representation has received considerable attention as a powerful tool for analyzing a variety of signals and systems. In particular, if the frequency content is time varying as in signals of biological origin which often do not comply with the stationarity assumptions, then this approach is quite attractive. In this dissertation, we explore the possibility of better representation of two particular biological signals, namely heart rate variability (HRV) and respiration. We propose the use of time-frequency analysis as a new and innovative approach to examine the physical and mental exertion attributed to exercise. Two studies are used for the main investigation, the "preliminary" and "anticipation" protocols.

In the first phase of this work, the application of five different bilinear representations on modeled HRV test signals and experimental HRV and respiration signals of the preliminary protocol is evaluated. Each distribution: the short time Fourier transform (STFT), the pseudo Wigner-Ville (WVD), the smoothed pseudo Wigner-Ville (SPWVD), The Choi-Williams (CWD), and the Born-Jordan-Cohen (RID) has unique characteristics which is shown to affect the amount of smoothing and the generation of cross-terms differently . The CWD and the SPWVD are chosen for further application because of overcoming the drawbacks of the other distributions by providing higher

resolution in time and frequency while suppressing interferences between the signal components.

In the second phase of this research, the SPWVD and CWD are used to investigate the presence of an anticipatory component due to the stressful exercise condition as reflected in the HRV signal from a change in behavior in the autonomic nervous system. By expanding the concept of spectral analysis of heart rate variability (HRV) into time-frequency analysis, we are able to quantitatively assess the parasympathetic (HF) and sympatho-vagal balance (LF:HF) changes as a function of time. As a result, the assessment of the autonomic nervous system during rapid changes is made.

A new methodology is also proposed that adaptively uncovers the region of parasympathetic activity. It is well known that parasympathetic activity is highly correlated with the respiration frequency. This technique traces the respiration frequency and extracts the corresponding parasympathetic activity from the heart rate variability signal by adaptive filtering.

BILINEAR TIME-FREQUENCY REPRESENTATIONS OF HEART RATE VARIABILITY AND RESPIRATION DURING STRESS

by
Rindala Saliba

A Dissertation
Submitted to the Faculty of
New Jersey Institute of Technology
in Partial Fulfillment of the Requirements for the Degree of
Doctor of Philosophy

Department of Electrical and Computer Engineering

January 1997

APPROVAL PAGE

BILINEAR TIME-FREQUENCY REPRESENTATIONS OF HEART RATE VARIABILITY AND RESPIRATION DURING STRESS

Rindala Saliba

Dr. Stanley S. Reisman, Dissertation Advisor
Professor of Electrical and Computer Engineering,
New Jersey Institute of Technology

Dr. Peter Engler, Committee Member
Associate Professor of Electrical and Computer Engineering,
New Jersey Institute of Technology

Dr. Joseph Frank, Committee Member
Associate Professor of Electrical and Computer Engineering,
New Jersey Institute of Technology

Dr. Bonnie Ray, Committee Member
Assistant Professor of Mathematics,
New Jersey Institute of Technology

Dr. Leon Cohen, Committee Member
Professor of Physics,
Hunter College, City University of New York

BIOGRAPHICAL SKETCH

Author: Rindala Saliba

Degree: Doctor of Philosophy

Date: January 1997

Undergraduate and Graduate Education:

- Doctor of Philosophy in Electrical Engineering,
  New Jersey Institute of Technology, Newark, NJ, 1997
- Master of Science in Electrical Engineering,
  New Jersey Institute of Technology, Newark, NJ, 1991
- Bachelor of Science in Electrical Engineering,
  New Jersey Institute of Technology, Newark, NJ, 1990
- Associates in Engineering Science,
  Bergen Community College, Paramus, NJ, 1987

Major: Electrical Engineering

Presentations and Publications:

M.V. Tazebay, R.T. Saliba and S.S. Reisman,
"Adaptive Time-Frequency Analysis of Autonomic Nervous System,"
Proceedings of the 17th IEEE Annual International Conference of the Engineering in Medicine and Biology Society, 1995, Montréal, Canada.

M.V. Tazebay, R.T. Saliba and S.S. Reisman,
"Adaptive Time-Frequency Analysis of Autonomic Nervous System,"
Proceedings of the 17th IEEE Annual International Conference of the Engineering in Medicine and Biology Society, 1995, Montréal, Canada.

R.T. Saliba, S.S. Reisman and W.N. Tapp,
"Vagal Response in Heart Rate Variability under Motion Sickness Stimulation,"
Proceedings of the 18th IEEE Annual Northeast Bioengineering Conference,
1992, University of Rhode Island, Rhode Island.

This thesis is dedicated to the three most precious people in my life,
my cherished parents, Touma and Hanna Saliba,
and my beloved husband, Elie Saadé.
They taught me how to love and how to aim high.
Their boundless support, guidance and encouragement kept me going
for as long as I can remember.

ACKNOWLEDGMENT

I would like to express my sincere gratitude to Dr. Stanley S. Reisman, who not only served as my research supervisor, providing valuable and countless resources and guidance, but also constantly gave me support, encouragement, and reassurance. He has been a father figure for the last six years. Without his help, this thesis would never have been completed.

Special thanks are extended to Dr. Peter Engler, Dr. Joseph Frank, Dr. Bonnie Ray, and Dr. Leon Cohen for their help and valuable input throughout the research.

I am also grateful to the Kessler Institute for Rehabilitation for providing the facility for this research, and my fellow colleagues for their friendship and support.

And finally, a special thanks goes to all my family members and friends that are deserving of recognition for roughing it out with me for the last few years and showing me what true friendship and sacrifice are all about. Gladys Gabriel, Fay Shabo, George Saliba, Gaby Saliba, Bob Gabriel, Hanna and Raafat Kamel, and Joe Aboukhalil, thank you especially for being there and for being who you are.

TABLE OF CONTENTS

TABLE OF CONTENTS
(Continued)

Chapter **Page**

TABLE OF CONTENTS
(Continued)

Chapter **Page**

TABLE OF CONTENTS
(Continued)

Chapter **Page**

LIST OF TABLES

Table **Page**

LIST OF FIGURES
(Continued)

LIST OF FIGURES
(Continued)

Figure **Page**

LIST OF FIGURES
(Continued)

Figure **Page**

LIST OF FIGURES
(Continued)

Figure **Page**

CHAPTER 1

INTRODUCTION

Biomedical engineering is the application of engineering and mathematical principles to medical science. The goal for its advancement is to develop tools for enhanced diagnosis and treatment of ailments that afflict mankind. The following work chronicles the research conducted on the utilization of time-frequency analysis as a non-invasive tool to quantify rapidly changing biological signals. The first step is to investigate the relevant physiology behind the human organs which are of interest.

1.1 The Heart

The cardiovascular system consists of blood vessels and the heart. In 1628, British physiologist William Harvey discovered that the cardiovascular system forms a circle, or circuit, so that blood pumped out of the heart through one set of vessels returns to the heart via a different set of vessels[1]. In actuality, there are really two circuits, both originating and terminating in the heart. Therefore, the heart, illustrated in Figure 1.1, is divided into two functional halves, each half containing two chambers: an atrium and a ventricle. The atrium of each side empties into the ventricle on that side. There is no direct flow between the two atria or the two ventricles in a healthy individual.

Blood is pumped by the pulmonary circuit from the right ventricle through the lungs and then into the left atrium. The blood is then pumped by the systemic circuit, from the left ventricle, through all the tissues of the body except the lungs, and then to the right atrium. In both circuits, the vessels carrying blood away from the heart are called

arteries, and those carrying blood from either the lung or all other parts of the body back to the heart are called veins.

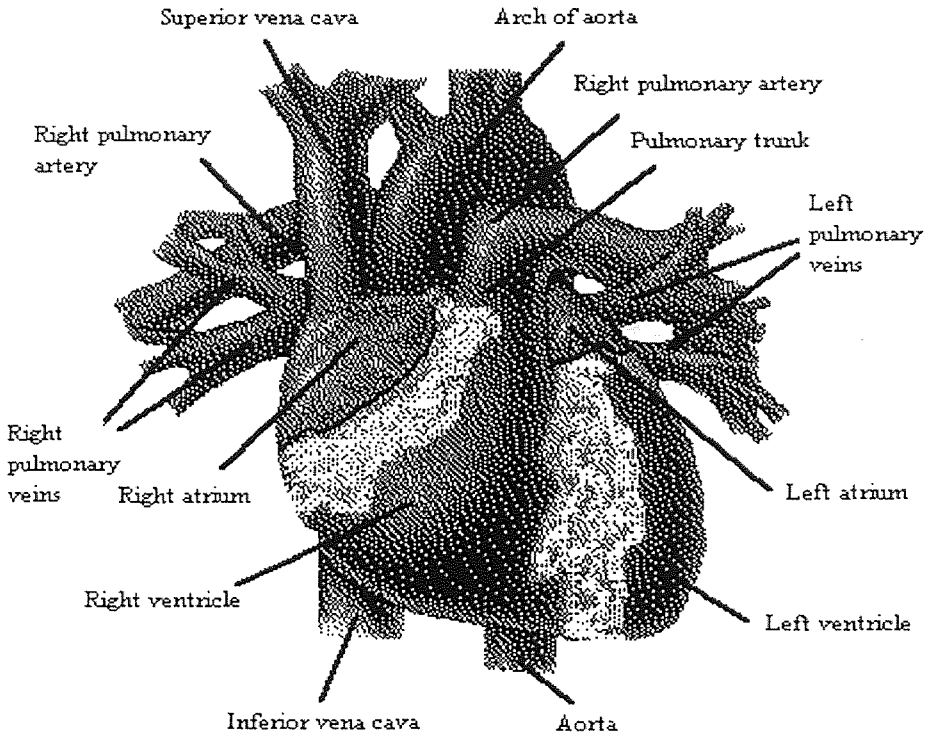

Figure 1.1 The heart
(from A.J. Vander, J.H. Sherman, and D.S. Luciano, *Human Physiology,* 1994)

The heart is a muscular organ which is enclosed in a fibrous sac called the pericardium[2]. The walls of the heart are primarily composed of cardiac-muscle cells called the myocardium. Cardiac-muscle cells combine properties of both skeletal muscle and smooth muscle. However, even more important, approximately one percent of the cardiac-muscle fibers have specialized features that are essential for normal heart excitation[1]. They constitute a network known as the conducting system of the heart and are connected to other cardiac-muscle fibers by gap junctions. The gap junctions allow

action potentials to spread from one cardiac-muscle cell to another. Thus, the initial excitation of one myocardial cell results in excitation of all cells, and as a result, the pumping action of the heart. The conducting system of the heart is shown in Figure 1.2.

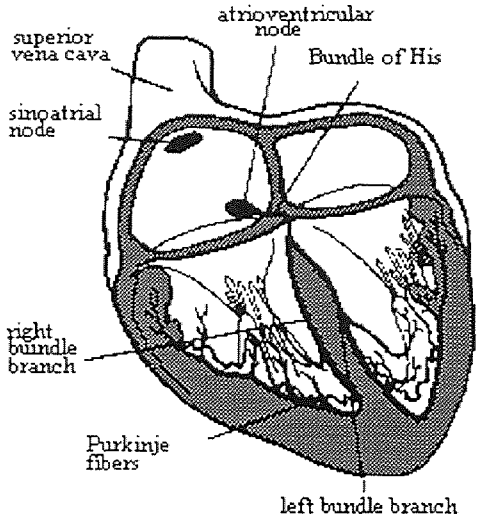

Figure 1.2 The conducting system of the heart
(from A.J. Vander, J.H. Sherman, and D.S. Luciano, *Human Physiology,* 1994)

The initial depolarization normally arises in a small group of conducting-system cells called the sinoatrial (SA) node. The SA node is located in the right atrium near the entrance of the superior vena cava. The SA node has the fastest inherent discharge rate of any of the myocardial cells with pacemaker activity. Therefore, the SA node is the normal pacemaker for the entire heart[1]. The action potential initiated in the SA node spreads throughout the myocardium, passing from cell to cell by way of gap junctions. The spread throughout the right atrium and the left atrium does not depend on fibers of the conducting system. The spread is rapid enough that the two atria are depolarized and contract at essentially the same time.

The spread of the action potential from the atria to the ventricles involves a portion of the conducting system called the atrioventricular (AV) node. The AV node is located at the base of the right atrium. The AV node has an important characteristic that makes the cardiac cycle more efficient. Because of the electrical properties of the cells that make up the AV node, the propagation of action potentials through the AV node results in a delay of approximately 0.1 seconds[1]. This delay allows the atria to finish contracting and, therefore, completely empty their contents of blood into their respective ventricles before ventricular excitation occurs.

Upon leaving the AV node, the action potential then travels to the septum, the area between the two ventricles, by the conducting-system fibers called the bundle of His[2]. The bundle of His then divides into the left and right bundle branches which eventually leave the septum and enter the walls of their respective ventricles. These fibers then make contact with the Purkinje fibers which are large conducting cells that rapidly distribute the action potential throughout most of the ventricles. The rapid conduction along the Purkinje fibers and the distribution of these fibers cause the depolarization of the left and right ventricular cells to occur approximately simultaneously, thus resulting in a single coordinated contraction. Figure 1.3 illustrates the sequence of cardiac excitation.

1.2 The Electrocardiogram

The electrocardiogram (ECG) is primarily a tool for evaluating the electrical events within the heart. The action potentials of cardiac muscles can be viewed as batteries that

cause charge to move throughout the body fluids. These moving charges, or currents, represent the sum of the action potentials occurring simultaneously in many individual cells and can be detected by recording electrodes at the surface of the skin[1]. Figure 1.4 illustrates a typical normal ECG recorded between the right and left wrists for one heart beat.

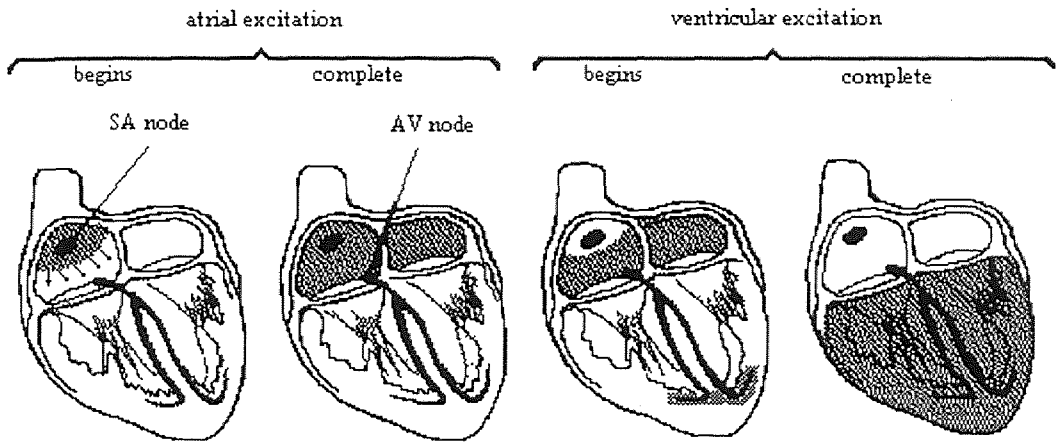

Figure 1.3 The sequence of cardiac excitation
(from A.J. Vander, J.H. Sherman, and D.S. Luciano, *Human Physiology,* 1994)

The first deflection, the P wave, corresponds to the current flow during atrial depolarization (contraction). The second deflection, the QRS complex, is a result of ventricular depolarization. The third and final deflection is the T wave. The T wave is a result of ventricular repolarization (relaxation). It should be noted that atrial repolarization is usually not evident in the ECG because it occurs at the same time as the QRS complex.

As mentioned earlier, the ECG is a measure of the electrical activity of the heart measured on the skin. The bipolar method of acquiring ECG detects electrical variations

measured on the skin. The bipolar method of acquiring ECG detects electrical variations at two different locations on the skin and displays the difference to obtain one waveform. Figure 1.5 is an illustration of the standard limb lead connections that form Einthoven's triangle. In addition, the diagram also shows the names of the respective leads. To record lead I, the negative terminal of the ECG monitor is connected to the right arm (RA) and the positive terminal is connected to the left arm (LA). To record lead II, the negative terminal of the ECG monitor is connected to the right arm and the positive terminal is connected to the left leg. To record lead III, the negative terminal of the ECG monitor is connected to the left arm and the positive terminal is connected to the left leg (LL). The reference point or ground is connected to the right leg (RL).

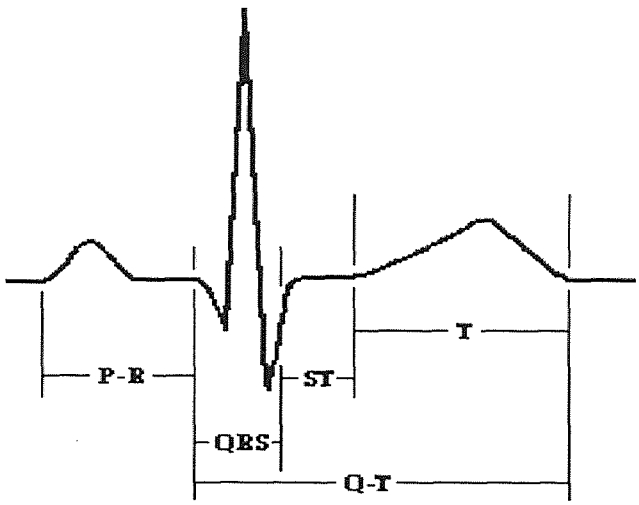

Figure 1.4 Illustration of a typical electrocardiogram

It is important to realize that depending on where the electrodes are attached, a different waveshape will be obtained for the same electrical events occurring in the heart.

obtaining different waveforms depending on the location of the electrodes, each individual has a unique ECG.

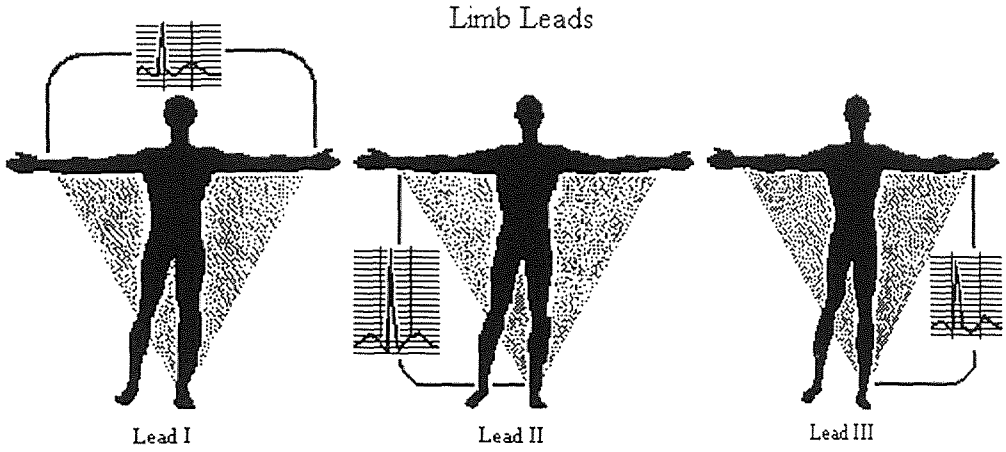

Figure 1.5 Standard ECG limb leads to form Einthoven's triangle
(from F. Netter. *The CIBA Collection of Medical Illustrations Volume 5,The Heart*,1981)

1.3 The Nervous System

Human behavior is controlled and regulated by two major communication systems, the endocrine system and the nervous system. The nervous system can be divided into two separate, but interconnected, parts. The first part consists of the brain and spinal cord and is called the central nervous system. The second part, which consists of nerves which extend from the brain and the spinal cord out to all points of the body, is called the peripheral nervous system.

The peripheral nervous system consists of both an afferent division and efferent division. The afferent division conveys information from primary receptors to the central nervous system. The efferent division carries signals from the central nervous system out

to effector cells such as muscles and organs. The efferent division is subdivided into a somatic nervous system and an autonomic nervous system. The somatic nervous system consists of all the nerve fibers going from the central nervous system to skeletal-muscle cells. The efferent innervation of all tissues other than skeletal muscle is done by the autonomic nervous system[1].

1.3.1 The Autonomic Nervous System

The autonomic nervous system is the part of the nervous system that controls the visceral functions of the body. Regulation of internal activities such as blood pressure, heart rate, gastrointestinal motility, and body temperature, among many others, is performed by the autonomic nervous system. Autonomic activity is controlled mainly by centers in the spinal cord, brain stem, and hypothalamus. Table 1.1 summarizes the effects of the autonomic nervous system on selected organs[1].

The autonomic nervous system is divided into two anatomical and functional units with opposite properties. The sympathetic nervous system is responsible for creating an increased level of activity in an organism. Anatomically, sympathetic nerves are composed of two neurons: a preganglionic neuron and a postganglionic neuron. These nerves pass from the spinal cord through the white ramus into one of the sympathetic ganglia before reaching their destination, Figure 1.6. Most postganglionic sympathetic nerve endings secrete norepinepherine, a neurotransmitter that activates excitatory receptors, but in some cases can inhibit certain organs. The sympathetic nervous system is

also responsible for the alarm or fight-or-flight response. This is caused by a mass discharge of all sympathetic nerve endings[2].

Table1.1 Autonomic effects on selected organs of the body
(from A.J. Vander, J.H. Sherman, and D.S. Luciano, *Human Physiology,* 1994)

Effector Organ	**Effect of Sympathetic Stimulation**	**Effect of Parasympathetic Stimulation**
Eyes		
Iris muscles	contracts (dilates pupil)	relaxes (constricts pupil)
Ciliary muscle	Relaxes (flattens lens)	Contracts
Heart		
SA node	Increases heart rate	Decreases heart rate
Atria	Increases contractility	Decreases contractility
AV node	Increases conduction velocity	Decreases conduction velocity
Ventricles	Increases contractility	Decreases contractility slightly
Arterioles		
Coronary	Dilates (β_2); constricts (α)	Dilates
Skin	Constricts	None
Skeletal muscle	Dilates (β_2); constricts (α)	None
Abdominal viscera	Dilates (β_2); constricts (α)	None
Salivary glands	Constricts	Dilates
Lungs		
Bronchial Muscle	Relaxes	Contracts
Stomach		
Motility, tone	Decreases	Increases
Sphincters	Contracts	Relaxes
Secretion	Inhibits (?)	Stimulates

The parasympathetic nervous system, by contrast, generally lowers the activity of an organism, and is associated with a relaxed state. Anatomically, parasympathetic fibers leave the brain through cranial nerves III, V, VII, IX, and X, and the second and third sacral spinal nerves as illustrated in Figure 1.7. Cranial nerve X is also called the vagus nerve, and since the vagus innervates much of the thorax and abdomen, especially the heart, for the parasympathetic nervous system, parasympathetic activity is often called

vagal activity. All parasympathetic nerve endings secrete acetylcholine. Although acetylcholine generally has an excitatory effect, it is also known to have inhibitory effects as well, such as the slowing of the heart by the vagus nerve[2].

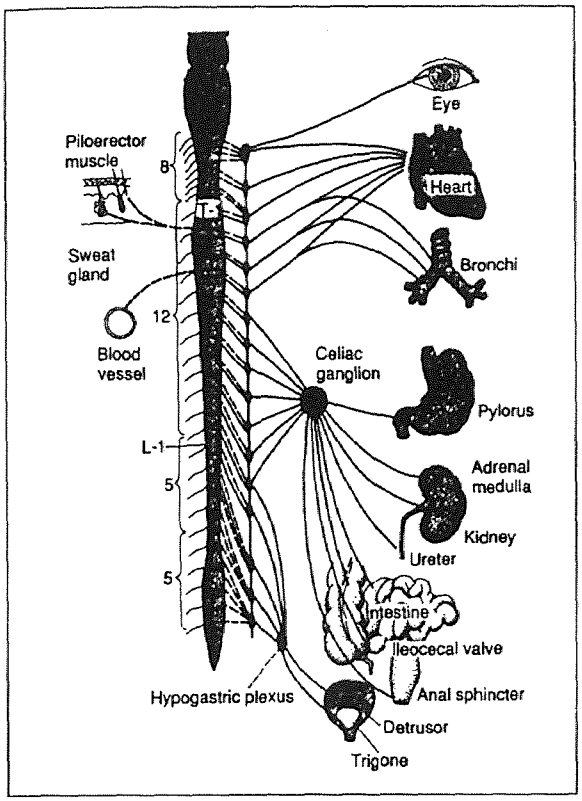

Figure 1.6 The sympathetic nervous system (from Guyton, A. C., *Textbook of Medical Physiology,* 1991)

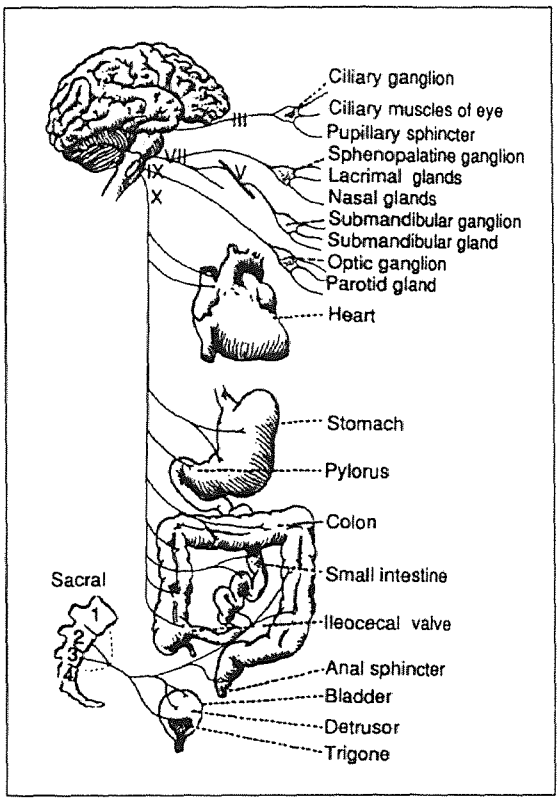

Figure 1.7 The parasympathetic nervous system (from Guyton, A. C., *Textbook of Medical Physiology,* 1991)

Both the sympathetic and parasympathetic nervous systems are continually active. These basal rates of activity are known as sympathetic and parasympathetic tone. The advantage of tone is that it allows a single nervous system to increase or decrease activity in an organ. For instance, normal sympathetic tone keeps the systemic arterioles constricted to approximately half their maximum diameter. By changing the degree of

sympathetic tone, the diameter of the arterioles can be increased or decreased. Without tone, the sympathetic nervous system can only cause vasoconstriction, never vasodilation.

1.4 Heart Rate Variability

1.4.1 Physiology of Changes in Heart Rate

Change in heart rate is sensitive to changes in body temperature, plasma electrolyte concentrations, and hormones[1]. However, the most important influence of beat-to-beat variations of heart rate comes from the autonomic nervous system. More specifically, sympathetic activity increases heart rate, whereas activity in the parasympathetic (vagus) nerves causes the heart rate to decrease. Due to considerably more parasympathetic activity to the heart than sympathetic activity in the resting state, the normal resting heart rate is below the inherent rate of 100 beats/minute.

The autonomic nervous system innervates the heart in a number of places. The sympathetic nervous system terminates at the SA node, the conduction system, atrial and ventricular myocardium, and coronary vessels. The parasympathetic fibers terminate in the SA and AV nodes, atrial and ventricular musculature, and coronary vessels. Interplay between the two systems will cause the heart to speed up or slow down, depending on which system is more active. Figure 1.8 illustrates autonomic innervation of the heart[3].

Perhaps the most important site of innervation of the autonomic nervous system on the heart occurs at the SA node. The SA node possesses an inherent discharge rate, often referred to as the pacemaker potential. The pacemaker potential is a slow depolarization of the cells of the SA node. The innervation of the sympathetic and

parasympathetic nervous system on the SA node changes the characteristics of depolarization within the SA node cells, thus changing heart rate. Figure 1.9 illustrates these changes due to autonomic innervation[1].

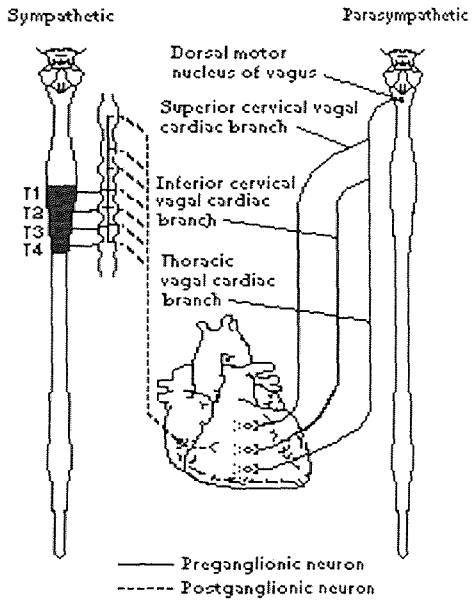

Figure 1.8 Autonomic innervation of the heart (from M.D. Kamath and E.L. Fallen, "Power spectral analysis of heart rate variability," *Crit. Rev. in Biomed. Eng.*, 1993)

For comparative purposes, the pacemaker potential labeled 'a' is the control. From the figure, one can observe that sympathetic stimulation increases the slope of the pacemaker potential. As a result, the SA node cells reach the threshold more rapidly, thus increasing the heart rate. Conversely, parasympathetic stimulation decreases the slope of the pacemaker potential. Consequently, the SA node cells reach the threshold more slowly, and heart rate decreases. In addition to decreasing the slope of the pacemaker potential, parasympathetic stimulation also hyperpolarizes the plasma membrane of the SA node cells so that the pacemaker potential starts from a more negative membrane

potential. As a result, the time it takes the SA node cells to reach the threshold increases, which decreases heart rate.

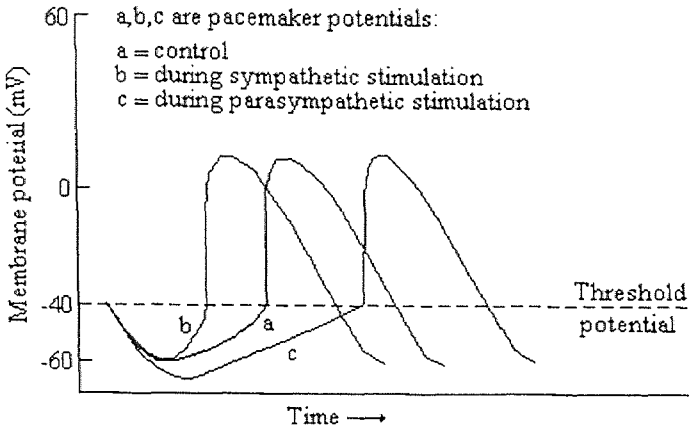

Figure 1.9 Effect of autonomic stimulation on the slope of the pacemaker potential (from A.J. Vander, J.H. Sherman, and D.S. Luciano, *Human Physiology,* 1994)

1.4.2 Heart Rate Variability as a Measure of Autonomic Function

Changes in heart rate usually involve the reciprocal action of the two divisions of the autonomic nervous system. An increased heart rate is the result of reduced parasympathetic tone coupled with an increased sympathetic activity. A decrease in heart rate is usually the result of increased parasympathetic tone and a simultaneous decrease in sympathetic tone. Therefore, changes in heart rate reflect the action of the sympathetic and parasympathetic nervous systems on the heart. However, under certain conditions, it is possible for heart rate to change by activity of only one division of the autonomic nervous system, independent of the other division, rather than reciprocal changes in both.

Initially, the effect of the autonomic nervous system on the heart was estimated by utilizing the traditional technique of average heart rate[3]. As a reference, the average heart rate was measured under normal resting conditions. Then the average heart rate was measured under the administration of drugs. The drugs used were atropine, which blocks the effects of the parasympathetic nervous system, and propranolol, which masks the effects of the sympathetic nervous system. A qualitative assessment can then be made of the autonomic nervous system by comparing the reference heart rate to the heart rate while under the administration of the drugs. This method looks at the average over time of heart rate. However, when the ECG is looked at on a beat-to-beat basis, rather than over a period of time, fluctuations in the heart rate are observed[3].

1.4.3 Power Spectral Analysis of Heart Rate Variability

Power spectral analysis of heart rate variability is a potentially powerful tool for evaluating the activity of the autonomic nervous system noninvasively. The time domain signal used for computing the heart rate variability power spectrum is known as the interbeat interval (IBI). Spectral analysis of this interval between the R-waves in the ECG results in a graph similar to that in Figure 1.10. Three distinct peaks are usually evident. These peaks are defined as: a very low frequency peak (0.02 Hz to 0.06 Hz), a low frequency peak (0.06 Hz to 0.15 Hz), and a high frequency peak (0.15 Hz to 0.4 Hz). Sometimes, a fourth peak is identified as the ultra low frequency peak which consists of frequencies less than 0.0033 Hz.

Past research in power spectral analysis of heart rate variability correlates the

three distinct peaks with certain physiological parameters[3]. The very low frequency band is associated with vasomotor control and temperature control. The low frequency band is associated with baroreceptor-mediated blood pressure control. The high frequency band has been linked with respiration.

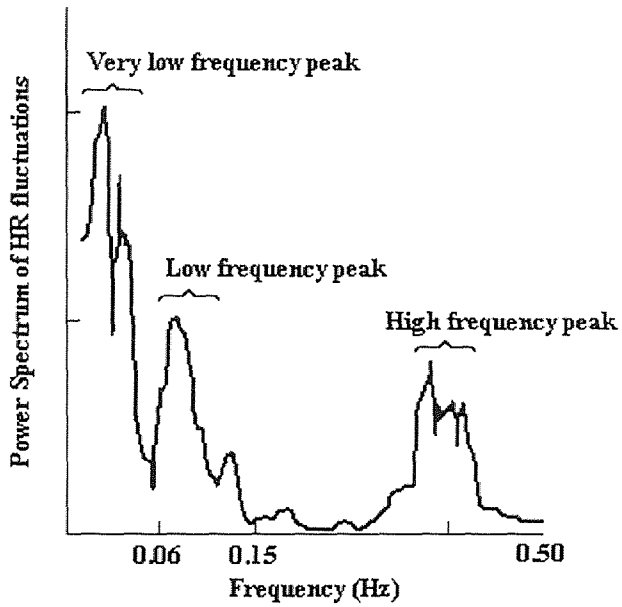

Figure 1.10 Typical power spectrum of HRV (from M. Kamath and E. Fallen, "Power spectral analysis of heart rate variability," *Crit. Rev. in Biomed. Eng.*, 1993)

To date, the best known and best defined peak in power spectral analysis of heart rate variability is the high frequency peak. The high frequency peak reflects changes in the interbeat interval that cycles up and down at the same frequency as respiration. This influence of respiration on heart rate has been known for more than one century and is called respiratory sinus arrhythmia (RSA). Properly defined, RSA is a rhythmical fluctuation in heart periods at the respiratory frequency that is characterized by a shortening and lengthening of heart periods in a phase relationship with inspiration and

expiration, respectively[4]. RSA is being used increasingly as a measure of vagal control of the heart. As a result, the high frequency peak, which often occurs at the same frequency as the respiration peak, corresponds approximately to the RSA and it is purely parasympathetic in origin[5].

From experience, one might contest that the frequency of respiration is not limited to within the narrow band of 0.15 Hz to 0.4 Hz. The normal respiration rate can be as low as only a few breaths per minute at rest and as high as up to 40 breaths per minute during intense exercise[2]. This stresses the fact that, when doing research on heart rate variability to determine parasympathetic activity, the frequency of respiration must be known. More specifically, the power spectrum of the respiration waveform should be computed. In most of the literature, the area under the frequency band between 0.15 Hz to 0.4 Hz is considered parasympathetic in origin. However, it has been proven that in cases of intense physical activity, the upper limit in this band can reach as high as 0.75 Hz[6].

Unlike parasympathetic activity, the sympathetic activity is not easily separated from the power spectrum of heart rate variability[3]. It has been hypothesized that the low frequency peak (0.06 Hz to 0.15 Hz) is a mixture of both parasympathetic activity and sympathetic activity. A better concept that is used to isolate the sympathetic activity is that of "sympatho-vagal balance" which recognizes both reciprocal and non-reciprocal parasympathetic and sympathetic influences on heart rate by computing the low frequency to high frequency ratio[7]. An increase in the low frequency to high frequency ratio indicates either an increase of sympathetic activity, a decrease in parasympathetic activity, or a reciprocal change in both.

1.5 Literature Review

1.5.1 Time-Frequency Analysis in Biological Signals

Standard spectral analysis by Fourier transform or variations of autoregressive models have been extensively applied in the attempt to evaluate quantitatively the fluctuations in beat-to-beat (R-R) intervals and respiration attributed to a regulatory function of the sympathetic and parasympathetic branches of the autonomic nervous system under steady-state conditions. Due to the limitations inherent in these methods, a compromise must always be made between frequency resolution and the choice of a time signal length short enough to suit the stationarity assumption. Analysis over a long time window, usually 5-10 min, does not show information about the time-varying structure of the spectra. Instantaneous changes of the signal content, typical for cardiovascular signals, are thus smeared out or appear as a wideband noise. Therefore, it is a common practice that a "reasonably stationary" part of the signal is identified and analyzed. However, the spectral estimation is dependent on the chosen observation window, and consequently the interpretability of the results is limited[8].

Recently, joint time-frequency signal representation has received considerable attention as a powerful tool for analyzing a variety of signals and systems. In particular, if the frequency content is time varying as in signals of biological origin which often do not comply with the stationarity assumptions, then this approach is quite attractive. Although either the time domain description or its Fourier transform carries complete information about the signal, none of them reveals explicitly the frequency spectrum at a particular time or the time at which a particular frequency component occurs. By mapping a one-

dimensional function of time or frequency into a two-dimensional function of time and frequency, the joint time-frequency representation (TFR) localizes the signal energy in both the time and frequency domains.

Traditionally, the short-time Fourier transform (STFT) or its modulus squared, called the spectrogram, has played an important role in visualizing the time-varying frequency content of various signals. It has been used extensively in the analysis of human speech[9] , and of brain electrical potentials (BEPs), primarily in the characterization of background electroencephalograms (EEGs)[10]. Using a model of heart sound generation/propagation, Durand, et al.,[11] have used the STFT to construct a time-varying transfer function and a coherence function relating intracardiac and extrathoracic vibrations. The STFT was also proposed to compute the energy distribution of the electrocardiogram (ECG). A major drawback inherent in the STFT is that a tradeoff also exists between temporal and spectral resolutions[12]. The spectrogram often presents serious difficulties when it is used to analyze rapidly varying signals. If the analysis window is made short enough to capture rapid changes in the signal, it becomes impossible to resolve signal components that are close in frequency within the analysis window duration. If one uses a longer sliding time window to obtain higher spectral resolution, then the underlying nonstationarity will be smeared out, resulting in lower temporal resolution.

The Wigner Distribution (WD) has been employed as an alternative to overcome this shortcoming of the STFT. The WD was first introduced in the context of quantum mechanics[13] and revived for signal analysis by Ville[14]. It possesses very high

resolution in both time and frequency, and it has many other nice properties as well. It has been successfully implemented for the analysis of several biological signals: circadian rhythms of carabid beetles[15], ECG signal[16], blood flow velocity wave-forms[17], ultrasonic Doppler signals[18], auditory neuron activity[19], and acoustic signals[20]. The applicability of the WD for the analysis of blood pressure, respiratory, and beat-to-beat fluctuations were also assessed by Novak, 1993[8]. It was shown that the discrete Wigner distribution follows well the instantaneous changes of spectral content of cardiovascular and respiratory signals which characterize the dynamics of autonomic nervous system responses. Two major drawbacks of the WD are that it is not necessarily nonnegative, and its bilinearity produces cross terms (or interferences) between two signal components located at different regions in the time-frequency plane. This may lead to serious misinterpretations regarding the signal spectral contents. Many attempted to rectify these shortcomings by incorporating a smoothing window function in both the time and frequency domains, thus defining the smoothed pseudo Wigner Distribution. This provided better resolution in time and frequency and reduced the interferences between the signal components.

In his pioneering work, Cohen incorporated many TFRs into a general class of time-frequency distributions. Cohen comprehensively discussed many aspects of time-frequency distributions and recent progress in the area[21]. Boashash also compared the performance of several time-frequency distributions in terms of resolution[22]. Desirable properties of a distribution and associated kernel requirements were extensively investigated by Claasen and Mecklenbrauker[23]. In 1989, Choi and Williams introduced

a new distribution with an exponential-type kernel[24]. The Choi-Williams distribution overcomes the aforementioned drawbacks of the STFT and the WD, and provides high resolution in time and frequency while suppressing interferences. Unfortunately, however, the Choi-Williams distribution does not completely satisfy the support properties in time and frequency. This kind of representation is well used in the biomedical field for various applications such as EEG characterizations[25] and electrocorticogram representation [26]. Zheng, et al.,[27] made use of the Choi-Williams distribution for EMG (motor unit potentials) description, and Sahiner and Yagle[28] applied it for blood flow speed determination and magnetic resonance imaging.

In 1992, a new class of time-frequency distributions, known as the reduced interference distribution (RID) was introduced, which has many desirable properties. It has been shown that this distribution provides a high resolution, easy to interpret localization of the signal energy spectrum in the time-frequency plane[29]. Many attempted to incorporate this emerging technique of time-frequency analysis to provide new insights into the nature of biological signals. Williams. et al.,[30] used the reduced interference distributions (RIDs) in the analysis of biosignals recorded in human epilepsy. It was shown that RID analysis of these signals resulted in research hypotheses which would be difficult or impossible to obtain using conventional techniques. The RID also demonstrated superior resolution in the detection and characterization of the first heart sound[31].

1.5.2 Stress and Behavioral Medicine research of the Cardiovascular System

Growing interest in behavioral medicine has focused attention on the function and control of the cardiovascular system, partly because of its involuntary responsiveness to emotional and stressful situations. The external manifestations of cardiovascular responses provide objective indications of the changing psychological status of normal subjects and patients. An expanding array of noninvasive techniques open opportunities for new and exciting research regarding the potential roles of psychological and behavioral factors in the development of dysfunction and disease[32].

In studies of stress, factors such as the context of the research situation, and subtle variations in the instructions presented can have significant effects on the resulting psychological, behavioral, and physiological responses. Specifically, both laboratory and field psychophysiology studies involve procedural elements, from the obtaining of informed consent to payment for participation, that can be significant sources of error variance that remain even if the most stringent experimental controls are instituted[33]. There is considerable evidence that the effects of physical stressors depend strongly on psychological factors, and that specific types of stressors can produce rather specific patterns of responses[34][35]. There are numerous ways of dimensionalizing the tasks and stimulus situations that produce different patterns of bodily responses. However, implicit in the description of a stressor as psychological is that the individual's response to a challenging or stressful stimulus depends on the way that stimulus is interpreted or appraised, the context in which that stimulus occurs, and the personal resources available for coping[36][37]. A body of research demonstrates that if situations are viewed as

harmful, threatening, or noxious, they can produce substantial physiological responses[34][37]. Conversely, when conditions are designed to change the demands of a stressor, or to reduce the psychological threat that might be engendered by potentially aversive procedures, they may produce smaller, and perhaps only minimal physiological responses and/or behavioral reactions[37].

1.5.2.1 Experimental Manipulations that Determine Intensity of Responding in Psychophysiological Studies: Considerable attention in recent years has been addressed to the study of psychophysiological reactivity (responsiveness) to psychological stress[33]. Numerous psychological stressors and tasks are employed in this research, and effort has been directed to identifying the dimensions of stressors that alter the intensity and patterning of cardiovascular and neuroendocrine responses. The intensity of a subjects' responses to an experimental task can be increased or decreased by varying the task instructions or the task characteristics according to a number of criteria. For example, increasing the positive or negative incentives for task performance, increasing the level of challenge in task instructions, and increasing the subjects' level of engagement/ involvement in the experimental situation can heighten physiological responses. Often these motivational dimensions overlap one another and covary in manipulations of experimental situations[33].

1.5.2.2 Level of Difficulty of the Experimental Task: Studies that have independently manipulated task difficulty have found that this variable does have an effect on subjects'

blood pressure and heart rate responses. It appears that the maximal physiological responses are produced by tasks that are seen as sufficiently difficult to put effort into, but not so difficult that subjects will give up on them. One explanation for this effect[38] is that tasks that elicit "active effortful coping" are thought to elicit a β-adrenergic pattern of cardiovascular responding characterized by increased heart rate and systolic blood pressure. For example, Obrist et al. (1978) found differences in cardiovascular reactions between easy and moderately difficult conditions where subjects responded to avoid shock. Here, it was hypothesized and found that a difficult criterion would be associated with greater effort and therefore with larger and more sustained increases in heart rate and systolic blood pressure compared to either a very easy or impossible reaction time criterion. However, Light and Obrist (1983) found somewhat different results using a reaction time task in which earning money was contingent upon performance[33].

Responding to control a difficult stressor may have different cardiovascular consequences than responding to control an easy stressor. Manuck and colleagues[39] studied the effects of coping on blood pressure reactions to tasks that were either difficult or easy. They found that responding to control an aversive stimulus led to greater cardiovascular reactions when working on a difficult task. However, when working on an easy task, there were no heightened cardiovascular reactions associated with coping. It is clear, however, that most studies only present subjects with a single level of task difficulty. Therefore, some populations of subjects may find specific tasks more difficult than others and may react physiologically more or less strongly to them. Ideally, tasks being considered for use in studies of cardiovascular reactivity should be carefully piloted

so that they are at a moderate level of difficulty for the subject population being studied[33].

1.5.2.3 Challenge, Harassment, and Competition: The level of challenge perceived to be involved in an experimental task refers to how demanding the subject perceives that task to be. Challenge is a psychological dimension that overlaps with many other dimensions, and is related to such factors as the type of incentive used, the difficulty of the task, whether competition is used as a motivator, or whether the subject is being evaluated in the experimental situation. A common technique employed by experimenters to heighten the level of challenge is to deliver a demanding instruction set for the tasks to be performed[33].

The use of instructions to manipulate challenge is illustrated by a study[40] that varied the level of challenge given to subjects prior to a cold pressor test. "High-challenge" instructions, delivered in a crisp tone of voice, informed subjects of the difficulty of the cold pressor task and the need for willpower, whereas, "low-challenge" instructions described the task as routine. Results indicated only minimal differences between Type A and B subjects in the low-challenge situation, and larger and statistically reliable differences in the high-challenge situation.

Harassment by the experimenter is a usual component of commonly used mental stress tasks, such as when subjects are told to count backwards as quickly as possible, being reminded in a crisp voice to go faster and be more accurate. Similar harassing statements have been used to heighten the reactivity to other types of cognitive and

psychomotor tasks. It is not clear whether harassment heightens physiological reactivity because it increases the level of challenge or because it heightens emotions such as anger[33]. Explicit and even subtle variations in these and other aspects of experimental instructions can make certain tasks effective elicitors of heightened physiological responses or can act to reveal or obscure individual differences in cardiovascular reactivity.

A social-psychological manipulation that can elicit physiological reactivity in subjects is the use of competition. To keep the level of competition standardized and controlled, competition has generally been created between subjects and either machines or confederates. Competition can also be used together with other manipulations, such as incentives and harassment, to elicit large magnitude changes in physiological response. Cardiovascular responses in competitive situations are of interest because competitiveness is a putative etiological factor in cardiovascular disorders[33]. Some subjects will treat any situation as a competitive one, whereas others will be reluctant to compete. This is illustrated by a study[41] that investigated the effects of competition with and without harassment on reactivity in Type A and B subjects. The investigators found that Type A's working against a harassing competitor showed greater heart rate and systolic blood pressure responses compared to Type B's and Type A's not being harassed. Thus, this study manipulation revealed that for Type A's, hostile competition was necessary to produce heightened cardiovascular and neuroendocrine responses. The effects of competition will play an important role in our research interpretation because our protocol involves interaction between the subject and the exercise cycle.

1.5.2.4 Cardiovascular Response to Vigorous Exercise: The cardiovascular system must be capable of adapting rapidly and effectively to changing requirements to enable the relatively small blood volume to serve the vital needs of the millions of cells in the various organs of the human body. Living cells survive, function, and thrive only in stable chemical and physical environments from which they can easily extract the essential nutrients and oxygen while eliminating toxic products derived from their metabolic activities. The many different functions of tissues require different and widely varying blood flow rates under various conditions. An extreme example is the transition from rest to vigorous exercise during which the blood flow through large muscle masses increases many fold in response to their greatly increased metabolic activity and energy release. At the same time, blood flow to the skin is increased to dissipate heat. Despite curtailed blood flow through inactive tissues, the total blood flow through the systemic circulation is increased and the pumping action of the heart is both accelerated and enhanced instantaneously or even in anticipation of exertion. Diverse, integrated patterns of response occur automatically under many different circumstances induced by neural and hormonal controls[32].

These involuntary control systems respond to various physical or psychological stresses by cardiovascular responses such as blushing, pallor, rapid pulse, fainting, or "palpitations' of the heart. The autonomic nervous system plays prominent roles in many aspects of cardiovascular response. As stated earlier, the parasympathetic nervous system acts through the vagus nerves to slow heart rate but has little direct influence on the peripheral vascular system. Conversely, the sympathetic nervous system acts to accelerate

heart rate, enhance the force of cardiac contraction, and can produce patterns of peripheral vascular responses that are appropriate for vigorous exertion. Since some of these reactions may emerge in anticipation of exercise, the central nervous system is the logical site of their origin[32].

Péronnet et al.[42] examined the cardiovascular and sympathetic profiles in response to a series of physical and mental challenges during recovery from an acute bout of aerobic exercise. Nine healthy men were tested on two occasions, once under an experimental (exercise) and once under a control (video watching) condition, in a counter-balanced order, one week apart. Although no differences in blood pressure were found in the two conditions, heart rate and plasma catecholamine concentrations were higher in exercise than in control session. These findings were partly attributed to elevated physiological levels "carried over" from exercise. They were also attributed to a possible anticipatory effect associated with exercising. Initially greater plasma NE (baseline) concentrations during the exercise session seemed to parallel these findings and could have been associated with exercise anticipation. However, subjects also knew that during video watching they would be only resting, which might be related to less vigorous, or even lethargic state. Thus, The higher vigor observed in the exercise session was left to reflect either an anticipation of the arousal inducing properties of exercise or the sedentary nature of the video watching. State anxiety and anger-hostility were reported lower in the post-experimental period than in the pre-experimental period. These findings were related to pre-experimental anticipation effects. The subjective knowledge

of no longer being faced with discomforts might have had an impact on anxiety and/or anger-hostility profile of the subjects.

1.6 Scope of Thesis

The ultimate goal of this research work is dedicated to the use of time-frequency analysis of heart rate variability as a new and innovative approach to investigate the physical and mental exertion attributed to exercise. Two studies are used for the main research. The first study is a twelve minute protocol designed by Fernando in 1992[43]. For distinctive purposes, we will refer to this protocol as the "preliminary protocol" for the remaining part of this thesis. The second study is an elaborate protocol designed by this researcher to specifically help understand more the effects of anxiety and anticipation on the heart rate variability signal during baseline control and stressful exercise conditions. The study involves two sets of protocols with two experiments, eighteen and twenty four minutes each, repeated twice for each subject, once only with the subject's awareness. We will refer to this study as the "anticipation protocol". Details of these studies are thoroughly discussed in chapter 2.

The aim of time-frequency analysis is to understand and develop tools that can describe rapid changes in time varying spectrum. Expansion of the concept of spectral analysis of heart rate variability into time-frequency analysis gives us the ability to quantitatively assess the parasympathetic and sympatho-vagal balance changes as a function of time. In the first phase of our research, time frequency analysis is performed on the entire heart rate variability and respiration signals of the preliminary protocol using

five classical kernels that fall under the general class of bilinear distribution. The aim of this process is to investigate the transitions between rest, exercise, and recovery, and to evaluate the different distributions and assess which distribution gives the most physiologically significant information. Each distribution used: the short time Fourier transform, the pseudo Wigner-Ville, the smoothed pseudo Wigner-Ville, The Choi-Williams, and the Born-Jordan-Cohen (RID), has unique characteristics which affect the amount of smoothing and the generation of crossterm interference differently. The vagal tone and the sympatho-vagal balance are the parameters used for comparison. They are assessed from the resulting 3-D time-dependent spectra by quantifying the area under the low frequency (0.06 Hz to 0.15 Hz) and high frequency (0.15 Hz to 0.75 Hz) ranges for each instant of time. Recall that the low frequency range is associated with the mixture of sympathetic and parasympathetic activity while the high frequency range corresponds to respiration and is thought to be purely parasympathetic in origin.

In the second phase of this research, the smoothed pseudo Wigner-Ville and the Choi-Williams distributions are performed on the heart rate variability signal to quantify the area under the low frequency and high frequency ranges during the anticipation protocol. The purpose of this investigation is to test the presence of an anticipatory component due to the stressful exercise condition as reflected in the heart rate variability signal from a change in behavior in the autonomic nervous system. We also want to compare pre- and post- exercise conditions between trials for each subject and between the total population of subjects.

The last phase of this work proposes a new methodology that adaptively uncovers the region of parasympathetic activity. It is well known that parasympathetic activity is highly correlated with the respiration frequency. This technique traces the respiration frequency and extracts the corresponding parasympathetic activity from the heart rate variability signal by adaptive filtering.

CHAPTER 2

METHODS

The main focus of this chapter is a thorough introduction to the methods and experimental protocols performed to acquire the biological signals of interest, namely the electrocardiogram and respiration signals. To begin with, a basic description is given of the theory behind the signal processing techniques used to analyze and acquire the signals. Because of the complexity of the signal processing, chapter three is provided for a more complete theoretical and practical discussion.

2.1 Time and Frequency Analysis

"Time analysis" is among the standard methodologies used to study the signal $x(t)$ as a function of time. Its main emphasis is on quantifying the energy, $|x(t)|^2 \Delta t$, which is the energy density in a small amount of time Δt, contained in that signal $x(t)$ [22]. However if we want to gain more understanding of the components that constitute our signal, it is customary to investigate an alternative way of looking at the signal, "frequency analysis". Therefore, if we expand the signal as

$$x(t) = \int_{-\infty}^{\infty} X(f) \cdot e^{j2\pi ft} df , \qquad (2.1)$$

we can think of $X(f)$ as the signal in the frequency-domain and $|X(f)|^2 \Delta f$ as the fractional energy in the frequency interval Δf at frequency f. Note that by inverting equation 2.1, we can define the signal in the frequency-domain[22].

$$X(f) = \int_{-\infty}^{\infty} x(t) \cdot e^{-j2\pi ft} dt \qquad (2.2)$$

$X(f)$ is referred to as the Fourier Transform (FT) of $x(t)$.

Thus, the Fourier Transform and its inverse establish a one-to-one relation between time and frequency domain. Although the FT allows the passage from one domain to the other, it does not allow a combination of the two domains. In particular, most time information is not easily accessible in the frequency domain. While the spectrum $X(f)$ shows the overall strength with which any frequency f is contained in the signal $x(t)$, it does not generally provide easy to interpret information about the *time localization* of spectral components[44].

In Figure 2.1, we illustrate two cases, where each contains three sine waves of equal duration time of 4 seconds and frequencies of 5 Hz, 20 Hz and 35 Hz. The only difference among cases (a) and (b) is that different frequencies occur at different times. The power spectrum, as shown in figure 2.2, is the same for the two signals. It shows that frequencies 5 Hz , 20 Hz and 35 Hz were present for both cases but does not show the specific duration of time they existed. To fully describe such a situation we have to give the frequencies for each particular time.

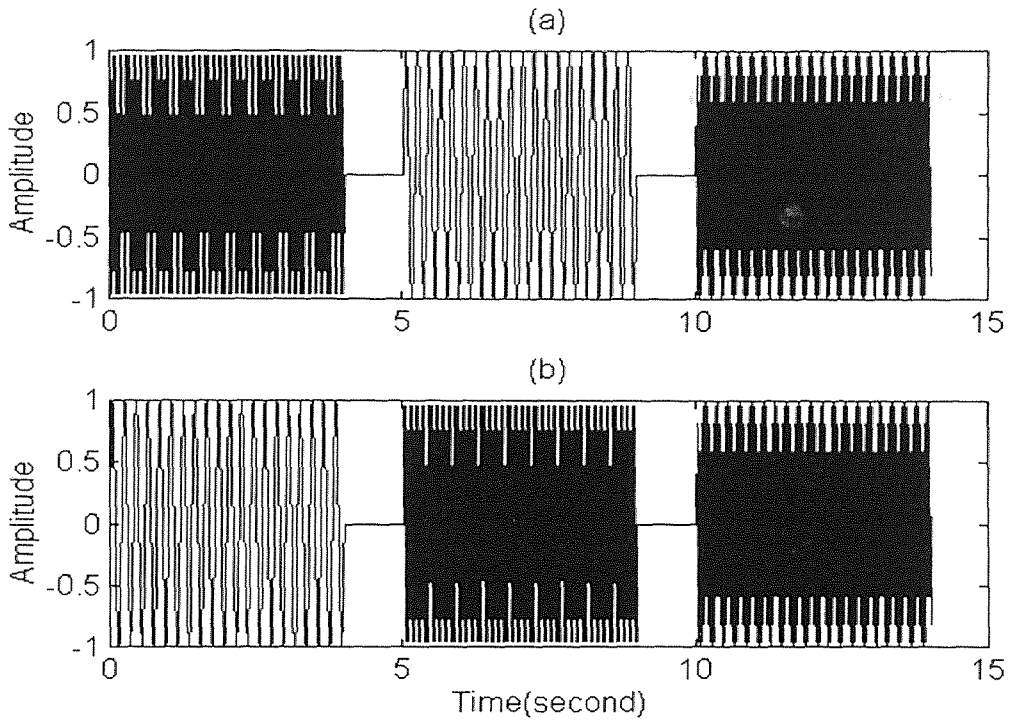

Figure 2.1 Two finite duration signals containing the same frequencies (5 Hz ,20 Hz and 35 Hz) occurring at different times

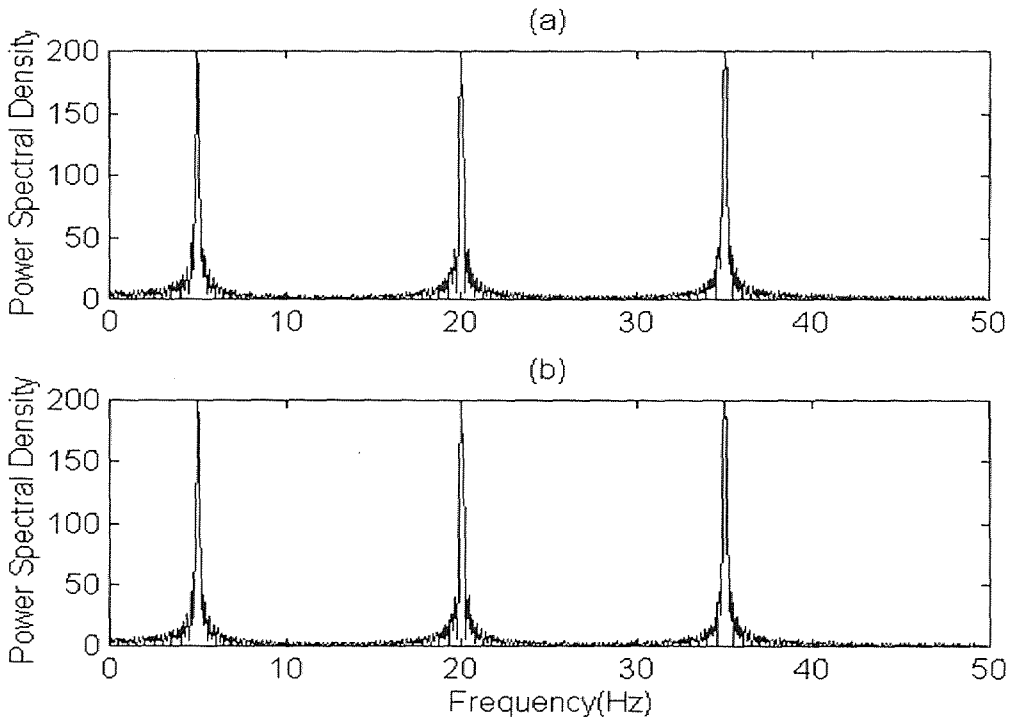

Figure 2.2 The power spectra for the two finite duration signals above The spectrum is an exact replica for each signal

2.2 Joint Time-Frequency Analysis

Time-frequency signal representations characterize signals over a joint time-frequency plane. They thus combine time-domain and frequency-domain analyses to yield a potentially more revealing picture of the temporal localization of a signal spectrum. Time-frequency distributions (TFDs) of signals map a one-dimensional function of time, $x(t)$, into a two-dimensional function of time and frequency, $\rho(t,f)$. Most TFDs are "time-varying representations" which are similar conceptually to a musical score with time running along one axis and frequency along the other axis. The values of the TFD surface above the time-frequency plane give an indication as to which spectral components are present at each particular time[44].

Time-frequency analysis was performed for the same signals (a) and (b) described in section 2.1 using the Choi-Williams distribution. Figure 2.3a shows that at the time intervals of [0 , 4], [5 , 9] and [10 , 14] seconds of the signal, frequencies of 20, 5 and 35 hertz exist respectively. Figure 2.3b shows that at the intervals of [0 , 4], [5 , 9] and [10 , 14] seconds of the signal, frequencies of 5, 20 and 35 hertz exist respectively.

The major drawback of time and frequency analysis is that they tell us the frequencies that existed for the total duration of the signal and not the duration when the different frequency components existed. However using time-frequency analysis shows that one can fully describe the existence of a specific frequency at each instant of time.

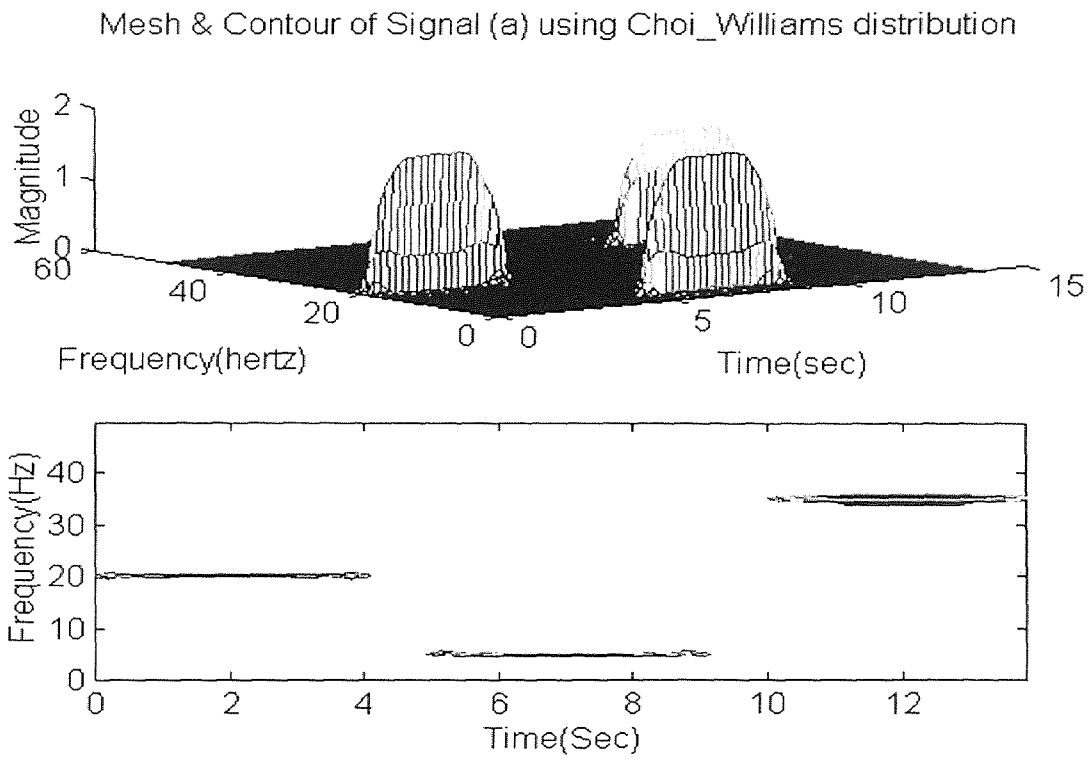

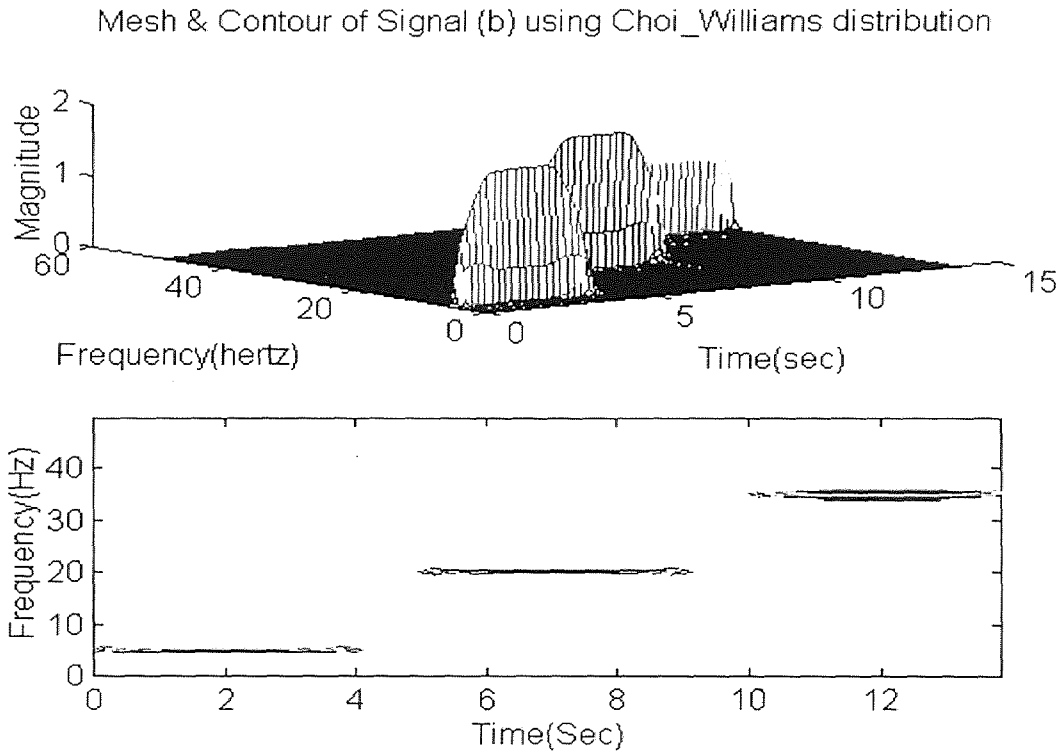

Figure 2.3 The mesh and contour plots of time-frequency analysis of signals (a) and (b) respectively

2.3 Analog-to-Digital Conversion

A discrete time signal is defined by specifying the value of an analog signal only at discrete times, called sampling instants[45]. Once the sampled values are quantized and encoded, a digital signal results. A digital signal is formed from a continuous-time, analog signal by a process called analog-to-digital(A/D) conversion. A block diagram of an analog-to-digital converter is shown in Figure 2.4.

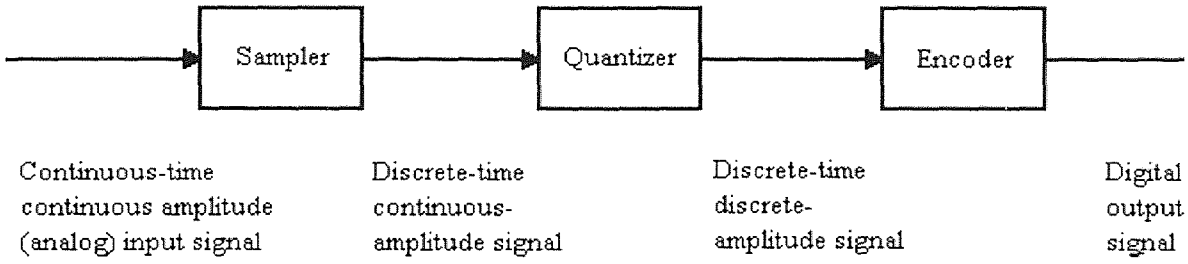

Figure 2.4 Block diagram of an analog-to-digital converter (from R. Ziemer, W. Tranter, and R. Fannin, *Signals and Systems: Continuous and Discrete*, 1989)

The first component is a sampler that extracts sample values from a continuous time, continuous amplitude (analog) input signal at specified sampling instants. The output of the sampler is a discrete time signal with a continuous amplitude because the sampled values assume the same continuous range of values assumed by the input signal. The second component in an A/D converter is a quantizer, which quantizes the continuous amplitude range of samples into a finite number of amplitude values. The last component is an encoder which maps each quantized sample value onto a digital word. For a binary representation, the number of quantizing levels q and the digital wordlength

n are related by

$$q = 2^n \tag{2.3}$$

In order to be able to reconstruct the original signal from the sampled signal, there are three important points that must be followed. The first point involves the sampling rate, and is covered by the sampling theorem which states that a bandlimited signal, having no frequency components above f_h hertz, is completely specified by samples that are taken at a uniform rate with a frequency greater than or equal to $2f_h$ hertz. In other words, the time between samples is no greater than $1/2f_h$ seconds. The frequency $2f_h$ is known as the Nyquist frequency. To understand why the sampling frequency must be greater than twice the highest frequency in the signal, the spectrum of the input signal and the spectrum of the sampled signal are displayed in Figure 2.5. Figure 2.5(a) shows that the spectrum of the input signal is double sided, consisting of power at both positive and negative frequencies. Figure 2.5(b) shows the spectrum of the properly sampled signal containing the spectrum of the original signal repeating at integer multiples of the sampling frequency. Figure 2.5(c) shows the effect of sampling at too low of a sampling rate. This effect is known as aliasing, and makes it impossible to recover the original signal.

The second important point to be made about the reconstructing of the original wave from the sampled wave, is that a low pass filter must be used to pass only those frequencies contained in the original spectrum. The final point concerns the number of quantization levels. Since the quantizing level is the only value retained after the sample

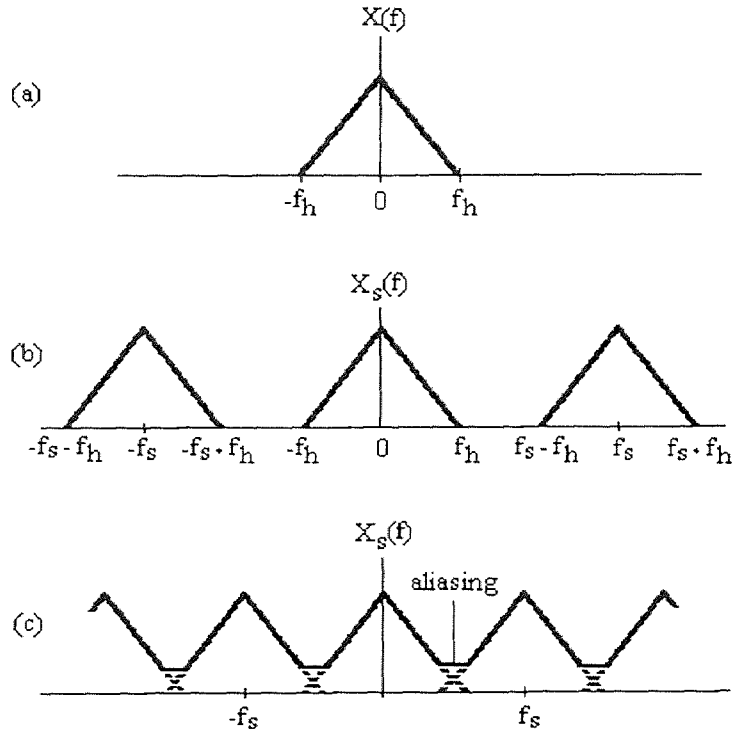

Figure 2.5 Spectrum of (a) the original signal (b) sampled signal and (c) improperly sampled signal (from R. Ziemer, W. Tranter, and R. Fannin, *Signals and Systems: Continuous and Discrete*, 1989)

values are quantized, errors are induced by the quantizing process that can not be removed by additional processing[45]. To reduce the quantization error, it is important to have enough quantization levels and to make sure the amplitude range of the signal uses all the quantization levels.

2.4 Subjects and Experimental Protocols

2.4.1 Preliminary Protocol

Ten subjects participated in an exercise protocol that Fernando designed in 1992. The protocol consisted of riding a cycle ergometer (Lifecycle, CA) at 80 rev/min as dictated by the visual speedometer readout. The initial workload involved pedaling at 80 rev/min

in an unloaded condition. Thereafter, the workload (resistance) was automatically varied by a computer algorithm to maintain the subject's heart rate at 70% of age predicted maximum. Age predicted maximum heart rate is calculated as 220 minus the age of the subject. The specific protocol required the subject to rest initially for two minutes on the bicycle with no physical activity. The subject was then instructed to pedal for two minutes until the heart rate achieved 70% of age predicted maximum. This pace was maintained for another four minutes for a total of 6 minutes of exercise. The subject was then asked to halt exercise and rest for another four minutes of recovery. The ECG lead II, the QRS sync pulse (a pulse that occurs at the time of the R-wave), and the respiration data were collected in a continuous 12 minute files[43].

2.4.2 Anticipation Exercise Protocol

Researchers have indicated that a greater heart rate response as well as an increase of systolic blood pressure during a stress exercise session may reveal an anticipatory effect associated with exercising[42]. They also indicated that the subjective knowledge of approaching (instead of no longer being faced with) discomforts may have had an impact on anxiety and/or anger/hostility profile of the subjects. In fact, these expectancy effects may have been more powerful than any treatment effects[42]. The role of these two processes should be tested experimentally. This study was devised to help understand more the effects of anxiety and anticipation on the heart rate variability and respiration signals.

A total of nine subjects, two females and seven males, participated in the study. The age of the subjects ranged from 21 to 39 years. All subjects were considered normal. In other words, they suffered from no known illnesses such as diabetes, heart disorders, etc. The only restriction on subjects were: (1) the subjects were between 20 and 40 years of age, (2) subjects did not suffer from any breathing disorders, and (3) pregnant women were not allowed. Each subject was instructed to have a light breakfast or lunch and to refrain from exercising and caffeine intake twenty four hours prior to testing. Smokers were also asked to abstain from smoking at least twelve hours before testing. Some general information on the subjects is shown in table 2.1.

Table 2.1 General information of each subject

Subject #	Sex	Age	Height	Weight	Smoker	Exercise fitness
1	M	21	5' 9"	170	no	Moderate
2	M	23	5' 10"	158	yes	Unfit
3	F	28	5' 3"	136	no	Unfit
4	M	22	5' 6"	170	no	Moderate
5	F	25	5' 1"	175	no	Unfit
6	M	32	5' 8"	154	yes	Unfit
7	M	37	5' 8"	148	no	Fit
8	M	39	5' 8"	149	no	Unfit
9	M	23	6'	195	no	Fit

The subjects were considered smokers if they had at least one cigarette per day. They were also classified in three levels of exercise fitness: (1) fit if they exercised at

least three times a week, for a minimum of 45 minutes, (2) moderately fit if they exercised two times a week, and (3) unfit if they exercised once a week or less. The participants were only told about the nature of the experiments (rest and exercise) without any specifics. Part of the details were then revealed in a page of written instructions that was read to them prior to the start of testing each time the experiment ran. It outlined the procedures and informed them about the rigorous exercise level.

The study involved two sets of protocols to be held at the same time of day but on two separate days. On the first experimental session (A), the subjects were first instructed that they would perform the protocol detailed below once, rest for 30 mins, and repeat it again. The first session ran as follows:

1) Rest for 2 mins.

2) Exercise for 6 mins (2 mins to reach desired HR and 4 mins maintaining it).

3) Rest for 10 mins.

4) Exercise for 3 mins (2 mins to reach desired HR and 1 min maintaining it).

5) Recovery for 3 mins.

The exercise consisted of riding a cycle ergometer (Lifecycle, CA) at 80 rev/min as dictated by the visual speedometer readout. The initial workload consisted of pedaling at 80 rev/min in an unloaded condition. Thereafter, the workload (resistance) was automatically varied by a computer algorithm to maintain the subject's heart rate at 70% of age predicted maximum. Age predicted maximum heart rate is calculated as 220 minus

the age of the subject. The specific protocol required the subject to rest initially for two minutes with no physical activity. Then the subject pedaled for two minutes until the heart rate achieved was 70% of age predicted maximum. This pace was to be maintained for another four minutes for a total of 6 minutes of exercise. The experimenter monitored the level of activity and intervened verbally to assure precision in completion of exercise. The subject then halted exercise and rested without physical exertion for ten minutes. Eight minutes into this rest period (minute 16), the subject was reminded that there was two minutes left for the onset of exercise. Pedaling resumed for a total of three minutes after that, two minutes to reach target heart rate and one minute maintaining it. Recovery followed the last exercise session where the subject was told again to halt all physical activity. Data was collected in a continuous 24 minute file. After thirty minutes of rest on a comfortable chair, the subject was seated back on the bicycle thinking that he/she would repeat the first protocol again. However, the second session was slightly changed. It actually included only:

1) Rest for 2 mins.

2) Exercise for 6 mins (2 mins to reach desired HR and 4 mins maintaining it).

3) Rest for 10 mins.

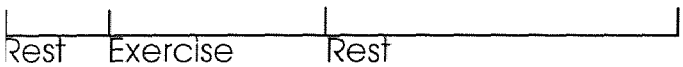

Thus, the first stage of the experiment was repeated. However, after reaching the end of the ten minutes recovery period, the session was ended for a total of 18 minutes of continuous data collection. Note that the subjects were intentionally not led to believe

that the early termination was a planned action. This was purposely done in an attempt to investigate and filter out changes in the physiological responses, if any, between doing the physical exercise versus the knowledge of repeating it. We therefore wanted to answer the question whether we could, between minutes 16 and 17, discover an anticipatory component attributed to the anxiety of performing the tedious exercise, and whether this component changed between performing the exercise and not performing it.

The second experimental session involved the same set of tests, but performed in the reverse order. The subjects were instructed in the beginning that they would perform the 18 minute protocol without the knowledge that they were repeating set 2 of experiment (A). They were told that they would perform the protocol detailed below, rest for 30 minutes, and then repeat it.

1) Rest for 2 mins.

2) Exercise for 6 mins (2 mins to reach desired HR and 4 mins maintaining it).

3) Rest for 10 mins.

The specific protocol required the subject to rest initially for two minutes with no physical activity. Then the subject was instructed to pedal for two minutes until the heart rate achieved was 70% of age predicted maximum. This pace was to be maintained for another four minutes for a total of 6 minutes of exercise. The subject was then asked to halt and rest without physical exertion for ten minutes. Eight minutes into the rest period,

the subject was reminded that there was two minutes left for the termination of the experiment. Data was collected in a continuous 18 minute files.

After thirty minutes of rest on a comfortable chair, the subject was now seated back on the bicycle thinking that he was to repeat the same procedure (B1) over again. Instead, the subject's second experiment (B2) included:

1) Rest for 2 mins.

2) Exercise for 6 mins (2 mins to reach desired HR and 4 mins maintaining it).

3) Rest for 10 mins.

4) Exercise for 3 mins (2 mins to reach desired HR and 1 min maintaining it).

5) Recovery for 3 mins.

Thus, after reaching the end of the ten minutes rest period which was supposed to indicate the termination of the experiment, the participant was asked to start pedaling again repeating the first protocol of the first visit. This was done again to investigate whether there would be any anticipatory component, now that the subject didn't have a prior knowledge of the exercise. Data was continuously collected for the 24 minute duration.

This study reevaluates the effect of stressful exercise on heart rate variability. Its main purpose is to test the presence of an anticipatory component due to the vigorous exercise condition as reflected in the heart rate variability signal from a change in

behavior in the autonomic nervous system. Thus, The study covered the two hypotheses of intervention. Each experimental procedure was covered in two states (told-done/told-not done). The physiological parameter investigated was the electrocardiogram. The experiments were conducted in the autonomic research lab at the Kessler Institute for Rehabilitation.

2.5 Data Acquisition

2.5.1 Acquisition of the Respiration Waveform

The respiration waveform was recorded using a method called impedance pneumography. A RESP I impedance pneumograph (UFI, Morrow Bay, CA) was used to measure trans-thoracic impedance changes which result from respiration. To produce a signal proportional to the trans-thoracic impedance, the RESP I causes a safe, high-frequency (30 Khz) alternating current to flow between two electrodes. As a result of the current, a voltage is produced which reflects the changes in impedance in the segment between the two electrodes. The RESP I senses this voltage and makes it available as its output in analog form.

For this study, two diagnostic ECG adhesive silver/silver chloride surface electrodes (Medtronic, Haverhill, MA) were placed on the left clavicles , and on the left rib below the pectoral muscles . To obtain a clean respiration signal, each skin site was prepared before the electrode application by thoroughly scrubbing with an alcohol prep to remove the outermost layer of dead skin (stratnum corneum). This helps reduce the dc offset and motion artifact from the skin-electrode interface. Next, a dry piece of gauze

pad was used to remove any alcohol and dead skin. Finally, application of the electrode to the prepared site was performed by placing the electrode on the skin, making sure that the gel made contact with the skin first, and then smoothing the electrode from the center out.

The analog voltage output of the RESP I was input to a DAS-16 analog-to-digital converter (Keithley MetraByte/Asyst, Natick, MA) which was installed in an IBM compatible 286, 25 MHz computer with 1 Mb of RAM and 107 Mb hard drive. However, before the output of the RESPI entered the DAS-16, it was isolated from the acquisition computer by an isolation amplifier which protects the subject from the 120V source required to power the acquisition computer. The connection between the RESPI and the isolation amplifier and the isolation amplifier and the A/D board were made with shielded cables.

The DAS-16 was configured to accept 8 different channels of data, each having an amplitude in the range of - 5 volts to + 5 volts. Each sample of data requires 2 bytes of hard disk space. Twelve of the sixteen bits are used for encoding the amplitude of the input signal, providing 4096 different quantization levels. One of the twelve bits is used to indicate if the signal has a positive or negative voltage. The remaining four bits are used to identify the different channels. Therefore, each quantization level is equivalent to 2.44 mV (5 Volts/ 2048).

The respiration is sampled at 200 samples per second and is stored in binary format. Because there is no filtering between the RESPI and the data acquisition board, the respiration was sampled at 200 samples per second to avoid aliasing due to 60 Hz

noise. Before the signal was acquired, the connection between the RESPI and the A/D board was checked with a program that plots the input to the A/D board on the screen. Once confirmed of the proper connection, the signal was acquired using Streamer v3.25 data acquisition software (Keithley MetraByte/Asyst, Natick, MA).

It should be mentioned that the RESPI is really an indirect measure of respiration. A direct measure of respiration would measure the air flow in and out of the lungs through the nose and mouth which would indicate both respiration rate and volume. The only way to do this is to place a mask over the subject's nose and mouth and connect the subject through a flexible tube to a spirometer or metabolic cart. Although this was an option, the RESPI was chosen for its simplicity to implement and comfort, keeping in mind that our investigation requires that no excess anxiety should be produced from external factors such as equipment. Another method considered to measure the respiration waveform was that of nasal thermistors. However, during exercise, people tend to breathe from both their nose and mouth. Unfortunately, the nasal thermistor would not measure the flow of air through the mouth. One possible solution to this problem is to put the nasal thermistor in the opening of a mask which covers the nose and mouth. Although this is a viable solution, it is also a problem since the mask is a minor nuisance that can become a major distraction during exercise techniques and thus contaminate the data. An advantage of the methods to measure respiration other than by impedance pneumography, is that they provide a very clean respiration tracing during all test conditions. Conversely, the RESPI tends to get noisy during exercise because of muscle electromyography, skin movement, and movement of the skin-electrode interface.

2.5.2 Acquisition of ECG

The ECG was acquired with a Quinton Q4000 Stress Test Monitor (Quinton Instrument Co., Seattle, WA), with electrodes placed in the three bipolar limb lead configuration. Output from the Q4000 were ECG leads I, II, and III, plus a sync pulse, all about 3 V_{p-p}. The sync pulse is a short duration square wave pulse that is synchronized with the QRS wave of the ECG. Three channels, the sync pulse and Lead I and II outputs, were connected by shielded cable to the data acquisition computer using the same procedure outlined in the previous section.

The skin of the subject was prepared in the same manner. Silver-silver chloride ECG electrodes (Medtronic Andover Medical, Haverhill, MA) were placed on the left and right clavicles (right arm and left arm positions), and on the left and right ribs below the pectoral muscles (right leg and left leg positions). These were connected to the Q4000 using its RA, RL, LA, and LL leads. It is important to note that subjects were seated facing away from the experimenter and equipment so that displays would not be a source of biofeedback.

2.6 Data Analysis

2.6.1 Converting Data from Binary Format to ASCII Format

Both the respiration signal and the ECG leads were collected using Streamer data acquisition software and a DAS16 data acquisition board. The signals were quantized to 12 bit words, and were stored on the root directory in a binary format that utilizes 2 bytes per sample. The software program used for analysis, MATLAB v4.2c (Math Works Inc.,

Natick, MA), can not convert the data from binary format into ASCII format. Therefore, a program called kunpack2 was utilized to convert the data from binary to ASCII format for MATLAB. The kunpack2 program converts the binary file to an ASCII file where each channel of data is represented as a column in a matrix and the columns are separated by spaces. This program is a modified version of the unpack program, a utility that Keithley MetraByte/ Asyst provided with the Das16 analog-to-digital conversion board.

2.6.2 Heart Rate Variability and Respiration Analysis

As mentioned in section 2.5.2, the ECG is converted from analog to digital form and stored in binary format on the data acquisition computer. The data is then transferred over the Novell network provided at Kessler Institute for Rehabilitation to a signal processing computer. In this study, the computer used to do the signal processing was an IBM compatible with a 90 Pentium processor with 65 Mb of RAM and a 2 GB hard drive. The initial step in the data analysis is to unpack the data from binary format to ASCII format using the kunpack2 program. Once in ASCII format, MATLAB is used to scan the data into a matrix form and then previously developed and modified software algorithms in MATLAB were used to obtain the HRV signal. The following is a description of the necessary steps to obtain IBI signal.

To begin the analysis, the sync pulse was chosen to identify the position of every R-wave in the ECG. This was achieved by providing a vertical threshold which the sync pulse must exceed. Once the R-waves are properly detected , an interbeat interval (IBI) signal can be constructed. To obtain the IBI signal, the distance in time between a

specific beat(T_m) and the beat previous in time(T_{m-1}) is calculated. This value of time difference then becomes the amplitude of the IBI signal at that specific beat. Mathematically, the IBI signal is computed by the formula $IBI_m = T_m - T_{m-1}$. See Figure 2.6 for a graphical representation.

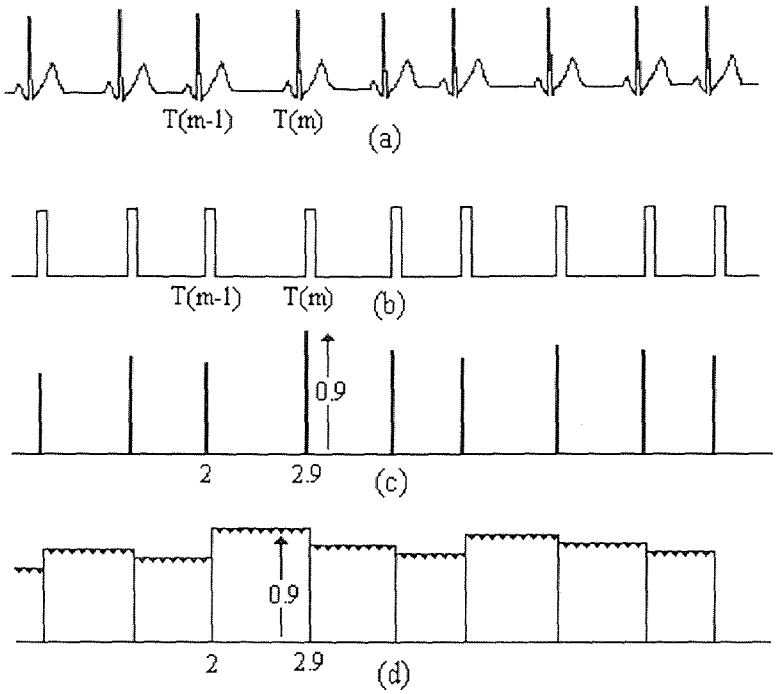

Figure 2.6 Figure depicting the construction of the IBI signal
(from S.J. Shin, W.N. Tapp, S.S. Reisman, and B.H. Natelson,"*Assessment of autonomic regulation of heart rate variability by the method of complex demodulation*," 1989)

Although the IBI represents the heart period at discrete points, the IBI signal is not suitable for FFT analysis because the discrete points, located at each R-wave, are not evenly spaced. In order to produce equidistant IBI samples suitable for analysis, the IBI signal must be interpolated[5].

The interpolation method used was that of a backward step function. This method assumes no new information about the direction of the time series is available until the next heart beat occurs. Therefore, the amplitude of all of the interpolated values between a beat at time T_{m-1} and the beat at T_m were set equal to the time difference between T_m and T_{m-1}. The interpolated interbeat interval(IIBI) is then sampled to produce an IIBI with evenly spaced samples. For example, in Figure 2.6(c) if a beat occurs at a time equal to 2 seconds and the next beat occurs at a time equal to 2.9 seconds, then the interpolated values between time 2 seconds and 2.9 seconds are all 0.9 seconds as shown in Figure 2.6(d). After the IIBI signal is obtained, it is detrended using a locally weighted robust regression algorithm. Essentially, this removes low frequency components below 0.05 Hz. If these low frequency components are not removed, they can dominate the power spectrum and decrease the detail of the components in the frequencies above 0.05 Hz. Another example of an IBI signal and an IIBI signal is shown in Figure 2.7.

The final step to obtain the HRV signal used in our analysis is to decimate the IIBI signal by a factor of ten (the ECG is sampled at 200 Hz). When the signal is decimated by a factor of ten, every tenth point of the original signal is kept, and the nine points in between are not used. In a time series of samples, every tenth point occurs at the same time as in the undecimated signal, except that there are no samples in between. In effect, decimating is similar to down-sampling. In other words, because the length of the IIBI signal is approximately the same length of the sampled ECG, which is acquired using a sampling frequency of 200 Hz, decimating the IIBI by a factor of ten, is similar to sampling the IIBI at 20 Hz. This can be done because the IIBI signal contains no

frequency components above 6 Hz.

Normally during heart rate variability studies a respiration signal is recorded simultaneously. To begin the analysis of the original respiration waveform, the data file is unpacked in DOS using the kunpack2 program. The ASCII file is then loaded into MATLAB and then decimated by a factor of ten since the samples of the respiration signal are already equidistant, 0.005 sec apart along the time axis. Therefore, there is no need for the interpolation procedure.

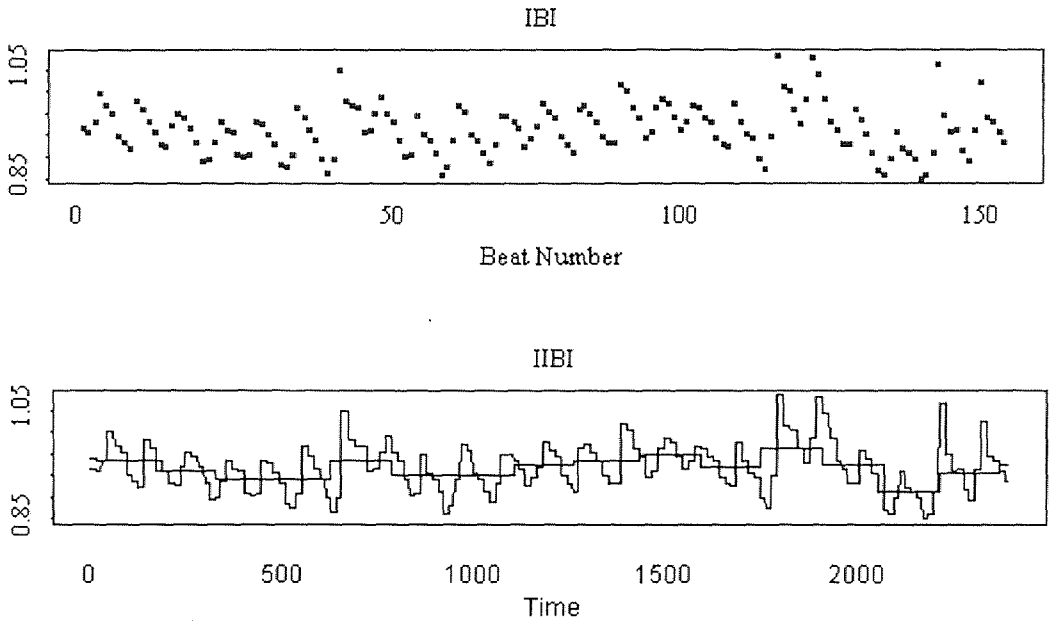

Figure 2.7 IBI signal and IIBI signal

2.6.3 Time Frequency Analysis

One of the drawbacks of the spectral analysis of heart rate variability is that it cannot track rapid changes in heart rate variability over time. The algorithms described in the

previous section were traditionally used to obtain the power spectrum on lengths of data on the order of minutes, so an average level of autonomic activity was represented. Often the level of autonomic activity can change in as rapidly as ten to fifteen seconds.

Time frequency analysis was performed on the entire IIBI and respiration files of using a series of the classical kernels that fall under the general class of bilinear distributions. Each distribution, as will be described in chapter 3, has unique characteristics which affect the processing and interpretability of the signals involved. The vagal tone and the sympatho-vagal balance were the physiological measures assessed from the resulting 3-D time-dependent spectra by quantifying the area under the low frequency and high frequency range for each instant of time. Adaptive filter processing was also used as an indicator for the high frequency range extraction of parasympathetic activity, as will be discussed in chapter 4.

CHAPTER 3

TIME-FREQUENCY REPRESENTATIONS

3.1 Categorization of Time-Frequency Distributions

3.1.1 Linear Time-Frequency Distribution

All linear time-frequency distributions (TFDs) satisfy the superposition or linearity principle which states that if $x(t)$ is a linear combination of some signal components, then the TFD of $x(t)$ is the same linear combination of the TFDs of each of the signal components[44].

$$x(t) = c_1 x_1(t) + c_2 x_2(t) \Rightarrow \rho_x(t,f) = c_1 \rho_{x1}(t,f) + c_2 \rho_{x2}(t,f) \qquad (3.1)$$

where $\rho_x(t,f)$, $\rho_{x1}(t,f)$, $\rho_{x2}(t,f)$ are time-frequency distributions of $x(t)$, $x_1(t)$ $x_2(t)$ respectively and c_1 , c_2 are constant coefficients.

Linearity is a desirable property in any application involving multicomponent signals because there already exist powerful analysis techniques for signals with such a property. One linear TFD of basic importance is the short-time Fourier transform. The basic idea is that by suitably pre-windowing the signal $x(t)$, we can obtain the time localization of its frequency components.

3.1.2 Quadratic Time-Frequency Distribution

Although linearity of the TFD is a desirable property, the quadratic(bilinear) structure of a TFD is an intuitively reasonable assumption when we want to translate a TFD as a time-

frequency energy distribution, since energy is a quadratic signal representation. All quadratic TFD satisfies the quadratic superposition principle which is defined as[44]

$$x(t) = c_1 x_1(t) + c_2 x_2(t) \Rightarrow \tag{3.2}$$

$$\rho_x(t,f) = |c_1|^2 \rho_{x1}(t,f) + |c_2|^2 \rho_{x2}(t,f) + c_1 c_2 \rho_{x1,x2}(t,f) + c_2 c_1 \rho_{x2,x1}(t,f) \tag{3.3}$$

where $\rho_x(t,f)$, $\rho_{x1}(t,f)$ and $\rho_{x2}(t,f)$ are the auto-time-frequency distributions, and $\rho_{x1,x2}(t,f)$ and $\rho_{x2,x1}(t,f)$ are the cross-time-frequency distributions of $x(t)$, $x_1(t)$, $x_2(t)$ respectively. c_1, c_2 are constant coefficients. Thus, for an n-component signal $x(t)$ the TFD $\rho_x(t,f)$ will comprise n signal terms and $\binom{n}{2} = n(n-1)/2$ cross terms[44], a fact that makes the visual analysis of the TFD of multicomponent signals difficult.

Among all the bilinear TFD with energetic interpretation, The Wigner distribution (WD) is the most widely studied and applied since it satisfies a large number of desirable mathematical properties.

3.1.3 Analytic Signal

In practical cases, the signals to be analyzed are real. An analytic signal $z(t)$ is a complex-valued signal whose spectrum is single-sided ($Z(f) \neq 0$ for $f > 0$ or $f < 0$). Because of this property of its spectrum, the imaginary part of an analytic signal is the Hilbert transform of the real part.

The Hilbert transform is defined as[46]:

$$\tilde{x}(t)=\frac{1}{\pi}\int_{-\infty}^{\infty}\frac{x(\lambda)}{t-\lambda}d\lambda \tag{3.4}$$

where $\tilde{x}(t)$ is the Hilbert transform of the signal $x(t)$.

Thus, to generate an analytic signal from a given signal $S_{original}(t)$, one should take the Hilbert transform of $S_{original}(t)$ which would become the imaginary part of analytic signal.

$$S_{\mathrm{Im}}(t)=\frac{1}{\pi}\int_{0}^{\infty}\frac{S_{original}(\lambda)}{t-\lambda}d\lambda \tag{3.5}$$

Note, the lower limit of the integral is zero , because $S_{original}(t)$ is a physical signal and is valid for the time interval $[0,\infty)$. Define $S_{\mathrm{Re}}(t)=S_{original}(t)$,

Then;

$$z(t)=S_{\mathrm{Re}}(t)+jS_{\mathrm{Im}}(t) \tag{3.6}$$

where $z(t)$is an analytic signal.

There are two basic reasons for using the analytic signal in calculating a joint time-frequency distribution:

First, the analytic signal does not have negative frequencies and therefore can not cause interference terms with positive frequencies; although it does not eliminate the interference of the positive frequencies with other positive frequencies. There will always be interference terms, no matter what part of the signal is eliminated, since that is an inherent property of bilinear distributions.

Second, consider a real signal $s(t)$. Its energy density spectrum, $|S(f)|^2$ is always

symmetric about the origin. This is illustrated in Figure 3.1 . Note, the average frequency will always become zero which is not what we want because it does not give us a sense of what is really going on with the signal. Also we want to obtain a value for average frequency which is roughly centered in the middle of the right hand bump. To achieve that, we have to neglect the left bump in the averaging. This is illustrated as follows:

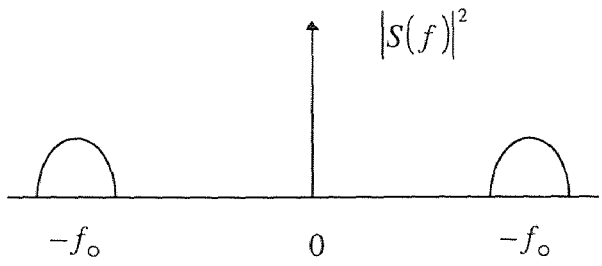

Figure 3.1 Energy density spectrum

Take the spectrum of the real signal $s(t)$

$$S(f) = \int_{-\infty}^{\infty} s(t) e^{-j2\pi ft} \cdot dt \tag{3.7}$$

Delete the negative part of the spectrum $S(f)$ such that;

$$S(f) \neq 0 \quad \text{for} \quad f > 0 \text{ and } S(f) = 0 \quad \text{for} \quad f < 0 \tag{3.8}$$

Take the inverse Fourier transform of the positive part of $S(f)$ to form the new complex signal $z(t)$. It turns out that the real part of signal $z(t)$ is the real signal $s(t)$ and the imaginary part is the Hilbert transform of $s(t)$ which is the definition of an analytic signal. Thus, to calculate the instantaneous frequency, the analytic signal should be used.

3.1.4 General Class of Time-Frequency Distributions

Most popular time-frequency representations can be expressed in terms of the general bilinear time-frequency distribution representations proposed by Dr. Leon Cohen. This allows one to generate all time-frequency distributions via a simple procedure. The mathematical formulation for the general class is[22];

$$\rho_z(t,f) = \iiint_{\infty} e^{j2\pi v(u-t)} g(v,\tau) z\left(u+\frac{\tau}{2}\right) z^*\left(u-\frac{\tau}{2}\right) e^{-j2\pi f\tau}\, dv\,du\,d\tau \qquad (3.9)$$

The $g(v,\tau)$ is an arbitrary function called the kernel and it determines the characteristics of the time-frequency distribution. Note that z is an analytic signal and z^* is the complex conjugate of z. If the integration with respect to v is performed, then equation (3.9) becomes:

$$\rho_z(t,f) = \iint_{\infty} G(t,\tau) z\left(u+\frac{\tau}{2}\right) z^*\left(u-\frac{\tau}{2}\right) e^{-j2\pi f\tau}\, du\,d\tau \qquad (3.10)$$

and the discrete time equivalent of equation (3.10) is:

$$\rho_z(n,k) = \sum_{m=-M}^{M} \sum_{p=-M}^{M} G(p,m) z(n+p+m) z^*(n+p-m) e^{-j4\pi mk/N} \qquad (3.11)$$

The advantage to using the discrete equation is that once the desirable kernel is chosen the distribution is fixed. The kernels which generate some of the most common distributions are listed in table 3.1.

3.1.5 Kernel Function

The kernel is particularly useful to study time-frequency distributions. They are easily generated, and the properties of the distribution can be observed by examining the kernel.

Table 3.1 Common distributions and their kernels
(from Cohen,L., *Introduction: A Primer on Time-Frequency Analysis*, edited by Boashash,B., *Time-Frequency Analysis Methods and Applications*, 1992).

Name	Kernel: $g(\nu,\tau)$	Distribution: $\rho(t,f)$
Wigner	1	$\int e^{-2j\pi\nu\tau} s^*\left(t-\tau/2\right)s\left(t+\tau/2\right)d\tau$
Wigner (windowed)	$h(\tau)$	$\int e^{-2j\pi\nu\tau} h(\tau)s^*\left(t-\tau/2\right)s\left(t+\tau/2\right)d\tau$
Margenau-Hill	$\cos(\pi\nu\tau)$	Real $s(t)S^*(f)e^{-2j\pi\nu t}$
Choi-Williams	$e^{-\nu^2\tau^2/\sigma}$	$\iint\sqrt{\frac{\pi\sigma}{\tau^2}}e^{-\pi^2\sigma(u-t)^2/\tau^2-j2\pi\nu t}$ $s^*\left(u-\frac{\tau}{2}\right)s\left(u+\frac{\tau}{2}\right)dud\tau$
Spectrogram	$\int h^*\left(u-\frac{\tau}{2}\right)e^{-2j\pi\nu u}$ $h\left(u+\frac{\tau}{2}\right)du$	$\left\lvert\int e^{-j2\pi ft}s(\tau)h(\tau-t)d\tau\right\rvert^2$
Zhao-Atlas-Marks	$g_1(\tau)\frac{\sin(2\pi\nu\lvert\tau\rvert/a)}{\pi\nu}$	$\int g_1(\tau)e^{-j2\pi\nu t}\int_{t-\lvert\tau\rvert/a}^{t+\lvert\tau\rvert/a}$ $s^*\left(u-\frac{\tau}{2}\right)s\left(u+\frac{\tau}{2}\right)dud\tau$

Also, when a new distribution is considered, its properties can readily be ascertained by examining its kernel. The kernel $g(\nu,\tau)$ can depend on time, frequency and the signal; however, we will consider the kernels which do not depend on the signal. The kernel

$g(\nu,\tau)$ is a function of ν and τ only. where ν,τ are the time and lag index respectively. The following is a list relating the properties of the distribution to the desirable properties of their kernels.

3.1.5.1 Properties

Nonnegativity:

A distribution should be positive for all values of time and frequency because it indicates how much of the total energy is in a particular time-frequency cell. However, most distributions contain negative as well as positive values. The positive part very often contains a time-frequency structure consistent with what we expect. The meaning of the negative regions is not yet completely understood. Sometimes the nonnegativity and cross terms are closely related, since the cross terms in the time-frequency domain are, in general, fluctuating and produce a plethora of negativity. In many cases, suppression of cross terms accompanies reduction of magnitude of negative values.

Realness:

The bilinear distributions are in general not positive definite, which implies that they are not strictly proper joint density functions. It has been argued that at least the kernel should be real[47]. That is for a given TFD $\rho_z(t,f)$;

$$\rho_z(t,f) = \iiint_{\infty} e^{j2\pi\nu(u-t)} g(\nu,\tau) z\left(u+\frac{\tau}{2}\right) z^*\left(u-\frac{\tau}{2}\right) e^{-j2\pi f\tau} d\nu du d\tau \qquad (3.12)$$

Take the complex conjugate;

$$\rho^{*}{}_{z}(t,f)=\iiint_{\infty} e^{-j2\pi v(u-t)}g^{*}(v,\tau)z^{*}\left(u+\frac{\tau}{2}\right)z\left(u-\frac{\tau}{2}\right)e^{j2\pi f\tau}\,dvdud\tau \qquad (3.13)$$

Let $$v\rightarrow -v \quad \text{and} \quad \tau\rightarrow -\tau \qquad (3.14)$$

We have;

$$\rho^{*}{}_{z}(t,f)=\iiint_{\infty} e^{j2\pi v(u-t)}g^{*}(-v,-\tau)z^{*}\left(u-\frac{\tau}{2}\right)z\left(u+\frac{\tau}{2}\right)e^{-j2\pi f\tau}\,dvdud\tau \qquad (3.15)$$

Therefore to assure that;

$$\rho_{z}(t,f)=\rho_{z}{}^{*}(t,f) \qquad (3.16)$$

the kernel should satisfy;

$$g(v,\tau)=g^{*}(-v,-\tau) \qquad (3.17)$$

Time and Frequency Shifts:

A desirable property is that if we translate the signal by amount t_0, we expect the whole distribution to be translated by the same amount. Similarly, if we shift the spectrum by a fixed frequency f_0, then the distribution should be shifted by an equivalent amount. That is if $z(t), s(t), \rho_z(t,f)$ and $\rho_s(t,f)$ are signal, shifted signal, distribution of signal and distribution of shifted signal respectively then;

$$s(t)=z(t-t_0)\Rightarrow \rho_s(t,f)=\rho_z(t-t_0,f) \qquad (3.18)$$

Similarly;

$$s(t)=z(t)\cdot e^{j2\pi f_0 t}\Rightarrow \rho_s(t,f)=\rho_z(t,f-f_0) \qquad (3.19)$$

The constraint for this property implies that the kernel should be independent of time and frequency.

Time and Frequency Marginals:

Another desirable property is that for a given time if we added up the bits of energy at different frequencies we will get the total energy $|z(t)|^2$ at that instant of time. Also if for a given frequency we add all the time pieces we should get the total energy at that frequency, $|Z(f)^2|$. That is if $z(t), \rho_z(t,f)$ are signal and distribution of signal respectively then;

$$\int \rho_z(t,f)df = z(t)\cdot z^*(t) = |z(t)|^2 \tag{3.20}$$

Similarly;

$$\int \rho_z(t,f)dt = Z(f)Z^*(f) = |Z(f)^2| \tag{3.21}$$

Let us integrate the left hand side of equation (3.20)

$$\int_{\infty} \rho_z(t,f)\cdot df = \int_{\infty}\iiint_{\infty} e^{j2\pi v(u-t)} g(v,\tau) z\left(u+\frac{\tau}{2}\right) z^*\left(u-\frac{\tau}{2}\right) e^{-j2\pi f\tau} dvdud\tau df \tag{3.22}$$

Using the definition of the Fourier transform we can write;

$$\int_{\infty} e^{-2j\pi f\tau} df = \delta(\tau) \tag{3.23}$$

Hence

$$\int_{\infty} \rho_z(t,f)\cdot df = \iiint_{\infty} \delta(\tau) e^{j2\pi v(u-t)} g(v,\tau) z\left(u+\frac{\tau}{2}\right) z^*\left(u-\frac{\tau}{2}\right) dvdud\tau \tag{3.24}$$

$$\int_{\infty} \rho_z(t,f)\cdot df = \iint_{\infty} e^{j2\pi v(u-t)} g(v,0)|z(u)|^2 dvdu \tag{3.25}$$

The only way equation (3.25) can be made equal to $|z(t)|^2$ is to take

$$\int_{\infty} e^{j2\pi\nu(u-t)} g(\nu,0) d\nu = \delta(t-u) \tag{3.26}$$

which forces;

$$g(\nu,0) = 1 \tag{3.27}$$

Similarly, we can show the condition on the kernel to satisfy the frequency marginal is

$$g(0,\tau) = 1 \tag{3.28}$$

Instantaneous Frequency:

If we fix time and ask for the expected value of frequency for that time, we obtain the first mean conditional frequency, given by:

$$\langle f \rangle_t = \frac{1}{\rho(t)} \int_{-\infty}^{\infty} f \cdot \rho(t,f) df \tag{3.29}$$

where $\rho(t)$ is the marginal in time

$$\rho(t) = \int_{-\infty}^{\infty} \rho(t,f) df \tag{3.30}$$

If the signal is analytic, the first moment of frequency for a given time is the instantaneous frequency because instantaneous frequency is defined in terms of the analytic signal. The instantaneous frequency is given in terms of the TFD:

$$\frac{\int f \cdot \rho_z(t,f) df}{\int \rho_z(t,f) df} = f_i(t) \tag{3.31}$$

where $f_i(t)$ is the instantaneous frequency. Constraint for the kernel is:

$$g(\nu,0) = 1 \quad \text{and} \quad \left. \frac{\partial g(\nu,\tau)}{\partial \tau} \right|_{\tau=0} = 0 \tag{3.32}$$

Group Delay:

From the point of view of joint time-frequency distributions we may think of the group delay as the mean time at a given frequency. Therefore everything we said for the expectation value of frequency at a given time allows us to write down the corresponding results for the expected value of time at a given frequency. That is

$$\frac{\int t \cdot \rho_z(t,f)dt}{\int \rho_z(t,f)dt} = \tau_g(f) \tag{3.33}$$

and the constraint for the kernel should be:

$$g(0,\tau) = 1 \text{ and } \left.\frac{\partial \cdot g(\nu,\tau)}{\partial \nu}\right|_{\nu=0} = 0 \tag{3.34}$$

Time and Frequency Support:

For a finite duration signal the distribution should be zero before the signal starts and zero after the signal ends which is known as weak finite support. But it would be much better if the distribution was zero whenever the signal was zero or strong finite support[1]. We can apply the same concept to the frequency axis. That is, if the signal has a spectrum that ranges between two frequencies f_1 and f_2 and is zero otherwise, than the distribution should be zero for frequencies smaller then f_1 and for frequencies greater than f_2 . This is summarized as follows; For the time axis:

$$z(t) = 0 \text{ for } |t| > t_c \Rightarrow \rho_z(t,f) = 0 \text{ for } |t| > t_c \tag{3.35}$$

and on the frequency axis

$$Z(f) = 0 \text{ for } |f| > f_c \Rightarrow \rho_z(t,f) = 0 \text{ for } |f| > f_c \tag{3.36}$$

and the associated kernel requirements should be respectively:

$$\psi(t,\tau) \equiv \int g(\nu,\tau) e^{-j2\pi\nu t} d\nu = 0 \quad \text{for} \quad |\tau| < 2|t| \tag{3.37}$$

$$\int g(\nu,\tau) e^{-j2\pi f t} d\tau = 0 \quad \text{for} \quad |\nu| < 2|f| \tag{3.38}$$

Reduced Interference:

The distribution should not contain cross terms between frequency components. For a multicomponent signal, the spectrum of each signal should be clearly seen without interference. The constraint for the kernel is that $g(\nu,\tau)$ be a 2-D low pass filter type. The summery of above properties and associated kernel requirements are presented in table 3.2.

3.1.6 Ambiguity Function Relationship

Let $R_z(t,\tau)$ be the instantaneous autocorrelation of a complex signal $z(t)$, defined as:

$$R_z(t,\tau) = z\left(t+\frac{\tau}{2}\right) z^*\left(t-\frac{\tau}{2}\right) \tag{3.39}$$

Then the symmetrical ambiguity function (AF) is defined as the inverse Fourier transform of $R_z(t,\tau)$ with respect to t.

$$A_z(\nu,\tau) = F_t^{-1}\left[R_z(t,\tau)\right] \tag{3.40}$$

This relationship may be combined with equation (3.9) to show that $\rho_z(t,f)$ may be found by:

$$\rho_z(t,f) = \iint A_z(\nu,\tau) \cdot g(\nu,\tau) \cdot e^{-j2\pi(\nu t + f\tau)} \cdot d\nu \cdot d\tau \tag{3.41}$$

Table 3.2 Distribution properties and associated kernel requirements (from Williams,W., Jeong,J., *Reduced Interference Time-Frequency Distributions*, edited by Boashash,B., *Time-Frequency Analysis Methods and Applications*, 1992)

Properties	Mathematical Description	Kernel Requirements
P0. Nonnegativity	$\rho_z(t,f) \geq 0 \forall t,f$	$g(\nu,\tau)$ is the AF of some $w(t)$
P1. Realness	$\rho_z(t,f) \in R$	$g(\nu,\tau) = g^*(-\nu,-\tau)$
P2. Time Shift	$s(t) = z(t-t_0) \Rightarrow$ $\rho_z(t,f) = \rho_z(t-t_0,f)$	$g(\nu,\tau)$ does not depend on t
P3. Frequency Shift	$s(t) = z(t)\cdot e^{j2\pi f_0 t} \Rightarrow$ $\rho_s(t,f) = \rho_z(t,f-f_0)$	$g(\nu,\tau)$ does not depend on f
P4. Time Marginal	$\int \rho_z(t,f)df = z(t)\cdot z^*(t) = \lvert z(t)\rvert^2$	$g(\nu,0) = 1$
P5. Frequency Marginal	$\int \rho_z(t,f)dt = Z(f)Z^*(f) = \lvert Z(f)^2\rvert$	$g(0,\tau) = 1$
P6. Instantaneous Frequency	$\frac{\int f\cdot \rho_z(t,f)df}{\int \rho_z(t,f)df} = f_i(t)$	$g(\nu,0) = 1$ and $\left.\frac{\partial g(\nu,\tau)}{\partial \tau}\right\rvert_{\tau=0} = 0$
P7. Group delay	$\frac{\int t\cdot \rho_z(t,f)dt}{\int \rho_z(t,f)dt} = \tau_g(f)$	$g(0,\tau) = 1$ and $\left.\frac{\partial \cdot g(\nu,\tau)}{\partial \nu}\right\rvert_{\nu=0} = 0$
P8. Time Support	$z(t) = 0$ for $\lvert t\rvert > t_c \Rightarrow$ $\rho_z(t,f) = 0$ for $\lvert t\rvert > t_c$	$\int g(\nu,\tau)e^{-j2\pi\nu t}d\nu = 0$ for $\lvert\tau\rvert < 2\lvert t\rvert$
P9. Frequency Support	$Z(f) = 0$ for $\lvert f\rvert > f_c \Rightarrow$ $\rho_z(t,f) = 0$ for $\lvert f\rvert > f_c$	$\int g(\nu,\tau)e^{-j2\pi f t}d\tau = 0$ for $\lvert\nu\rvert < 2\lvert f\rvert$
P10. Reduced Interference	$\rho_{z1*z2}(t,f) = \rho_{z2*z1}(t,f) = 0$	$\rho_z(\nu,\tau)$ is a 2-D low pass filter type

Thus, any member of Cohen's class of distributions may be found by first multiplying the kernel, $g(\nu,\tau)$, by the symmetric ambiguity function and then carrying out the double Fourier transform[22]. The generalized ambiguity function, $g(\nu,\tau)A(\nu,\tau)$ is a key concept which helps one in clearly seeing the effect of the kernel in determining $\rho_z(t,f)$.

We illustrate this concept in Figure 3.2[22], where the ambiguity function of two sine wave signals is given. The auto terms of the two signals are placed near the center of Figure 3.2 and the cross-terms are placed in the upper right and lower left corner. Thus, to determine a desirable distribution, the kernel function should emphasize the auto terms near the center and de-emphasize the cross terms in the corners.

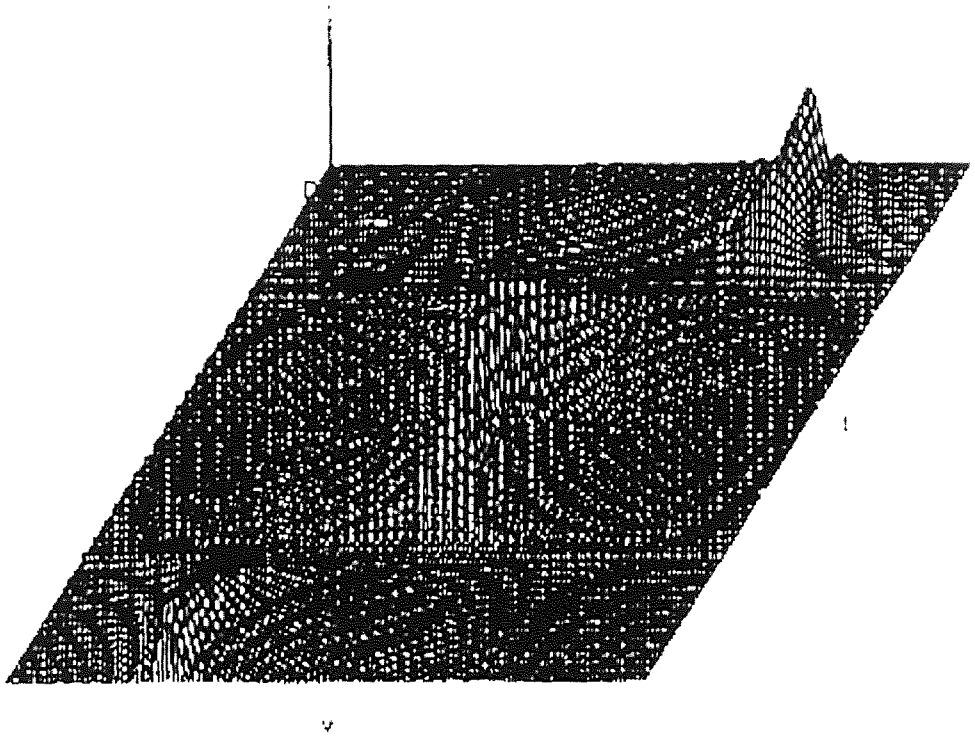

Figure 3.2 Ambiguity function of two sine wave signals
(from Williams,W., and Jeong,J., *Reduced Interference Time-Frequency Distributions*, edited by Boashash,B., *Time-Frequency Analysis Methods and Applications*, 1992).

3.2 Comparison of Time-Frequency Distributions

3.2.1 Short Time Fourier Transform

The short time Fourier transform was the first tool devised for analyzing a signal in the time-frequency domain[47]. This is done by extracting a small piece of the signal and taking its Fourier transform, and by continuing this process we show the existing frequency components at each instant of time. We can present this idea mathematically by first designing a window function, $h(\tau - t)$which will emphasize the times around the fixed time of interest t. We then multiply the signal with the window function and take its Fourier transform:

$$S_t(f) = \int_{t-\Delta}^{t+\Delta} s(\tau)h(\tau - t)e^{-j2\pi f\tau}\,d\tau \tag{3.42}$$

As this process is continued for each particular time ,we obtain a different spectrum. The totality of these spectra makes a time-frequency distribution. The energy density of the signal at the fixed time t is

$$\rho_{sp}(t,f) = \left|\int_{t-\Delta}^{t+\Delta} s(\tau)h(\tau - t)e^{-j2\pi f\tau}\,d\tau\right|^2 \tag{3.43}$$

where $\rho_{sp}(t,f)$is called the spectrogram. The spectrogram can be also written in terms of the Fourier transforms of the signal and window function.

$$\rho_{sp}(t,f) = \left|\int_{f-\Delta}^{f+\Delta} S(f')H(f - f')e^{-j2\pi f't}\,df'\right|^2 \tag{3.44}$$

where $H(f)$, $S(f)$are Fourier transforms of the signal and window function respectively. Note, equation (3.44) can be used to study the behavior of the signal around the fixed frequency of interest f. The spectrogram should not be thought of as a different

distribution because it is a member of a general class of distributions[21].

How large should the window be?, or , How should we weigh each piece of the signal? To answer these questions we need to understand the time-bandwidth relation, or the uncertainty principle.

Let us define the duration of a signal $s(t)$ by Δt ;

$$(\Delta t)^2 = \int (t-\bar{t})^2 |s(t)|^2 dt \tag{3.45}$$

where $\bar{t}$ is mean time and is defined as;

$$\bar{t} = \int t |s(t)|^2 dt \tag{3.46}$$

Let us also define the bandwidth of the signal $S(f)$ in the frequency domain by Δf ;

$$(\Delta f)^2 = \int (f-\bar{f})^2 |S(f)|^2 df \tag{3.47}$$

where $\bar{f}$ is mean frequency and is defined as;

$$\bar{f} = \int f |S(f)|^2 df \tag{3.48}$$

The time bandwidth relation is;

$$\Delta t \cdot \Delta f \geq \frac{1}{4\pi} \tag{3.49}$$

The physical interpretation of time bandwidth is that the duration and bandwidth can not be both made narrow because $|s(t)|^2$ and $|S(f)|^2$ can not be changed independently[46]. The advantage of the short-time Fourier transform is that it has an easily understandable interpretation and is positive every where. This is a desirable property when we want to interpret the spectrogram as the signal energy distribution in the time-frequency plane.

One of the shortcomings of the short-time Fourier transform is the trade off

between time and frequency resolution. Consider two extreme choices of the analysis window $h(t)$. The first case is that of perfect time resolution, that is, if the analysis window $h(t)$ is a Dirac impulse,

$$h(t) = \delta(t) \Rightarrow \rho_{STFT}(t,f) = s(t)e^{-2j\pi ft} \tag{3.50}$$

where $s(t)$, $\rho_{STFT}(t,f)$ are the signal and short time Fourier transform of the signal respectively. In this case, the short time Fourier transform essentially reduces to the signal $s(t)$, preserving all time variations of the signal but not providing any frequency resolution. The second case is that of perfect frequency resolution obtained with the all-constant window $h(t) = 1$, then;

$$H(f) = \delta(f) \Rightarrow \rho_{STFT}(t,f) = S(f) \tag{3.51}$$

where $H(f)$, $S(f)$ are Fourier transform of window and signal respectively. Here the short time Fourier transform reduces to the Fourier transform and does not provide any time resolution. Therefore, because of the uncertainty principle, both $h(t)$ and $H(f)$ can not be made arbitrarily narrow.

Another shortcoming of the spectrogram is that it does not satisfy time and frequency marginal properties at the same instant. If we write the signal $s(t)$ and window $h(t)$ in terms of their amplitudes and their phase;

$$s(t) = A(t)e^{j\vartheta(t)} \text{ and } h(t) = A_h(t)e^{j\vartheta_h(t)} \tag{3.52}$$

and similarly for their Fourier transforms

$$S(f) = B(f)e^{j\varphi(f)} \text{ and } H(f) = B(f)e^{j\varphi_H(f)} \tag{3.53}$$

Then the marginals are;

$$\int \rho_{STFT}(t,f)df = \int A^2(t')A_h{}^2(t'-t)dt' \tag{3.54}$$

$$\int \rho_{STFT}(t,f)dt = \int B^2(f')B_H{}^2(f-f')df' \tag{3.55}$$

These do not equal the instantaneous energy or energy density spectrum, namely $A^2(t)$ and $B^2(f)$ [21]. But they do approach them as we narrow the window in the respective domains. However window $h(t)$ and $H(f)$ can not be narrowed concurrently.

The short time Fourier transform is a linear signal decomposition, and there are no cross terms between signal components. However, the spectrogram is also a bilinear signal energy distribution due to the magnitude squaring operation. Thus, the spectrogram has cross terms that are not noticeable because they are inherently filtered out by a low-pass filter defined by the ambiguity function of the window[47].

3.2.2 Wigner Distribution

Among all the bilinear TFD, The Wigner distribution (WD) is the most studied and applied [23]. The Wigner distribution can be obtained from the general class equation (3.9) by taking $g(\nu,\tau)=1$:

$$\rho_w(t,f) = \int_{-\infty}^{\infty} z\left(t-\frac{\tau}{2}\right)z^*\left(t+\frac{\tau}{2}\right)e^{-2j\pi f\tau}d\tau \tag{3.56}$$

where $\rho_w(t,f)$, $z(t)$ and $z^*(t)$ are the Wigner distribution, an analytic signal and the complex conjugate of the analytic signal respectively. From equation (3.56) we see that for each particular time we are adding up pieces made from the product of the signal at a

past time multiplied by the signal at an equal future time. The Wigner distribution satisfies many properties, which are described as follows:

The WD is a real valued function that is;

$$\rho_w(t,f) = \rho_w^*(t,f) \tag{3.57}$$

Since the kernel of the WD is one for any value of ν and τ, then the complex conjugate of the kernel is always one. That is;

$$g(\nu,\tau) = g^*(-\nu,-\tau) = 1 \tag{3.58}$$

This is the constraint of the kernel for the distribution to be real from section 3.1.5.1 .

The WD satisfies the time and frequency shift properties as long as the kernel of the WD is not a function of time and frequency that is;

$$s(t) = z(t-t_0) \Rightarrow \rho_s(t,f) = \rho_z(t-t_0,f) \tag{3.59}$$

$$s(t) = z(t)\cdot e^{j2\pi f_0 t} \Rightarrow \rho_s(t,f) = \rho_z(t,f-f_0) \tag{3.60}$$

where $z(t), s(t), \rho_z(t,f)$ and $\rho_s(t,f)$ are the signal, the shifted signal, the distribution of signal and the distribution of the shifted signal respectively. To prove this property one should take the kernel of the WD independent of time and frequency and set it equal to one, that is:

$$g(\nu,\tau) = 1 \text{ where } \nu \notin R_{time} \text{ and } \tau \notin R_{frequency} \tag{3.61}$$

Let $\rho_z(t,f), \rho_s(t,f)$ represent the WD of the signal $z(t)$ and the shifted signal $s(t)$, then

$$\rho_s(t,f) = \int_{-\infty}^{\infty} z\left(t-\frac{\tau}{2}-t_o\right) z^*\left(t+\frac{\tau}{2}-t_o\right) e^{-2j\pi f\tau} d\tau \tag{3.62}$$

and

$$\rho_s(t,f)=\int_{-\infty}^{\infty} z\left(t-\frac{\tau}{2}\right)z^*\left(t+\frac{\tau}{2}\right)e^{-2j\pi f(\tau-t_o)}d\tau=\rho_z(t-t_o,f) \qquad (3.63)$$

To prove the frequency shifting one can use a similar argument.

The WD is uniquely related to the signal up to a constant phase factor[21]. To understand this idea, take the inverse Fourier transform of equation 3.56 with respect to f,

$$z\left(t-\frac{\tau}{2}\right)z^*\left(t+\frac{\tau}{2}\right)=\int \rho_w(t,f)e^{2j\pi f\tau}df \qquad (3.64)$$

Then, let :

$$t+\frac{\tau}{2}\rightarrow t' \;;\; t-\frac{\tau}{2}\rightarrow t \quad \text{and} \quad \tau\rightarrow t-t'$$

which gives;

$$z(t)z^*(t')=\int \rho_w\left(\frac{1}{2}(t'+t),f\right)e^{2j\pi(t-t')f}df \qquad (3.65)$$

Taking a particular value for $t'=0$ and dividing both sides by $z^*(t')$, we obtain;

$$z(t)=\frac{1}{z^*(0)}\int \rho_w\left(\frac{1}{2}t,f\right)e^{j2\pi tf}df \qquad (3.66)$$

One can therefore recover the original signal from the Wigner distribution for a given resolution. The preceding relation can be used to determine whether a signal exists which will generate a given $\rho_w(t,f)$.

The Wigner distribution also satisfies the marginals properties. To prove these, one can use the constraint of the kernel for marginals properties ,that is;

$$g(v,0)=1 \text{ and } g(0,\tau)=1 \qquad (3.67)$$

By inspection, the kernel of the Wigner distribution $g(\nu,\tau)=1$, satisfies both marginals. Thus, the Wigner distribution satisfies the total energy. Note the converse is not true[21]. For the first conditional moment at a fixed time, the Wigner distribution gives the instantaneous frequency and at a fixed frequency the first conditional moment would be the group delay.

For a finite duration signal the Wigner distribution is zero before the signal starts and after the signal ends[21]. If we have a band limited signal, the Wigner distribution will be zero for all frequencies that are not included in that band. These properties are called the support properties of the Wigner distribution. In general the Wigner distribution is not zero when the signal is zero[47].

Consider the multicomponent signal $z(t)$:

$$z(t)=z_1(t)+z_2(t) \tag{3.68}$$

The Wigner distribution is:

$$\rho_w(t,f)=\rho_{w_{11}}(t,f)+\rho_{w_{22}}(t,f)+\rho_{w_{12}}(t,f)+\rho_{w_{21}}(t,f) \tag{3.69}$$

where $\rho_w(t,f)$, $\rho_{w_{11}}(t,f)$ and $\rho_{w_{22}}(t,f)$ are the auto Wigner distributions of $z(t), z_1(t)$ and $z_2(t)$ respectively. The terms $\rho_{w_{12}}(t,f)$ and $\rho_{w_{21}}(t,f)$ are called the cross Wigner distributions. Therefore the Wigner distribution of the sum of the two signals is not the sum of their respective Wigner distributions. In general the Wigner distribution puts cross terms in between any two frequencies and any two times[21].

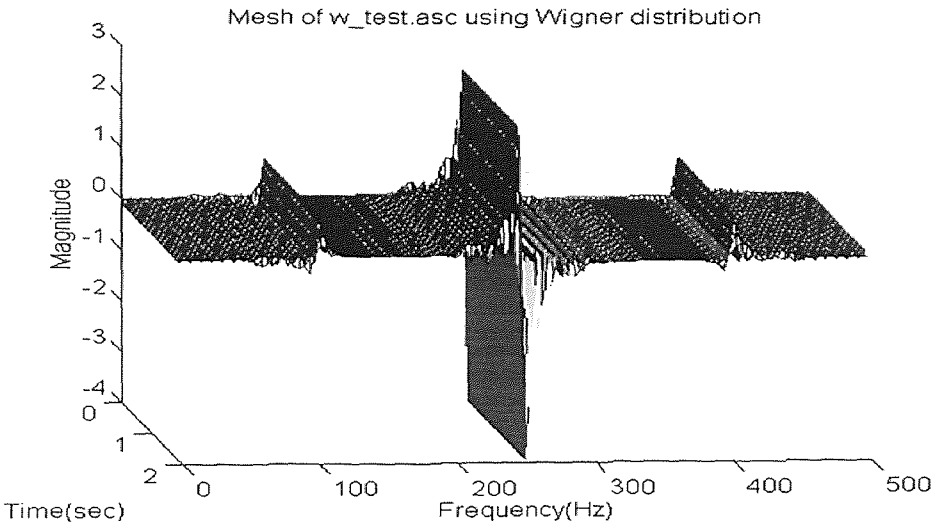

Figure 3.3 The Wigner distribution of the sum of two finite duration sine waves

Figure 3.3 presents the Wigner distribution of a signal which is the sum of two sine waves of one second duration with frequencies of 100 and 400 hertz. Note the cross term in the middle of the two frequencies at 250 hertz. This is the most important draw back of the Wigner distribution (WD).

Another draw back of the Wigner distribution is that it always has negative regions throughout the time-frequency plane, except in the case of the Gaussian signal where the amplitude is modulated[22].

3.2.2.1 Windowed Wigner Distribution

In practice one is forced to calculate the Wigner distribution using equation (3.70):

$$\rho_w = \int_{t-\Delta}^{t+\Delta} h(\tau) z\left(t-\frac{\tau}{2}\right) z^*\left(t+\frac{\tau}{2}\right) e^{-2j\pi f\tau}\, d\tau \qquad (3.70)$$

where $h(t)$ is a window function. This is due to the finite nature of the data. The resulting distribution has the effect of smoothing the Wigner distribution over frequency and is

called the Pseudo Wigner distribution (PWD)[46]. The PWD sometimes results in a better looking distribution in that certain cross terms are suppressed. One can clean the cross terms by smoothing the Pseudo Wigner distribution over time which is called the Smoothed Pseudo Wigner distribution (SPWD). Smoothing the Pseudo Wigner distribution is performed as follows:

$$\rho_{ws}(t,f) = \iint_{window(L)} L(t-t', f-f') \cdot \rho_w(t', f') dt' df' \tag{3.71}$$

where L, $\rho_{ws}(t,f)$ and $\rho_w(t,f)$ are smoothing function, the Smoothed Pseudo Wigner distribution and the Pseudo Wigner distribution respectively. The advantages of the Smoothed Pseudo Wigner distribution are that for certain types of smoothing, a positive distribution is obtained and the cross terms are suppressed. However smoothing destroys some of the desirable properties of the Wigner distribution: if L is taken to be independent of the signal, then the only way to obtain a positive distribution is by sacrificing the marginals properties[22].

3.2.3 The Exponential Distribution

A new approach was presented by Choi and Williams where they address the main draw back of the Wigner distribution (cross terms)[47]. In section 3.2.2.1 a method was described to remove the cross terms but this usually involves violating some of the desired properties like the marginals. Choi and Williams investigated using a generalized ambiguity function[47]. They chose an exponential kernel, that is;

$$g(\nu,\tau) = e^{-\nu^2\tau^2/\sigma} \tag{3.72}$$

Substituting equation (3.72) in equation (3.9) and integrating with respect to v one obtains;

$$\rho_{cw}(t,f)=\iint\sqrt{\frac{\pi\sigma}{\tau^2}}e^{-\pi^2\sigma(u-t)^2/\tau^2-j2\pi\tau f}z^*\left(u-\frac{\tau}{2}\right)z\left(u+\frac{\tau}{2}\right)dud\tau \qquad (3.73)$$

where $\rho_{cw}(t,f), z(t)$ and $z^*(t)$ are the Choi-Williams distribution, an analytical signal and complex conjugate of the analytical signal. The ability to suppress the cross terms comes by controlling σ .

In Figure 3.4, we illustrate three cases, where each contains two sine waves with frequencies of 100 and 400 hertz. The Choi Williams distribution was performed for the three cases but with different values for σ . Note, in case "a" we are taking σ to be 10000 which makes the kernel effectively one and we have the Wigner distribution. In case "b" and "c" we are taking σ to be 50 and 1, respectively which produces a kernel which is peaked near the origin in the v,τ plane and hence offers better cross term suppression.

Hence one can control the relative suppression of the cross terms by reducing the value of σ . The Choi Williams distribution satisfies many of the desirable properties, as described below:

The Choi Williams distribution is real. To prove this, one can replace the v,τ with $-v,-\tau$ respectively in to the kernel function and perform the manipulation;

$$g^*(-v,-\tau)=e^{-(-v)^2(-\tau)^2/\sigma}=e^{-v^2\tau^2/\sigma}=g(v,\tau) \qquad (3.74)$$

(a)

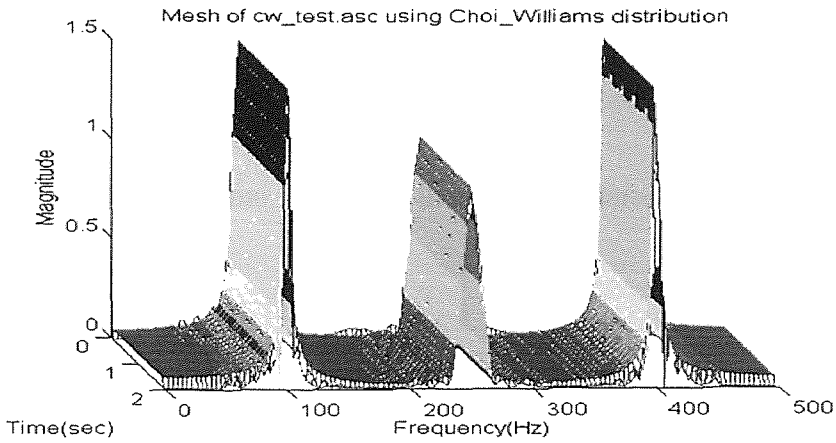

(b)

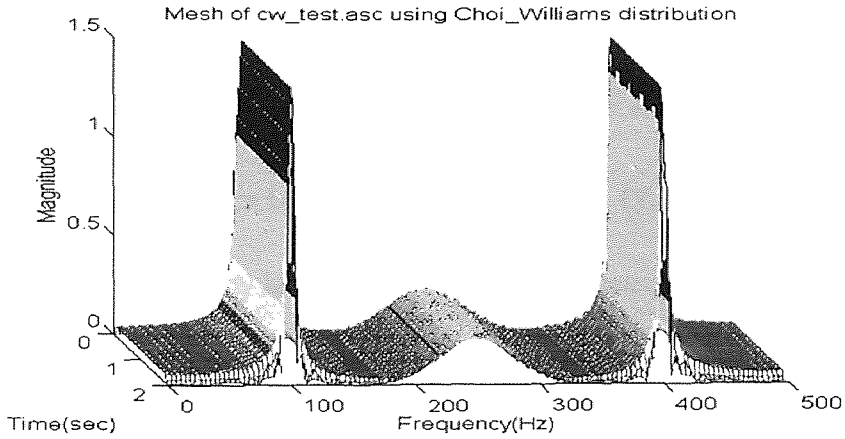

(c)

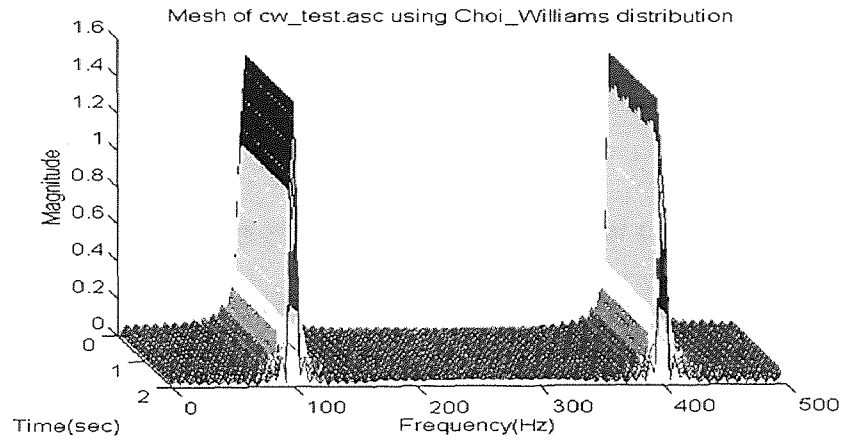

Figure 3.4 Performance of the Choi Williams distribution upon three cases with a) $\sigma = 1000$, b) $\sigma = 50$ and c) $\sigma = 1$

The Choi Williams distribution satisfies both the marginals properties, since;

$$g_{cw}(\nu,0) = e^{-0^2\tau^2/\sigma} = 1 \tag{3.75}$$

and similarly for the other marginal. Since the marginal properties are satisfied, the total energy property will be satisfied.

The Choi Williams distribution does not satisfies the finite support properties. To show this we introduce the following condition for determining whether a distribution is zero before a signal starts and after the signal ends. This work was done by Claasen and Mecklenbrauker[23] and is expressed as follows:

$$\int g(\nu,\tau)e^{-j\nu t}d\nu = 0 \quad \text{for} \quad |\tau| < 2|t| \tag{3.76}$$

Similarly, for the signal that is bandlimited in the region (f_1, f_2) the distribution should be zero for values of frequency less than f_1 and greater then f_2.

$$\int g(\nu,\tau)e^{-j2\pi f\tau}d\tau = 0 \quad \text{for} \quad |\nu| < 4\pi|f| \tag{3.77}$$

If we replace the kernel of the Choi Williams distribution in equation (3.76) and carry out the integration using a table of integrals[11], we obtain:

$$\int e^{-\nu^2\tau^2/\sigma} e^{-2j\nu t}d\nu = \frac{\sqrt{\pi}}{\sqrt{\tau^2/\sigma}} e^{-\frac{t^2}{4\tau^2/\sigma}} \tag{3.78}$$

Note, the right hand side of equation (3.78) is not equal to zero; therefore, The Choi Williams distribution does not satisfy the support properties.

3.2.4 Reduced Interference Distribution (RID)

Incorporating the idea of interference reduction in the Choi Williams distribution (P10 in

Table 3.2) with other desirable properties (P0-P9 in Table 3.2), a new class of time-frequency distributions, called reduced interference distributions, has been introduced [29]. While not satisfying P0, the RID does satisfy P1-P10 and provides high resolution in time and frequency. To meet the requirements for P1-P10, the RID kernel should be a cross shaped low pass filter, satisfying[29]

$$|g(\nu,\tau)| \ll 1 \quad \text{for} \quad |\nu\tau| > 0 \tag{3.79}$$

The following is the procedure to design a RID kernel[29].

Step 1: Design a primitive real valued function $h(t)$ that satisfies the following:

R1: $h(t)$ has unit area, i.e., $\int h(t)dt = 1$.

R2: $h(t)$ is a symmetrical function of time, i.e., $h(t) = h(-t)$.

R3: $h(t)$ is time limited on $\left[-1/2 \;, 1/2\right]$, i.e., $h(t) = 0 \quad for \quad |t| > 1/2$.

R4: $h(t)$ tapers smoothly towards both ends so that its frequency response has little high frequency content. That is, $|H(\nu)| << 1 \quad for \quad |\nu| >> 0$, where $H(\nu)$ is the Fourier transform of $h(t)$.

Step 2: Take the Fourier transform of $h(t)$, i.e., $H(\nu) = \int h(t)e^{-j\nu t}dt$.

Step 3: Replace ν by $\nu\tau$ in $H(\nu)$: $g(\nu,\tau) = H(\nu\tau)$.

Since $g(\nu,\tau)$ is a function of the product of ν and τ , R1 implies that the RID satisfies both marginals properties. That is:

$$g(\nu,0) = H(0) = \int h(t)e^{-\nu 0t}dt = \int h(t)\cdot 1 dt = 1 \tag{3.80}$$

Similarly one can show the RID satisfies the frequency marginal. Condition R2

produces a real $H(v)$, which in turn implies the realness (P2) of the RID. Condition R2 also implies the instantaneous frequency and group delay exists under the condition that $dH(v)/dv$ exists[48]. The RID satisfies the time and frequency shift properties since the kernel does not depend on time or frequency. R3 does imply the time and frequency support properties[47]. To prove it, one should take the Fourier transform of the kernel with respect to v and use the scaling property of the Fourier transform to carry out the integral. That is:

$$G(t,\tau)=\int g(v,\tau)e^{-jvt}dv=\frac{2\pi}{|\tau|}h\left(\frac{-t}{\tau}\right) \tag{3.81}$$

Based upon the kernel requirements in table 3.2, equation 3.76 has to equal zero in order to satisfy the time support. That is:

$$G(t,\tau)=\int g(v,\tau)e^{-jvt}dv=\frac{2\pi}{|\tau|}h\left(\frac{-t}{\tau}\right)=0 \quad if \quad |\tau|<2|t| \tag{3.82}$$

By symmetry, one can also show that the RID satisfies the frequency support. R4 plays the role of suppressing the interference. In most cases, the auto terms are located near the origin of the ambiguity domain, while the cross terms occur far away from the origin[29]. Therefore, a low pass filter type kernel imposed by R4 can effectively reduce interference while retaining the resolution of the auto terms. Using a primitive function $h(t)$ designed according to requirements R1-R4, the RID has the following integral expression.

$$\rho_{RID}(t,f)=\iint\frac{1}{|\tau|}h\left(\frac{u-t}{\tau}\right)z\left(u+\frac{\tau}{2}\right)z^{*}\left(u-\frac{\tau}{2}\right)e^{-2j\pi f\tau}du\,d\tau \tag{3.83}$$

where $\rho_{RID}(t,f)$, $z(u)$ and $z^*(u)$ are the reduced interference distribution (RID), an analytical signal and complex conjugate of the analytical signal. The requirements on $h(t)$ and their counterparts are shown in table 3.3.

Table 3.3 Requirements on $h(t)$ and their counterparts

R1. unit area: $\int h(t)dt = 1$	P4 , P5
R2. symmetrical: $h(-t) = h(t)$	P1 , P6 , P7
R3. time limited: $h(t) = 0 \quad \forall \lvert t \rvert > \frac{1}{2}$	P8 , P9
R4. low pass type: $\lvert H(v) \rvert << 0 \quad for \quad \lvert v \rvert >> 0$	P10
Note: In this kernel design procedure, P2 and P3 are always satisfied, while P0 is not satisfied.	

The RID is not dedicated to a certain type of signal. The idea underlying the RID is to develop TFDs that satisfy many desirable properties. One can find signals that will not be effectively handled by the RID; for example, a chirp. Since the RID has a cross shaped kernel in the ambiguity domain, if the ambiguity function of the chirp falls on a 45° diagonal line, then it will not intersect well with the RID kernel, resulting in low time and frequency resolution[29]..

One example of a RID distribution where $h(t) = \prod(t) = \prod_{-1/2}^{1/2} 1$ corresponds to the Born-Jordan distribution. It satisfies all of R1-R4, and properties P1-P10 are also satisfied. Since $h(t)$ is flat on $\left[\frac{-1}{2}, \frac{1}{2}\right]$, the resultant $H(v\tau)$ has a very narrow

bandwidth. Hence, the Born- Jordan kernel provides very good interference at the expense of autoterm resolution[29].

3.3 General Approach to Computation of Time-Frequency Distributions

The discrete time definition of Cohen's class of time-frequency distributions given in equation (3.11), reproduced here for convenience,

$$\rho_z(n,k) = \sum_{m=-M}^{M} \sum_{p=-M}^{M} G(p,m) z(n+p+m) z^*(n+p-m) e^{-j4\pi mk/N} \qquad (3.84)$$

forms the basis of the general approach to implementation of time-frequency distributions. This approach can be expanded to three steps[22]:

1. Form the bilinear product $K_z(n,m) = z(n+m)z^*(n-m)$. The bilinear product has Hermitian symmetry[49], that is:

$$K_z(n,m) = \begin{cases} z(n+m)z^*(n-m) & for\, m \geq 0 \\ K_z^*(n,-m) & for\, m < 0 \end{cases} \qquad (3.85)$$

This means that values of the bilinear kernel need only be calculated for positive time lags[48]. The efficient way to compute the bilinear product is to calculate them as they are required.

2. Convolve the bilinear product with the desired kernel function $G(n,m)$ in the n (time) dimension for each time instant. In an actual implementation, either the product kernel matrix or the selection kernel matrix $G(n,m)$, may be computed at the point of use (in the convolution). This saves memory and time. The kernel matrix $G(n,m)$ is known to be symmetrical in both time and lag dimensions, and so values are only used from the

positive quadrant.

3. Calculate the discrete Fourier transform of this result, to produce the time slice of the desired distribution.

The time-frequency distributions (TFDs) used in this work and their determining kernel functions $G(n,m)$ are shown in table 3.4. These code fragments were originally written in FORTRAN code by Boashash in 1992[22]. The equivalent code was initially transferred to MATLAB by Adib in 1995[50]. A new modified and much more thoroughly tested version was written for the present research to accommodate for the processing of both the heart rate variability and respiration signals.

Table 3.4 TFDs and their determining function $G(n,m)$
(from Boashash, B., *Time-Frequency Analysis Methods and Applications*, 1992)

Time-Frequency Representation	$G(n,m)$
Pseudo Wigner Distribution (PWD) using rectangular window	$\delta(n) \quad m \in \left[\frac{-(M-1)}{2}, \frac{(M-1)}{2}\right]$ 0 otherwise
Smoothed Pseudo Wigner Distribution using a rectangular window of odd length P	$\frac{1}{P} \quad n \in \left[\frac{-(P-1)}{2}, \frac{(P-1)}{2}\right]$ 0 otherwise
STFT using a rectangular window of odd length P	$\frac{1}{P} \quad \lvert m+n \rvert \leq \frac{(P-1)}{2}$ 0 otherwise
Born -Jordan- Cohen (RID)	$\frac{1}{\lvert m \rvert + 1} \quad \lvert m \rvert \leq \lvert n \rvert$ 0 otherwise
Choi-Williams (parameter σ)	$\frac{\sqrt{\sigma/\pi}}{2m} e^{-\sigma n^2/4m^2}$

CHAPTER 4

TIME-FREQUENCY ANALYSIS OF HEART RATE VARIABILITY AND RESPIRATION

Signals of practical interest often do not conform to the requirements of realistic application of Fourier principles. The approach works best when the signal of interest is composed of a number of discrete frequency components so that time is not a specific issue. Examples are a constant frequency sinusoid or a signal that exists for a very short time so that its time occurrence is considered to be known. Much of what we know implies that signals that can not be satisfactorily represented in these ways must be forced into the mold or abandoned[29].

Standard spectral analysis by Fourier transform or variations of autoregressive models have been extensively applied in the attempt to evaluate quantitatively the fluctuations in beat-to-beat (R-R) intervals and respiration attributed to a regulatory function of the sympathetic and parasympathetic branches of the autonomic nervous system under steady-state conditions. Due to the limitations inherent in these methods, a compromise must always be made between frequency resolution and the choice of a time signal length short enough to suit the stationarity assumption. Analysis over a long time window, usually 5-10 minutes, does not show information about the time-varying structure of the spectra. Instantaneous changes of the signal content, typical for cardiovascular signals, are thus smeared out or appear as a wideband noise. Therefore, it is a common practice that a "reasonably stationary" part of the signal is identified and

analyzed. However, the spectral estimation is dependent on the chosen observation window, and consequently the interpretability of the results is limited[8].

Recently, joint time-frequency signal representation has received considerable attention as a powerful tool for analyzing a variety of signals and systems. In particular, if the frequency content is time varying as in signals of biological origin which often do not comply with the stationarity assumptions, then this approach is quite attractive. Although either the time domain description or its Fourier transform carries complete information about the signal, neither of them reveals explicitly the frequency spectrum at a particular time or the time at which a particular frequency component occurs. By mapping a one-dimensional function of time or frequency into a two-dimensional function of time and frequency, the joint time-frequency representation (TFR) localizes the signal energy in both the time and frequency domains.

The ultimate goal of this research work is dedicated to the use of time-frequency analysis of heart rate variability and respiration as a new and innovative approach to investigate the physical and mental exertion attributed to exercise.

4.1 Heart Rate Variability Test Signals

Although time-frequency analysis has been extensively studied and universally used, there is not much experience in its application to very low frequency ranges (less than 1 Hz). Even its prior use on the beat-to-beat variations was limited to the use of one particular distribution under resting and posture conditions[8]. A series of sinusiods and chirps were first created to test the behavior of the five distributions in the high frequency

ranges (100 Hz to 400 Hz). Each distribution used: the short time Fourier transform (STFT), the pseudo Wigner-Ville (WV), the smoothed pseudo Wigner-Ville (SPWV), The Choi-Williams (CW), and the Born-Jordan-Cohen (RID), has unique characteristics which affect the amount of smoothing and the generation of crossterm interference . Despite the validation of their proper responses, it was important to be able to test the application of these distributions on a signal modeled as closely as possible to the long term heart rate variability signal over the frequency range of interest, namely, for frequencies less than 0.7 Hz.

In Figure 4.1, we illustrate the first case, where the HRV signal is modeled as a continuous sum of three sine waves of equal amplitude of one and duration time of 200 seconds, containing frequencies 0.1 Hz, 0.3 Hz and 0.5 Hz. The power spectrum shows the presence of the exact three frequencies.

Time-frequency analysis was performed on the same signal described above using the five different distributions with the same specifications (FFT and window size equal to 512). It is evident from looking at the results in Figures 4.5-4.7 that all the distributions show the auto-terms at the specified frequencies (0.1 Hz, 0.3 Hz, and 0.5 Hz) for all time. However, note that the STFT distribution displays the lowest frequency resolution. There is an inherent tradeoff between time and frequency resolutions. If the analysis window is made short enough to capture rapid changes in the signal, it becomes impossible to resolve frequency components of the signal which are closer in frequency than the analysis window duration. On the other hand, the WVD provides a high resolution representation in time and in frequency for non-stationary signals. In addition, it has the

important property of satisfying the time and frequency marginals in terms of the instantaneous power in time and energy spectrum in frequency. However, its energy distribution is not non-negative, and it often possesses severe cross-terms, or interference terms, between components in different time-frequency regions. This potentially leads to confusion and misinterpretation of the signal content. Note the cross-terms at 0.2 Hz, 0.3 Hz and 0.4 Hz in Figure 4.5.

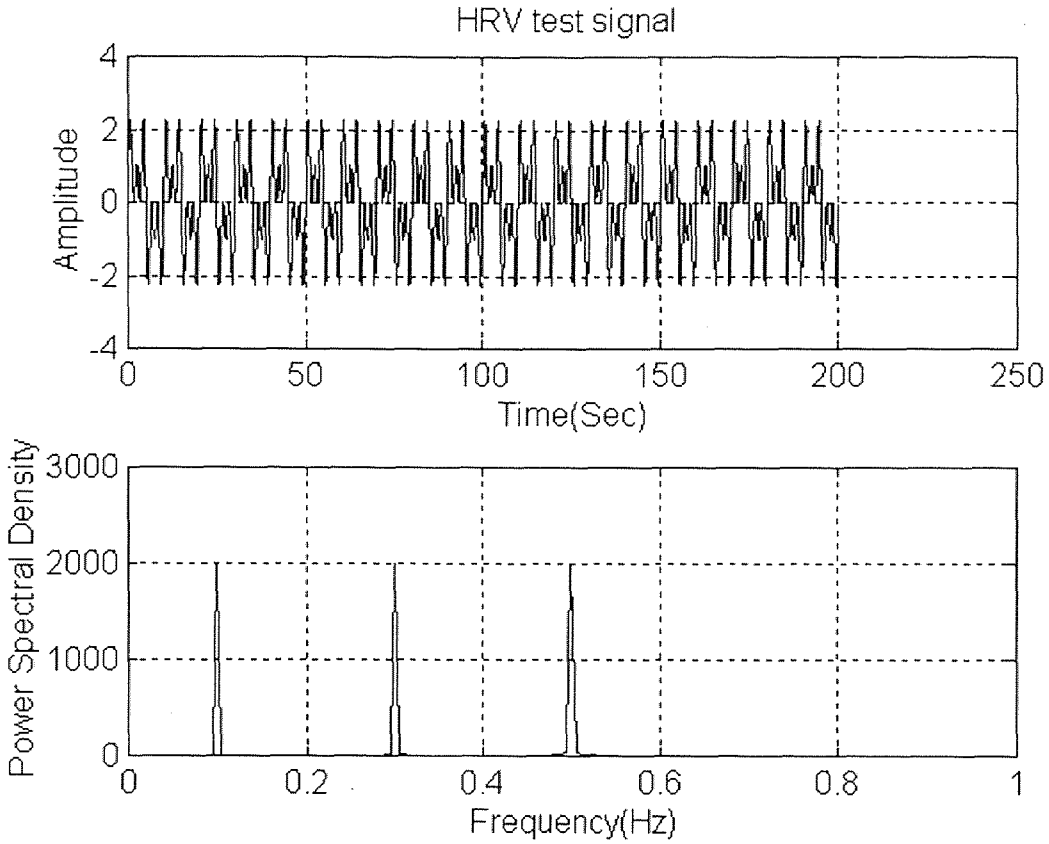

Figure 4.1 The HRV signal modeled as three continuos sine waves containing the frequencies (0.1 Hz,0.3 Hz and 0.5 Hz)

The RID is not a non-negative distribution as is the spectrogram. However, we have observed that the RID is more non-negative than the WVD. This may be due to the

fact that the WVD cross-terms often exhibit quite sizable negative values. The RID reduces negativity as a consequence of reducing the size of the cross-terms, but it also provides a high resolution and easy to interpret localization of the signal spectrum in the time-frequency plane as demonstrated in Figure 4.6.

The CW and the SPWVD overcome the aforementioned drawbacks of the other distributions and provide high resolution in time and frequency while suppressing interferences between the signal components as seen in Figures 4.6 and 4.7.

In Figure 4.2, we illustrate the second case, where the HRV signal is modeled as a continuous sum of three sine waves of equal duration time of 200 seconds, containing frequencies 0.1 Hz, 0.3 Hz and 0.5 Hz with added filtered Gaussian noise producing a signal-to-noise ratio of 2.8312 (i,e SNR=4.52 dB). Using a first order Butterworth filter with a cutoff frequency of 0.01 Hz, the Gaussian noise is filtered in an attempt to approach as closely as possible the $1/f$ spectral behavior exhibited by the long term HRV frequency response. The power spectrum shows the presence of the three frequencies with noise.

It is clear from looking at the results in Figures 4.8-4.10 that all the time-frequency distributions show the auto-terms at the specified frequencies (0.1 Hz, 0.3 Hz, and 0.5 Hz) for all time. The distributions all behave in a similar manner as described before with the addition of a noise component to our signal. In Figure 4.8, we note that the STFT barely distinguishes the low frequency noise component from the 0.1 Hz signal component. However, there is no interaction between the noise and the 0.3 Hz and 0.5 Hz frequencies. The WVD and the RID are no longer limited to cross-terms between signal

components. Now there is added interference between each of the three frequencies 0.1 Hz, 0.3 Hz and 0.5 Hz and the noise component as demonstrated in Figures 4.8 and 4.9. The CW and SPWV distributions are shown to distinguish well between the signal and noise components with the SPWVD being even more precise.

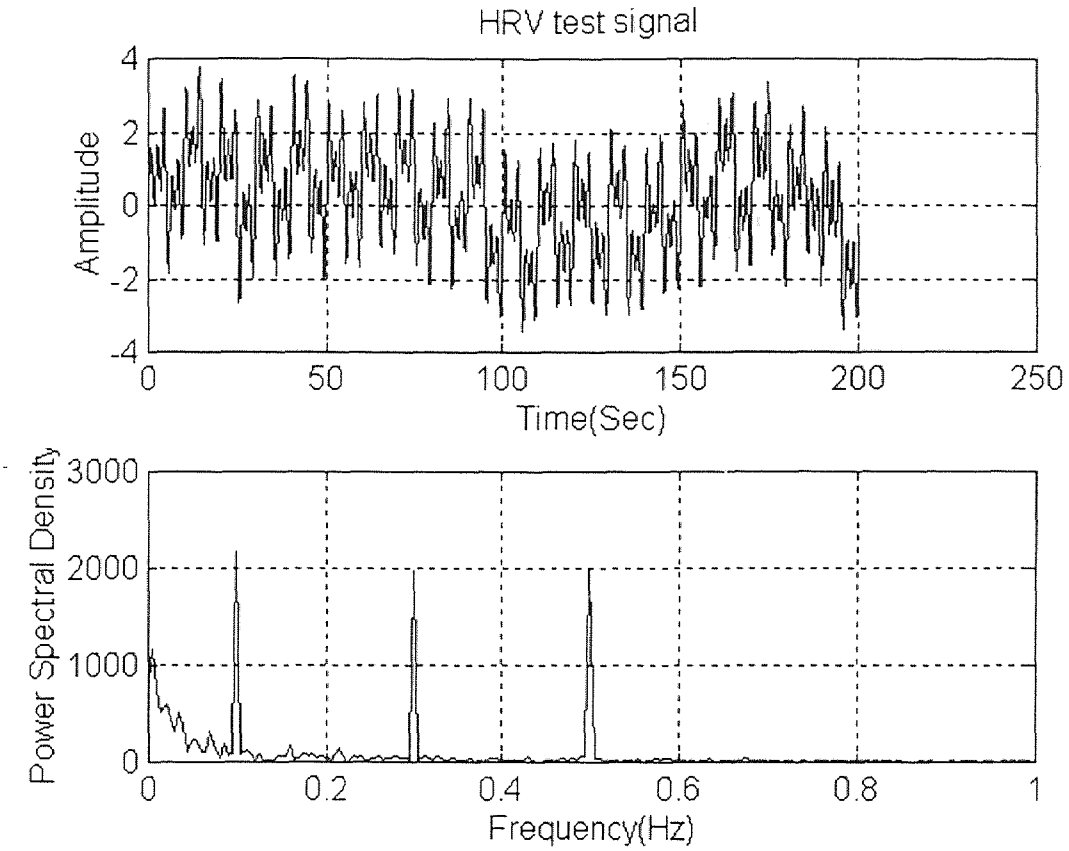

Figure 4.2 The HRV signal modeled as three continuos sine waves containing the frequencies (0.1 Hz,0.3 Hz and 0.5 Hz) with added noise (SNR=4.52dB)

In Figures 4.3 and 4.4, we illustrate the third and fourth cases, where the HRV signal is modeled as the sum of three sine waves of equal duration time of 50 seconds, separated by 25 seconds with frequencies of 0.3 Hz, 0.1 Hz and 0.5 Hz respectively. The difference between the two signals is again the presence of the added filtered Gaussian

noise at all time producing a signal-to-noise ratio, in Figure 4.4, of 0.778 (i,e SNR= -1.09 dB). The power spectra show that the frequencies 0.1 Hz , 0.3 Hz and 0.5 Hz are present for both cases, but it does not show the specific duration of time they existed. Figure 4.4 also shows the strong presence of noise in the very low frequency region that mostly affects the 0.1 Hz signal component.

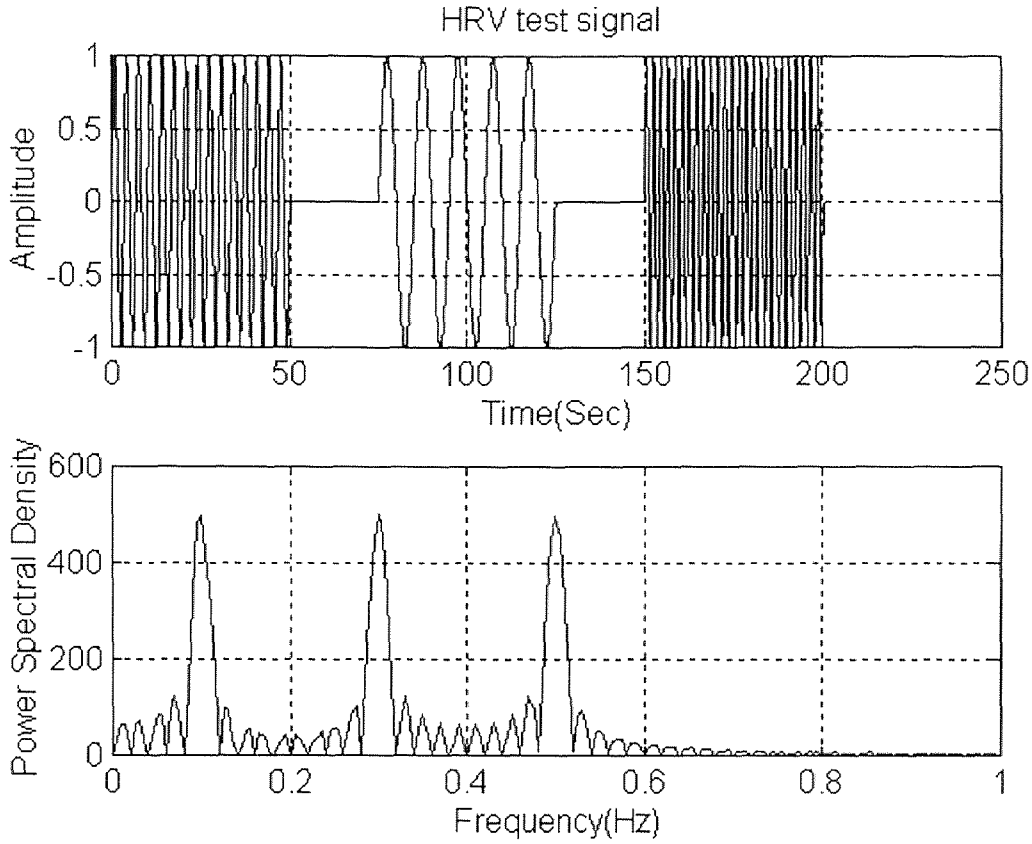

Figure 4.3 The HRV signal modeled as short duration sine waves containing the frequencies (0.1 Hz,0.3 Hz and 0.5 Hz)

Looking at Figures 4.11-4.13, we note that all five distributions show distinctly the presence of the three frequencies at the specific duration of time. At the time intervals of [0,50], [75,125] and [150,200] seconds of the signal, frequencies 0.3 Hz, 0.1 Hz and

0.5 Hz exist respectively. Note that the differences between the distributions are mainly in the signal intensity and the ability to maintain both accurate time and frequency resolutions. Also recall that since the signal does not exist for all time, we do not see cross-terms between different frequency components. Only one frequency is present at each specific duration of time.

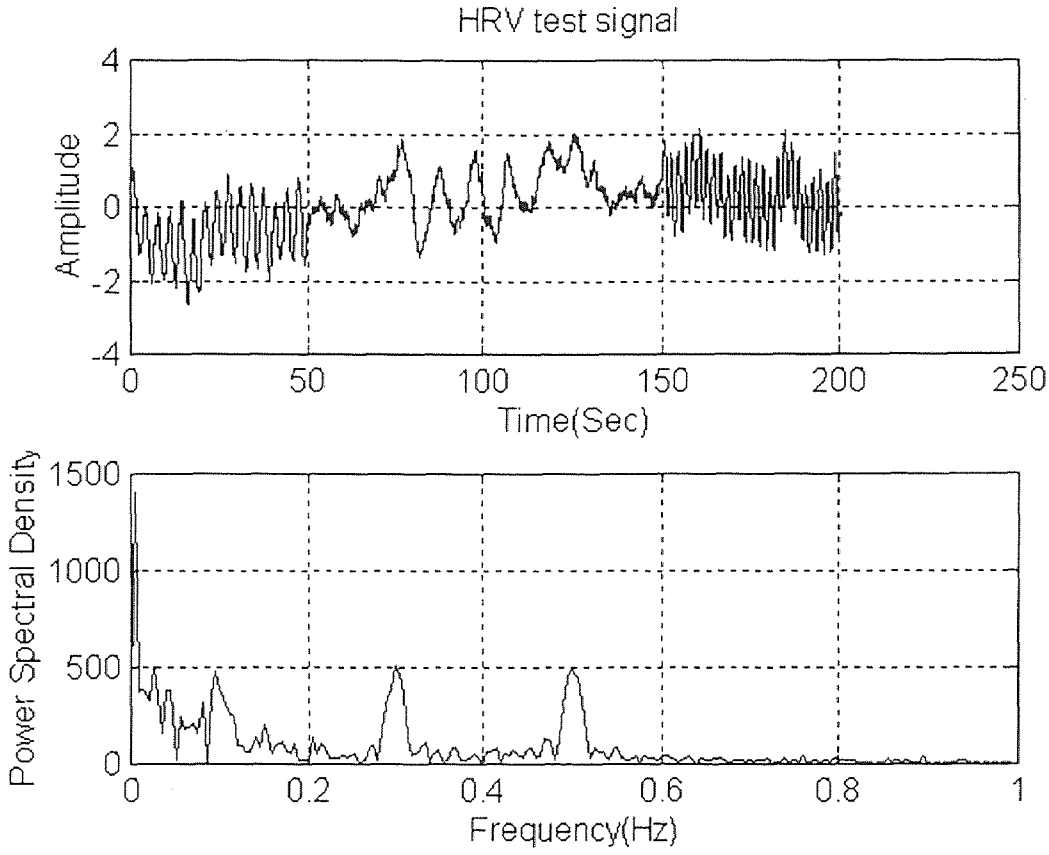

Figure 4.4 The HRV signal modeled as three short duration sine waves containing the frequencies (0.1 Hz,0.3 Hz and 0.5 Hz) with added noise (SNR=-1.09dB)

Figures 4.14-4.16 reveal a similar situation. However, now with the presence of a strong noise component, we note a considerable interaction with the 0.1 Hz signal. Yet, the other signal frequencies can be easily distinguished. Note that with the presence of

noise at all time, the WVD and the RID reveal the cross-term interaction between the signal and noise components. The CWD and the SPWVD present high resolution in both time and frequency while suppressing cross-term interactions between the signal and noise components.

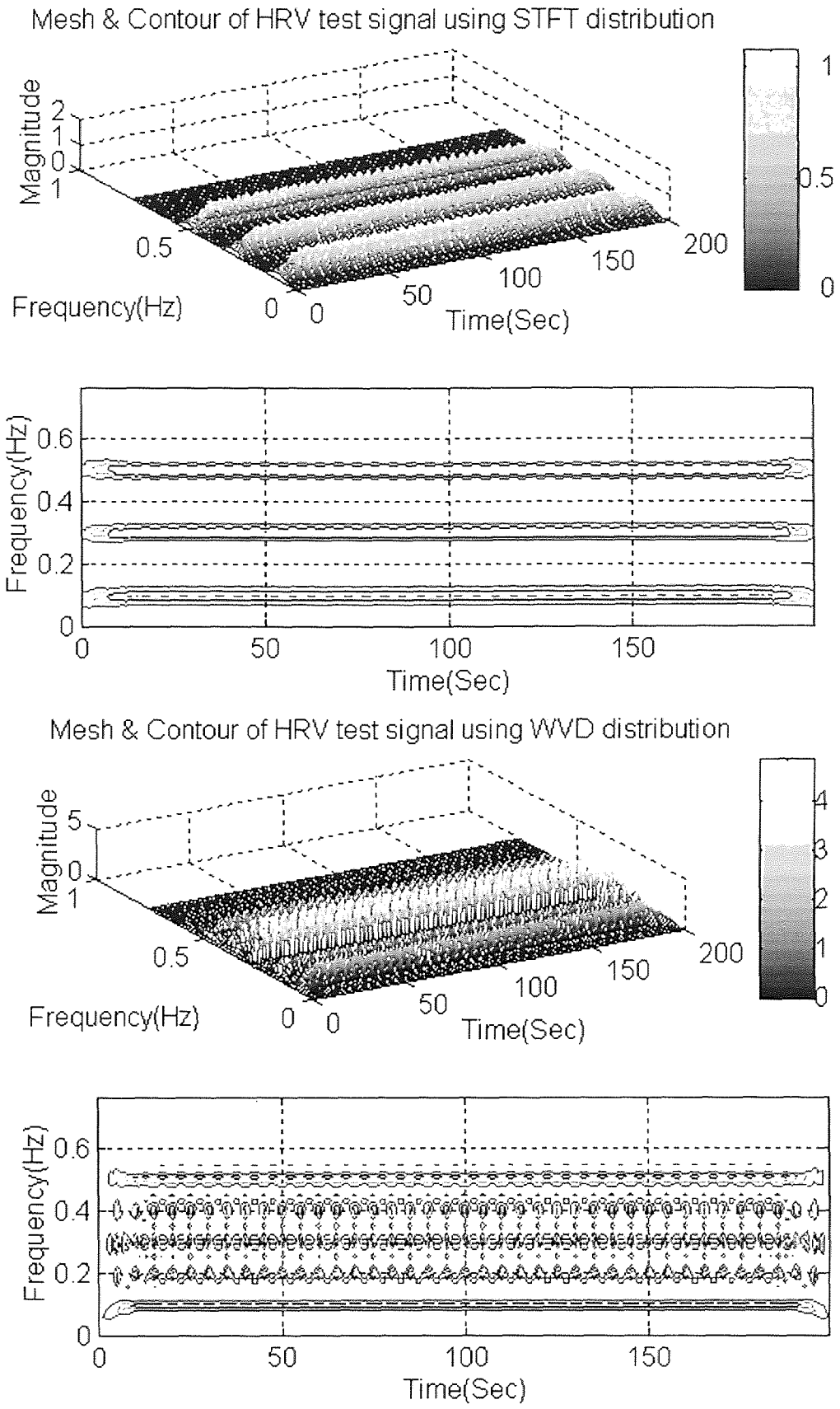

Figure 4.5 The STFT & the WVD of the noiseless continuous HRV test signal

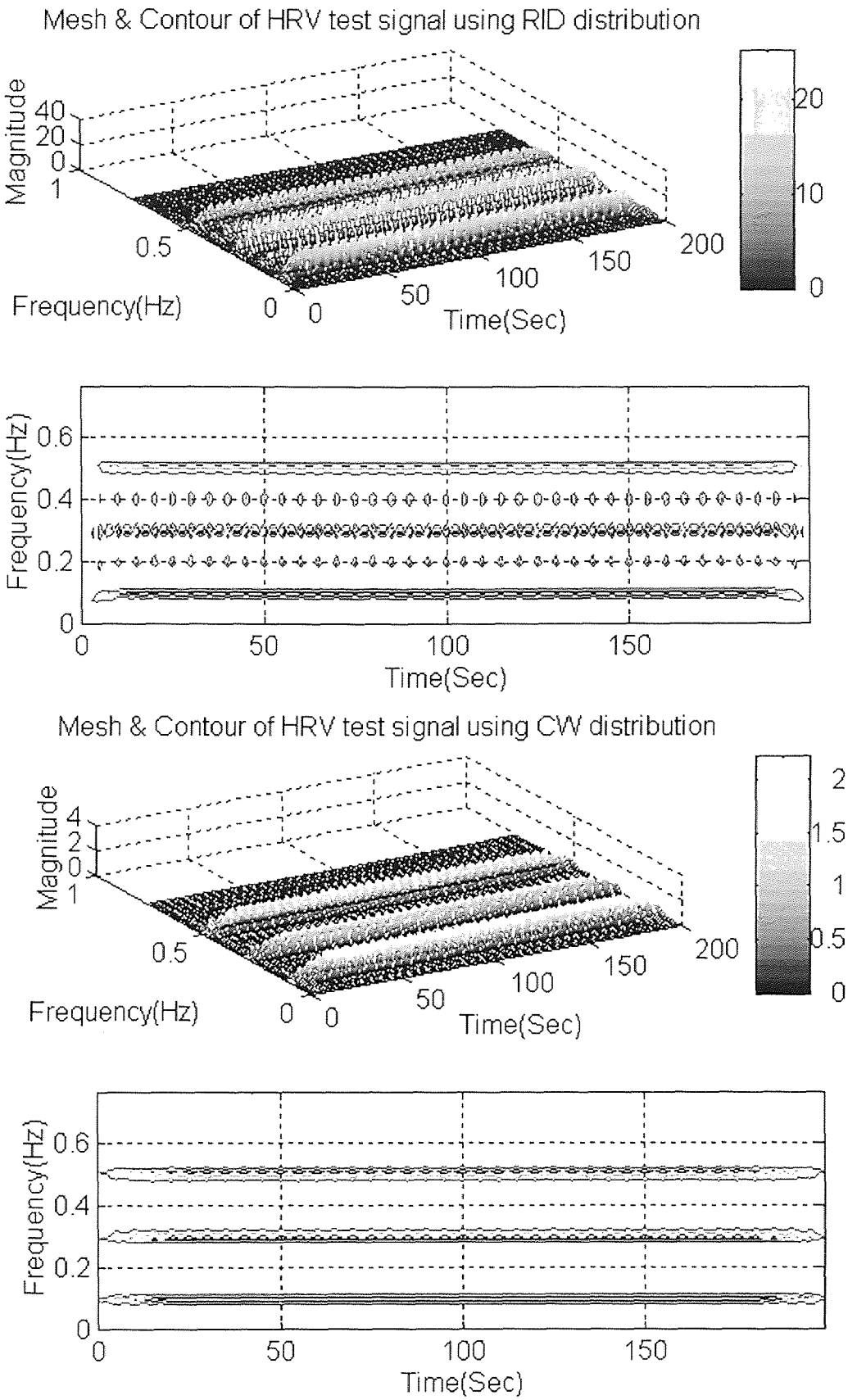

Figure 4.6 The RID & the CWD of the noiseless continuous HRV test signal

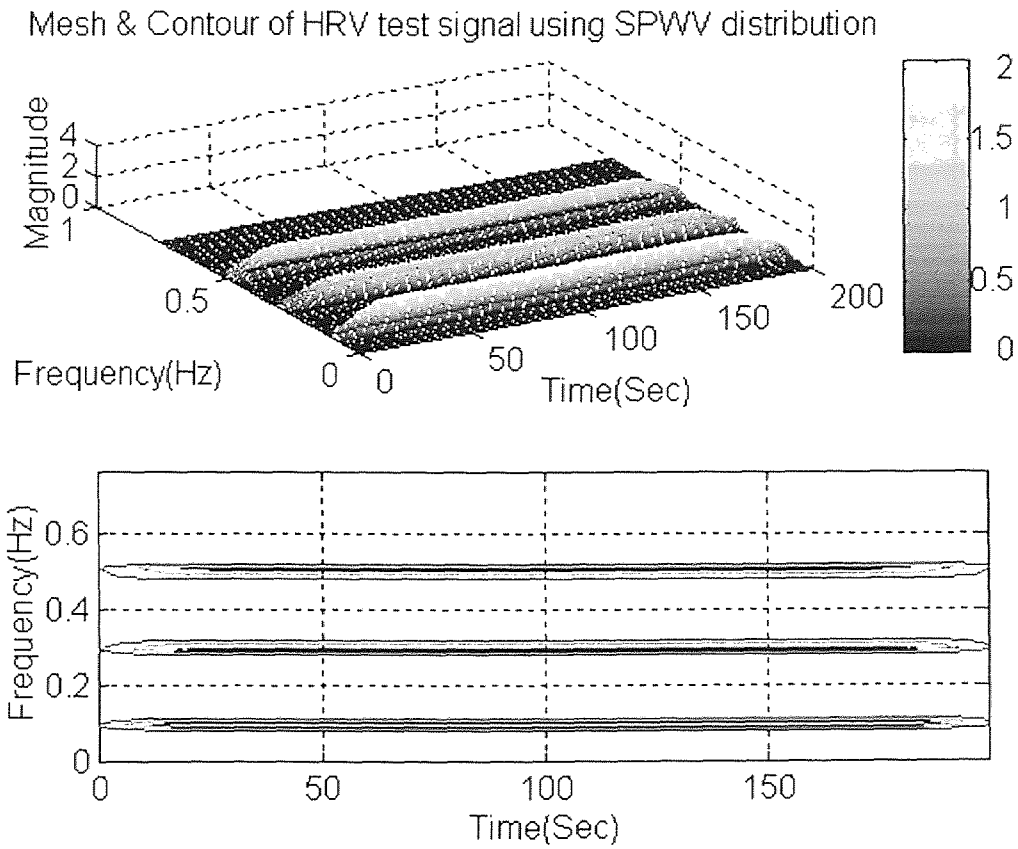

Figure 4.7 The SPWVD of the noiseless continuous HRV test signal

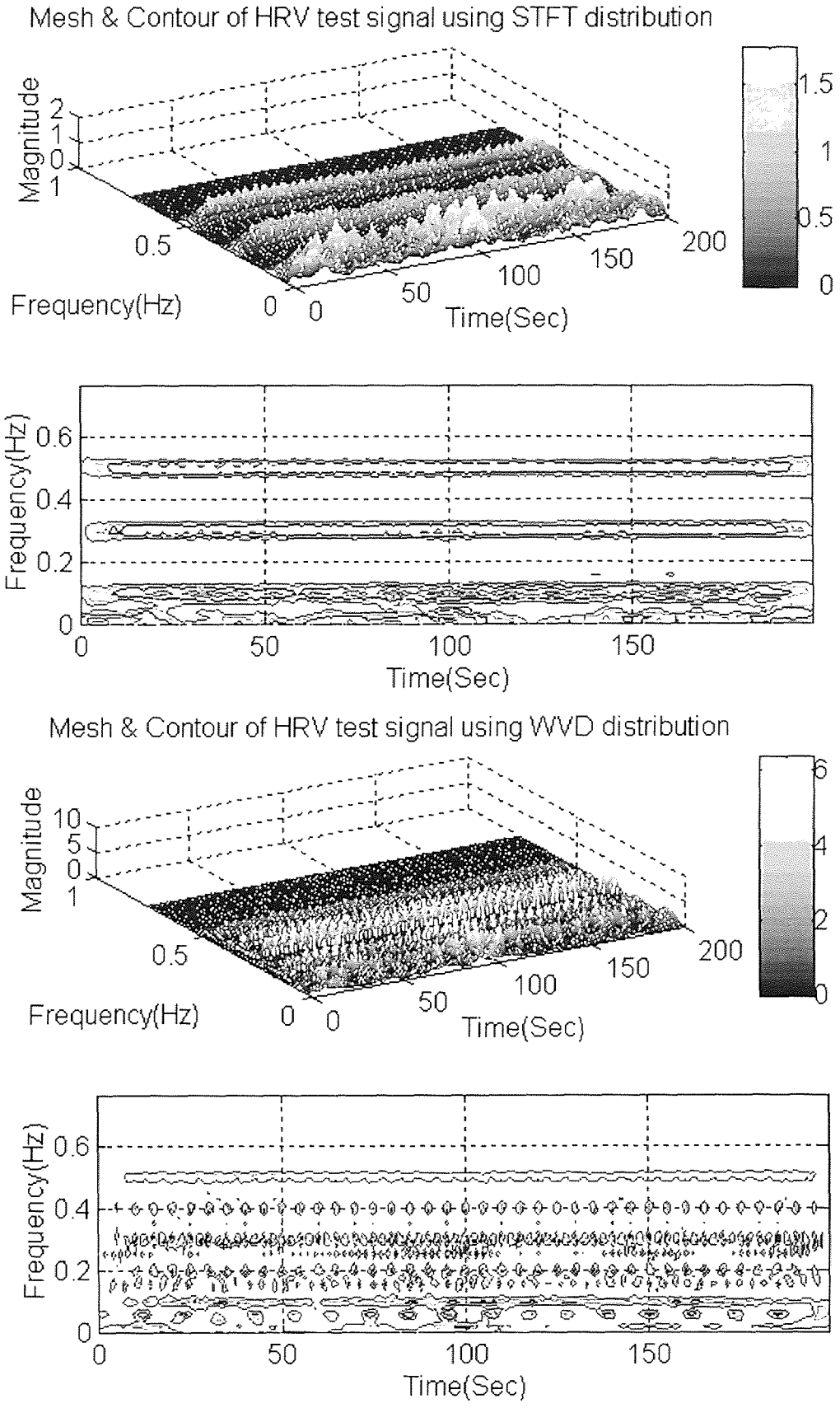

Figure 4.8 The STFT & the WVD of the continuous HRV test signal (SNR=4.52dB)

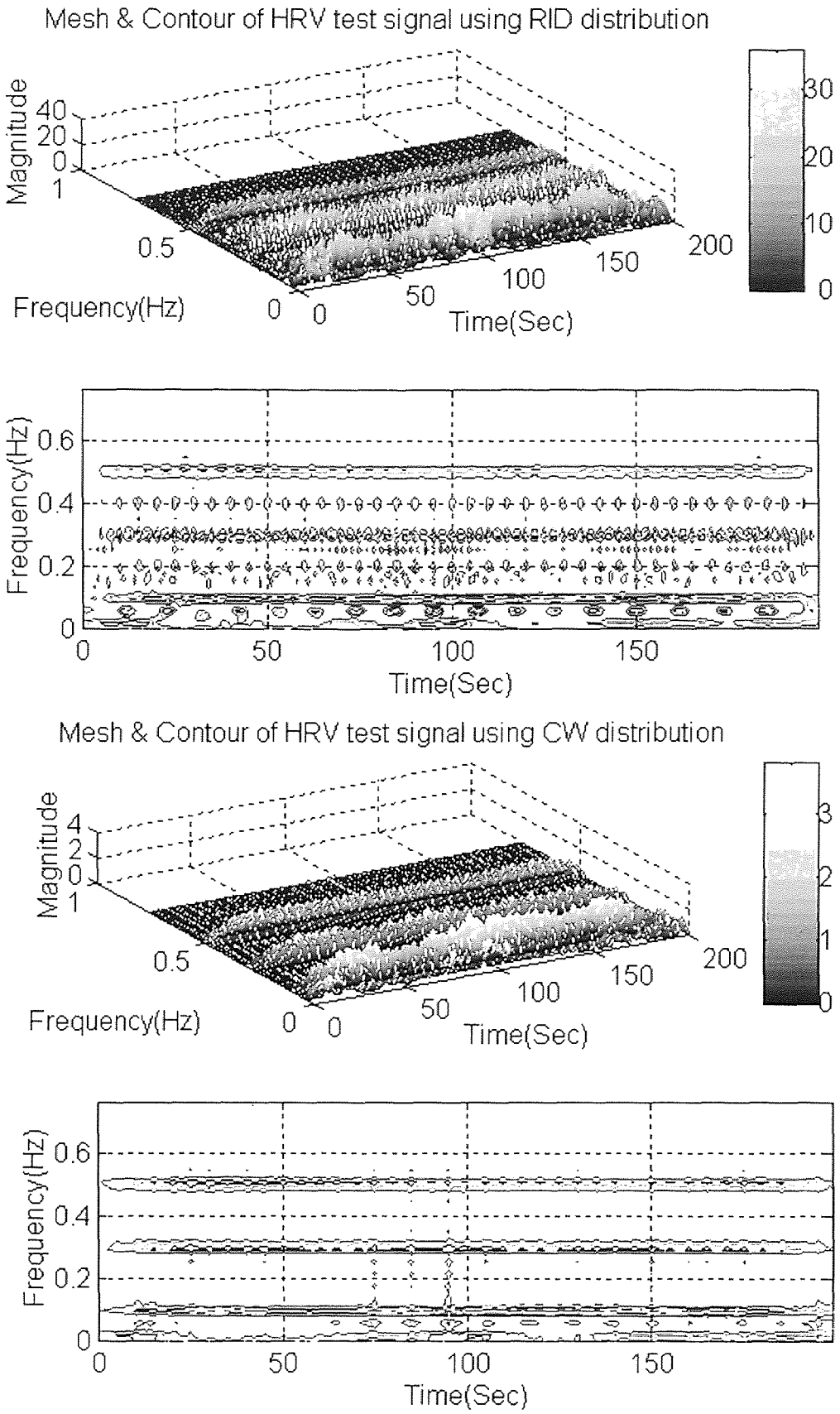

Figure 4.9 The RID & the CWD of the continuos HRV test signal (SNR=4.52dB)

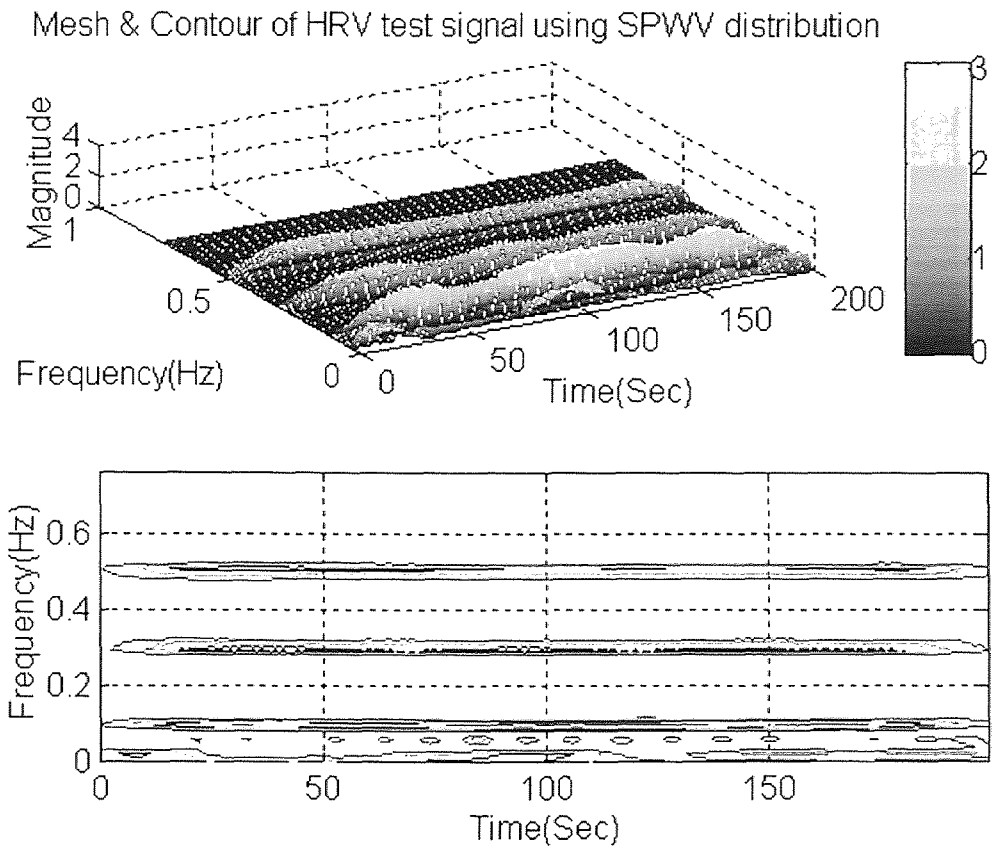

Figure 4.10 The SPWVD of the continuous HRV test signal (SNR=4.52dB)

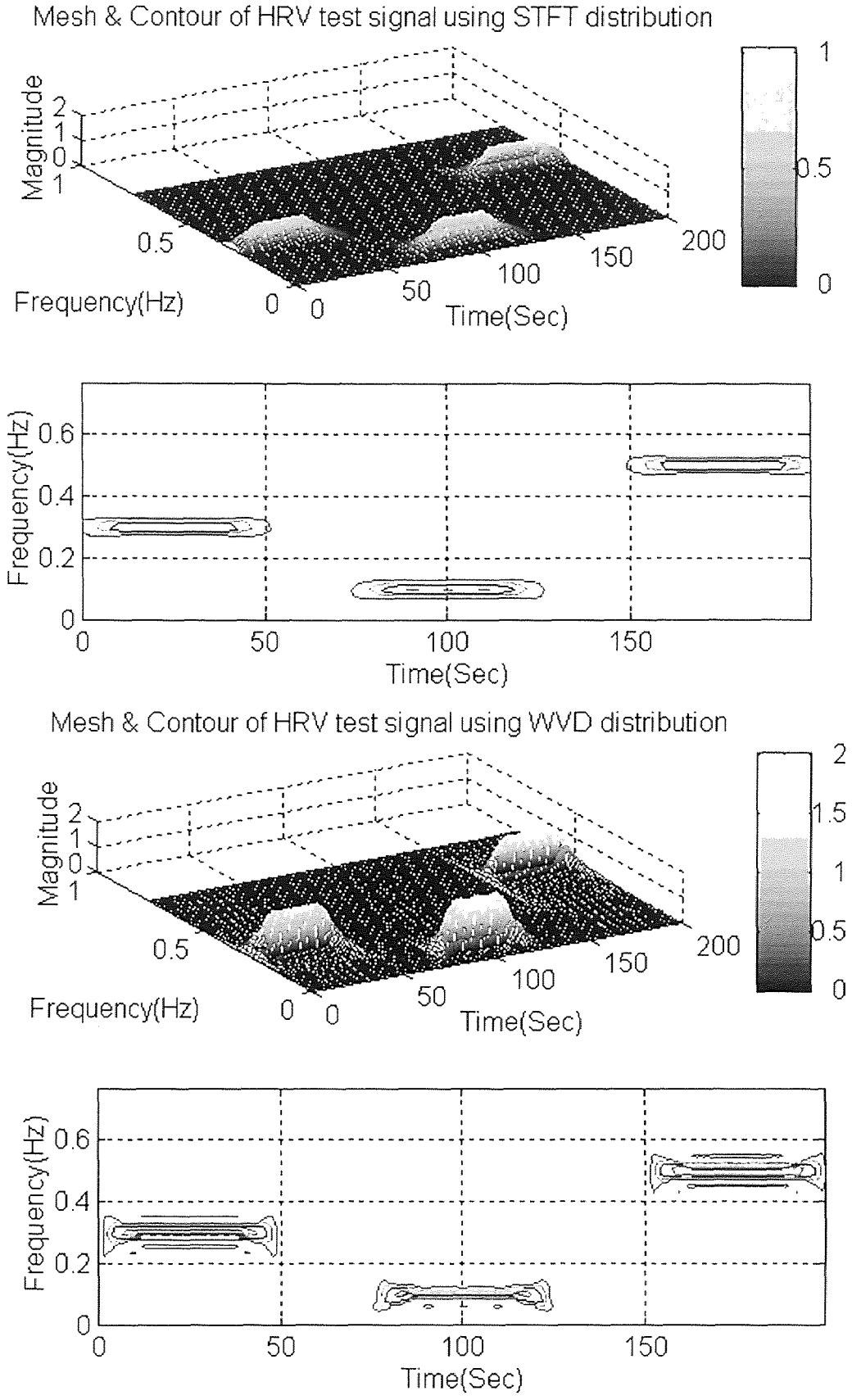

Figure 4.11 The STFT & the WVD of the short duration HRV test signal

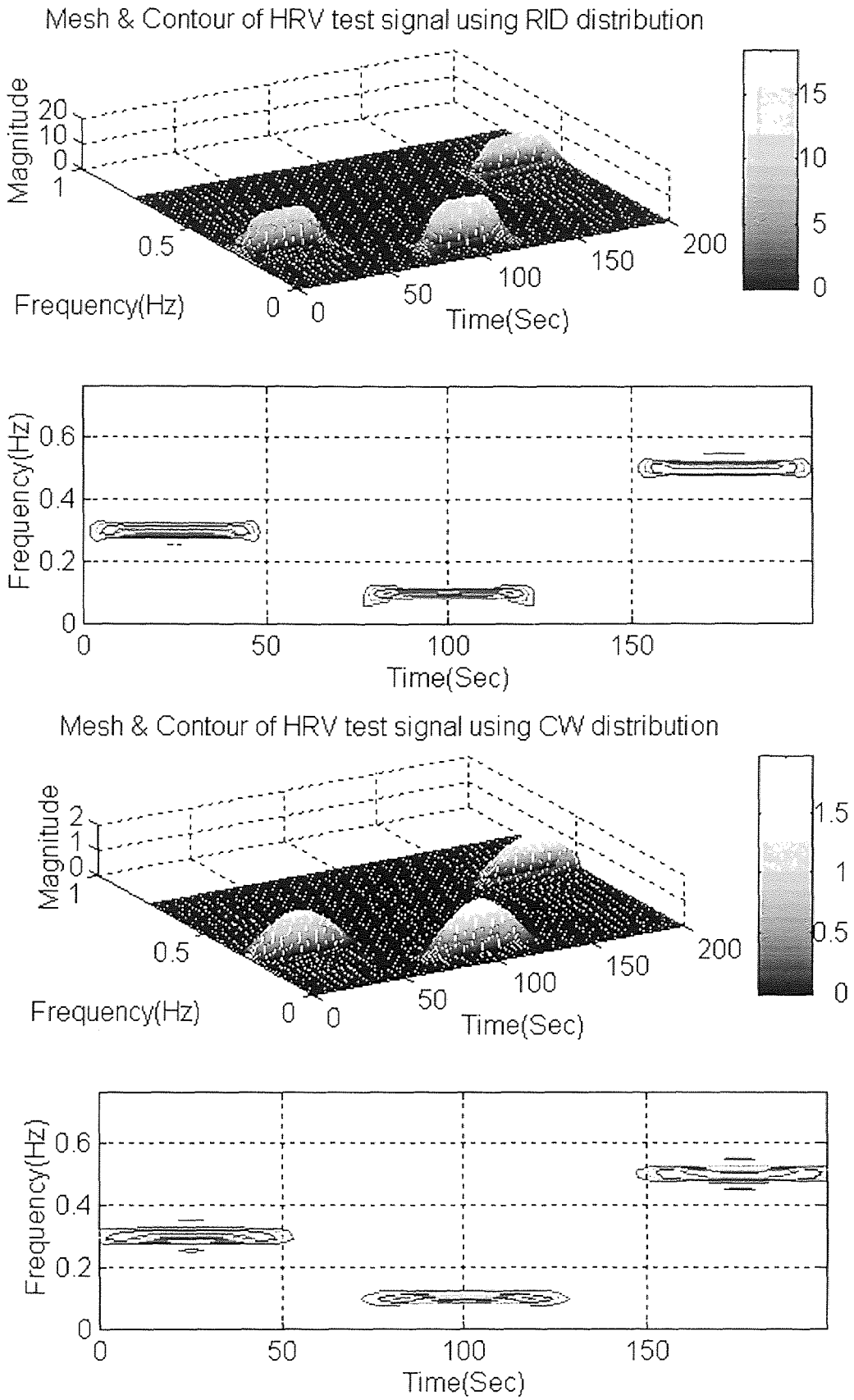

Figure 4.12 The RID & the CWD of the short duration HRV test signal

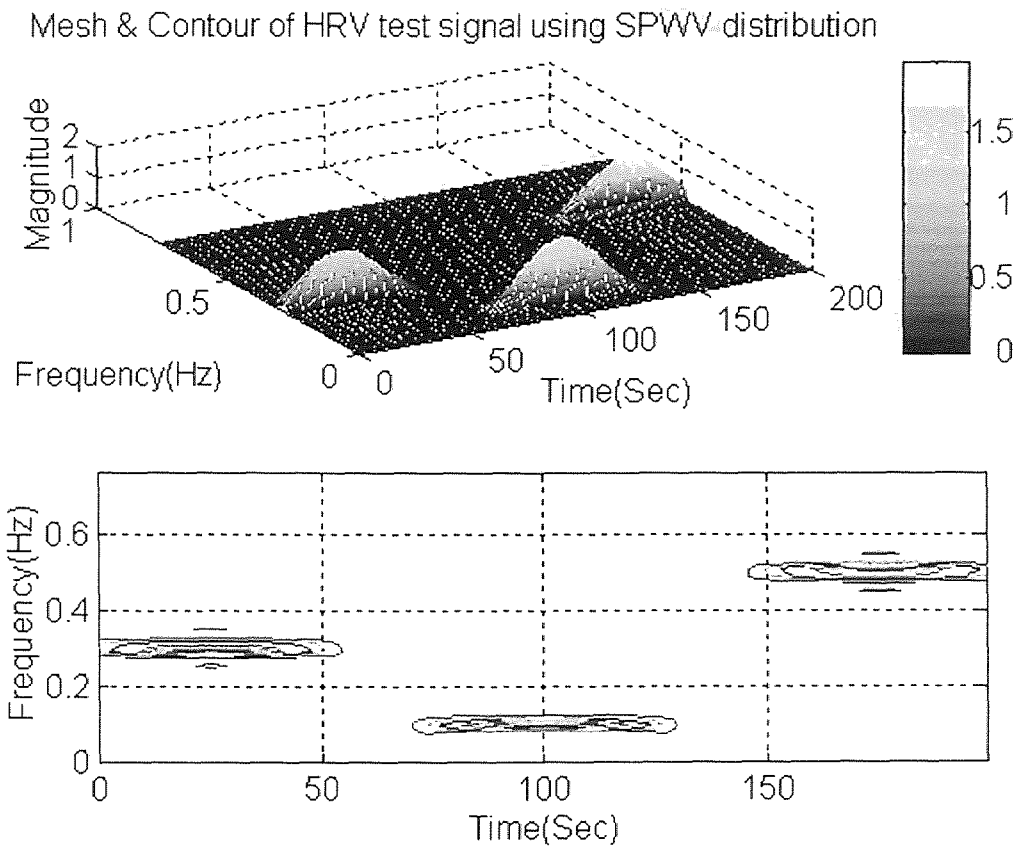

Figure 4.13 The SPWVD of the short duration HRV test signal

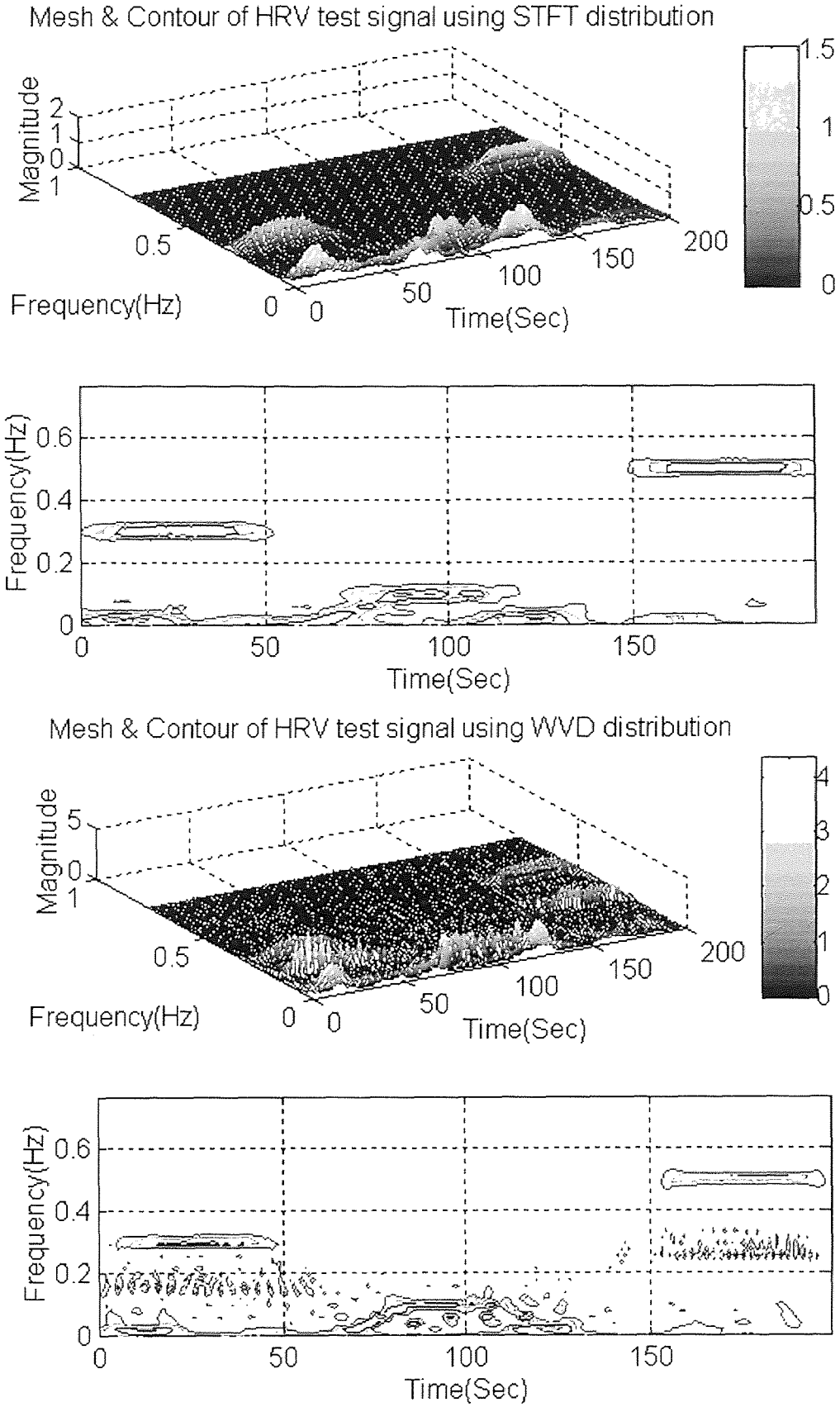

Figure 4.14 The STFT & WVD of the short duration HRV test signal (SNR=-1.09dB)

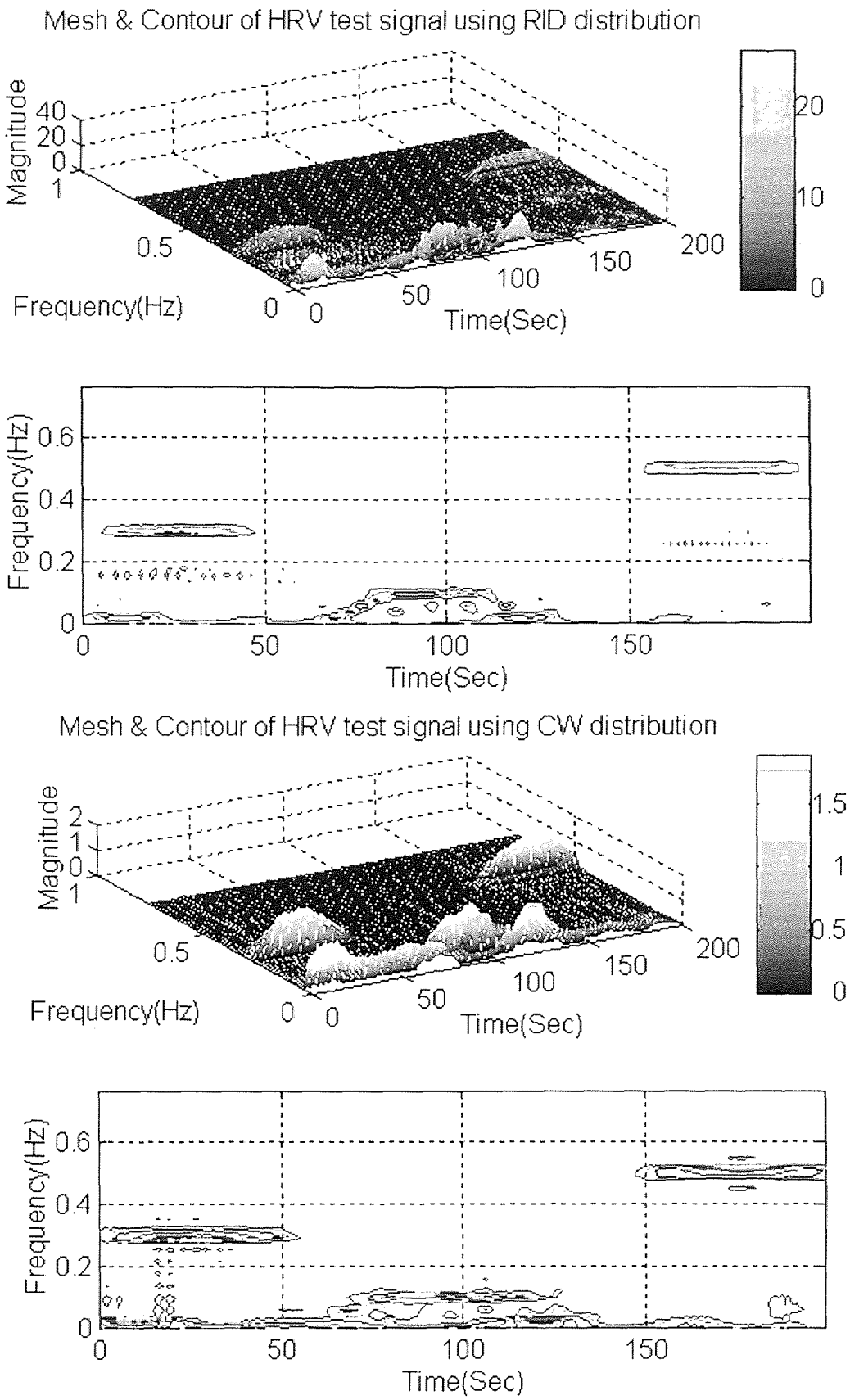

Figure 4.15 The RID & CWD of the short duration HRV test signal (SNR=-1.09dB)

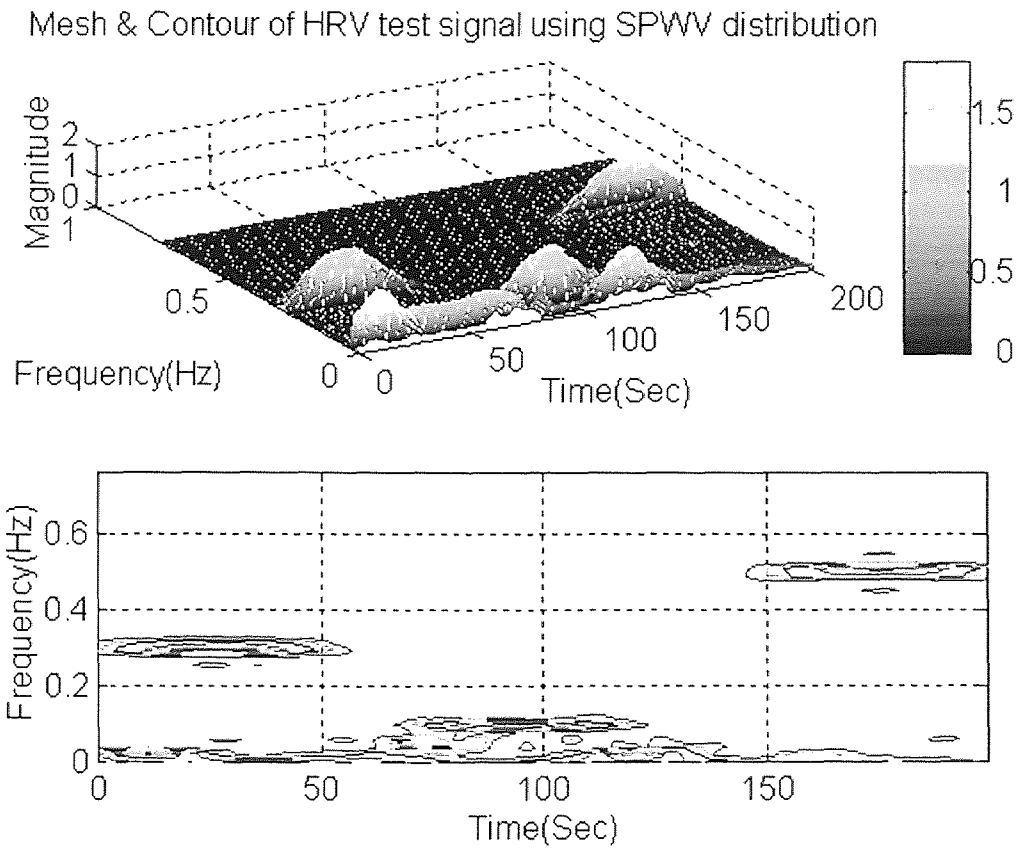

Figure 4.16 The SPWVD of the short duration HRV test signal (SNR=-1.09dB)

4.2 Time-Frequency Analysis of the Preliminary Protocol

The aim of time-frequency analysis is to develop tools that can describe rapid changes in time varying spectra. Expansion of the concept of spectral analysis of heart rate variability into time-frequency analysis gives us the ability to quantitatively assess the high frequency and the low frequency changes as a function of time. In the following sections, we will evaluate the use of the five classical kernels described in chapter 3 and section 4.1 to analyze the respiration and heart rate variability signals of the preliminary protocol. The aim of this process is to investigate the transitions between rest, exercise, and recovery, and to assess which distribution gives the most physiologically significant information. The vagal tone and the sympatho-vagal balance are the parameters used for comparison. They are assessed from the resulting 3-D time-dependent spectra by quantifying the area under the low frequency (0.06 Hz to 0.15 Hz) and high frequency (0.15 Hz to 0.75 Hz) ranges for each instant of time. Recall that the low frequency range is associated with the mixture of sympathetic and parasympathetic activity while the high frequency range is purely parasympathetic in origin.

4.2.1 Respiration Analysis

Figure 4.17 displays a typical respiration response to the twelve minute preliminary cycling investigation. The specific protocol required the subject to rest initially for two minutes, start pedaling for another two minutes to reach the vigorous exercise stage, exercise for an additional four minutes, and then rest for the last four minutes of recovery. Note that one can clearly distinguish the different phases of this study in the plot of the

raw respiration signal. After mean removal, the detrended respiration signal is used for further analysis.

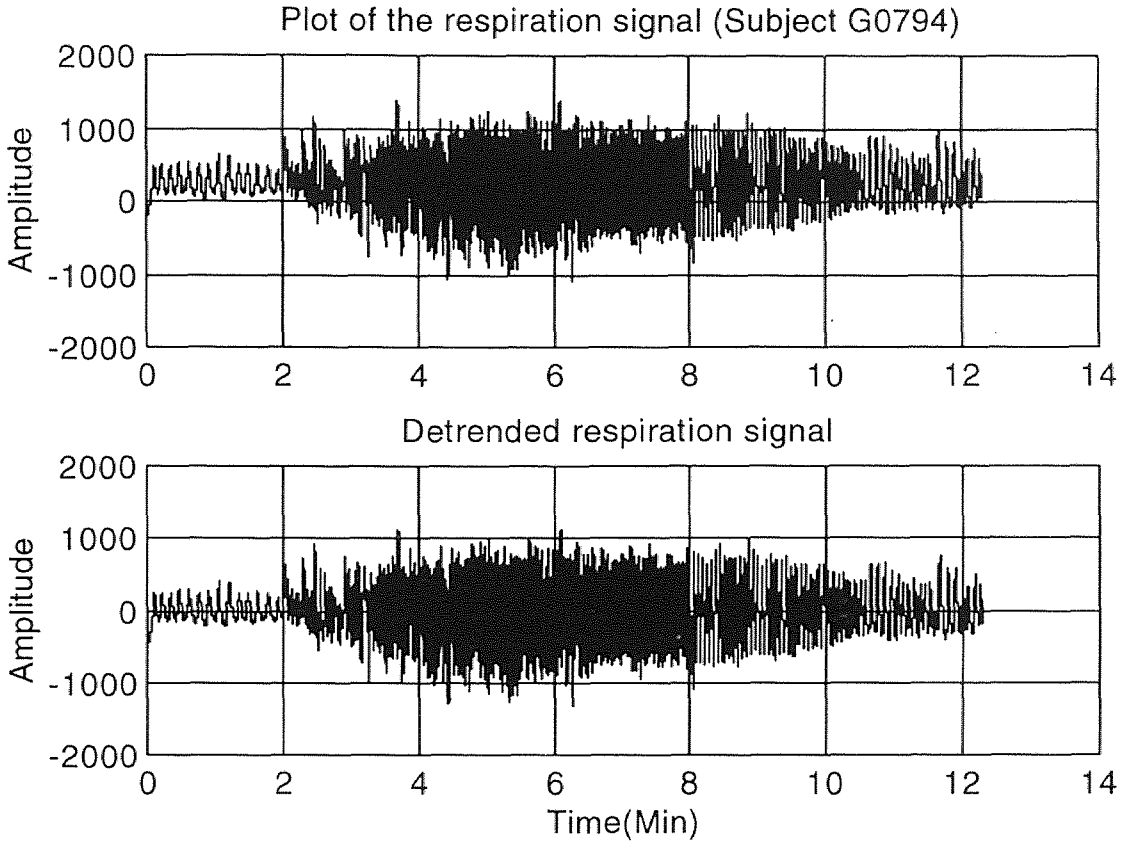

Figure 4.17 The raw and detrended respiration signal for subject G0794

Time-frequency analysis was performed on the detrended respiration signal of the ten subjects that participated in this study. The same FFT and window size of 512 was used for all the distributions. Figures 4.19-4.28 display the results for the same subject described above (G0794).

Figure 4.19 illustrates the mesh and contour plots of the 3-D resultant spectra using the STFT . Note that the contour plots are displayed in the two frequency regions

of interest. Looking at the mesh along with the contour plots, we clearly see the shift in the frequency of respiration between the rest, exercise and recovery stages. At rest [0-2 mins], the major activity is concentrated in the low frequency region (0.06 Hz to 0.15 Hz). In the exercise period [2-8 mins], we note the increase in the frequency of respiration starting from the onset of cycling at minute 2 to reach the maximum intensity between (0.5 Hz to 0.65 Hz) during the vigorous cycling level. Note the significant drop in frequency , from approximately 0.6 Hz to 0.25 Hz, at the onset of recovery and termination of motion (minute 8), and the further decline into lower frequencies from minute 10 to the end of the experiment.

Figure 4.20 presents the low frequency and high frequency activity as obtained by summing the area in the two specified bands at each instant of time throughout the whole experiment. These plots display exactly the same information as in Figure 4.19 as a function of the intensity at all time. The normalized low frequency and high frequency activity plots are obtained by dividing at each instant of time the LF and HF power by the sum of both respectively;

$$NLF=\frac{LF}{LF+HF} \qquad \text{and} \qquad NHF=\frac{HF}{LF+HF}$$

These plots show that at rest, the relative power is concentrated in the low frequency region, thus indicating that the subject is breathing at a rate below 0.15 Hz. With the onset of exercise, there was a relative transient shift to the high frequency range. Respiration remains in the high frequency range throughout indicating that the challenging exercise level forced the subject to breathe faster, thus forcing his respiration frequency into the high region. The normalized power does not show a recovery until

minute 10 when the transition to the low frequency region begins. The ratio of low frequency to high frequency emphasizes again the dominance of the LF activity during rest and the HF activity during exercise.

Figures 4.21-4.28 replicate these same findings displayed using the Wigner-Ville, Born-Jordan-Cohen, Choi-Williams, and smoothed pseudo Wigner-Ville distributions. The differences between these distributions relate back to their inherent characteristics that are thoroughly discussed and compared in the previous section. The WVD and the RID still present the problem of generating cross-term interference, although with different intensity, between the low and high frequency signal components as seen in Figures 4.21-4.24. The CWD addresses this drawback. However, the clarity of replication and the smoothest distribution can still be most demonstrated in the use of SPWVD.

It is important to note that the respiration signal under this particular exercise condition is a very good candidate to demonstrate the benefits of the application of time-frequency analysis. The findings listed above validate the physiological states the subjects are in. With rest and relaxation, the breathing rate is decreased producing a low respiration frequency. With exercise and exertion, the breathing rate increases to supply the body with more oxygen and remove more carbon dioxide, thus shifting the frequency of respiration into higher ranges that can reach as high as 0.75 Hz. This prominent shift in frequency between different durations of time is best observed using time-frequency distributions as clearly demonstrated here and in the previous test signals.

4.2.2 Heart Rate Variability Analysis

Figure 4.18 displays the heart rate variability response in the same subject during the twelve minute preliminary protocol. The purpose of this study was to investigate two important questions:

I) Is there an evident change in heart rate variability due to the stressful exercise condition imposed on each subject?

II) Is recovery from exercise different either qualitatively or quantitatively from initiation of exercise?

Looking at the heart rate variability signal shown below, one can easily distinguish the three stages of rest, exercise, and recovery by noting the changing trend in amplitude and

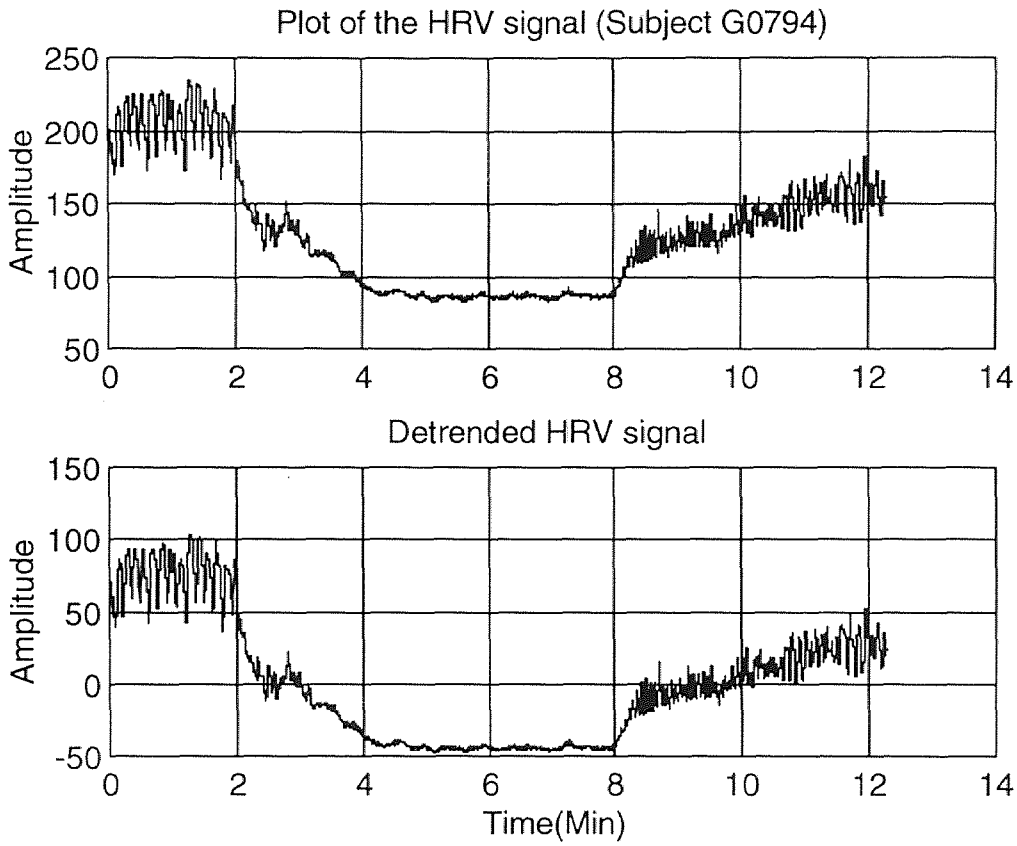

Figure 4.18 The raw and detrended HRV signal for subject G0794

variability at each phase of the experiment. There are also pronounced transitions between these stages.

After mean removal, time-frequency analysis was performed on the detrended HRV signal of the ten subjects using the same specifications of window and FFT size of 512. Figures 4.29-4.34 display the resulting distributions for the same subject (G0794). Note that as stated earlier, the same findings are observed in all the distributions with the differences limited to the interference between frequency components, the power and the smoothing effects. The SPWVD still exhibits the best time and frequency resolutions. It displays the smoothest envelope or trend of the resulting 3-D power spectra. Looking at the mesh and contour plots of Figure 4.29 we note that all the major power of the HRV signal is concentrated in the very low frequency region (less than 0.06 Hz). It is hard to point out any change in our area of interest by just looking at these plots. Figure 4.30 shows the mesh and contour plots of the low frequency and high frequency regions respectively. It clearly indicates that the major activity occurs at rest in both frequency ranges, which corresponds to the highest amplitude and variation in the inter-beat-interval signal. While average heart rate speeds up during exercise, the variability in the heart rate slows down, which is demonstrated in the lower power during the exercise phase. Note that this information is replicated and is easily seen in the LF and HF activity plots in Figure 4.29 . These plots also show clearly the transitions between the three states of rest and exercise, and exercise and recovery.

4.2.2.1 Statistical Analysis of the Heart Rate Variability Signal: In order to verify our findings using time-frequency analysis and to answer the questions posed in the previous section, statistical analysis was also performed on the HRV signal. The first test compared the mean heart rate between rest [0-2 mins], exercise [4-6 mins], and recovery [10-12 mins] for the ten subjects. With the assumption that the 3 observations on each of the 10 subjects were independent, we tested for a difference between the three phases. The null hypothesis stated that no significant differences exist between one or more of the means. The test was conducted at the 5% significance level. After assessing the normality of the data using a normal quantile plot, a repeated measures ANOVA showed an F value with a probability significantly less than 0.05. This indicated that there are indeed differences between rest and exercise, exercise and recovery, and rest and recovery, as demonstrated in the raw data itself.

The second statistical method used a correlation test to compare the slopes into and out of exercise under the assumption that the slopes were jointly normally distributed. The null hypothesis stated no correlation between the slopes (i,e r=0). the 20 observations used the slopes of the first minute into [min 2-3] and first minute out of [min 8-9] exercise for each subject. After passing the normality check, the data indicated a strong inverse correlation between the transition from rest to exercise and from exercise to recovery with an r=-0.848. This may indicate that subjects with quick transition into exercise tend to recover quickly out of exercise.

Therefore, along with the time-frequency representations, the statistical analysis shows that a stressful exercise level drastically changes the heart rate variability signal. It

also shows that there is a significant difference between rest and recovery which indicates that four minutes out of exercise is not enough for the heart rate to reach its normal resting state.

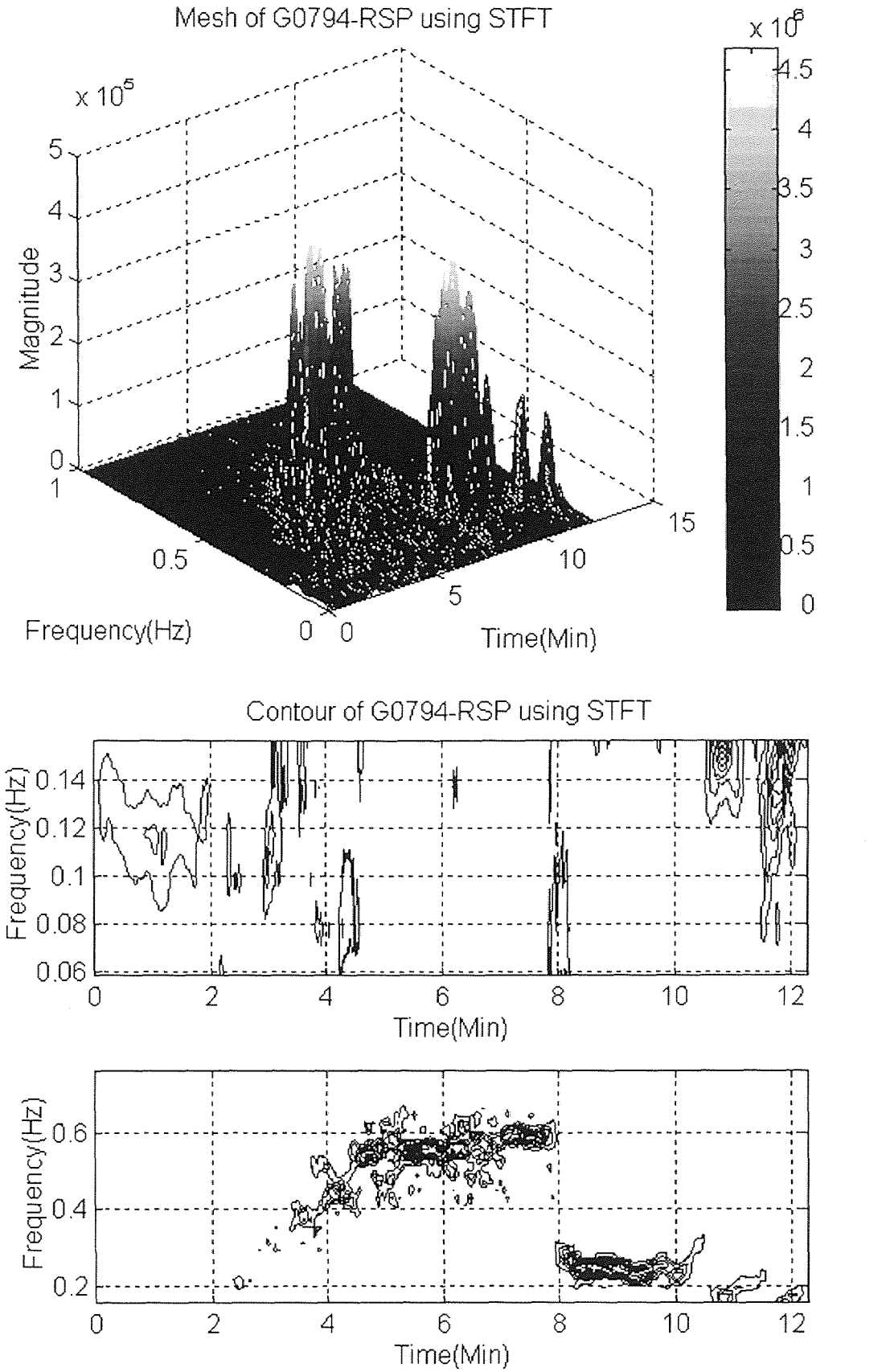

Figure 4.19 Mesh and contour of the STFT of the respiration signal (Subject G0794)

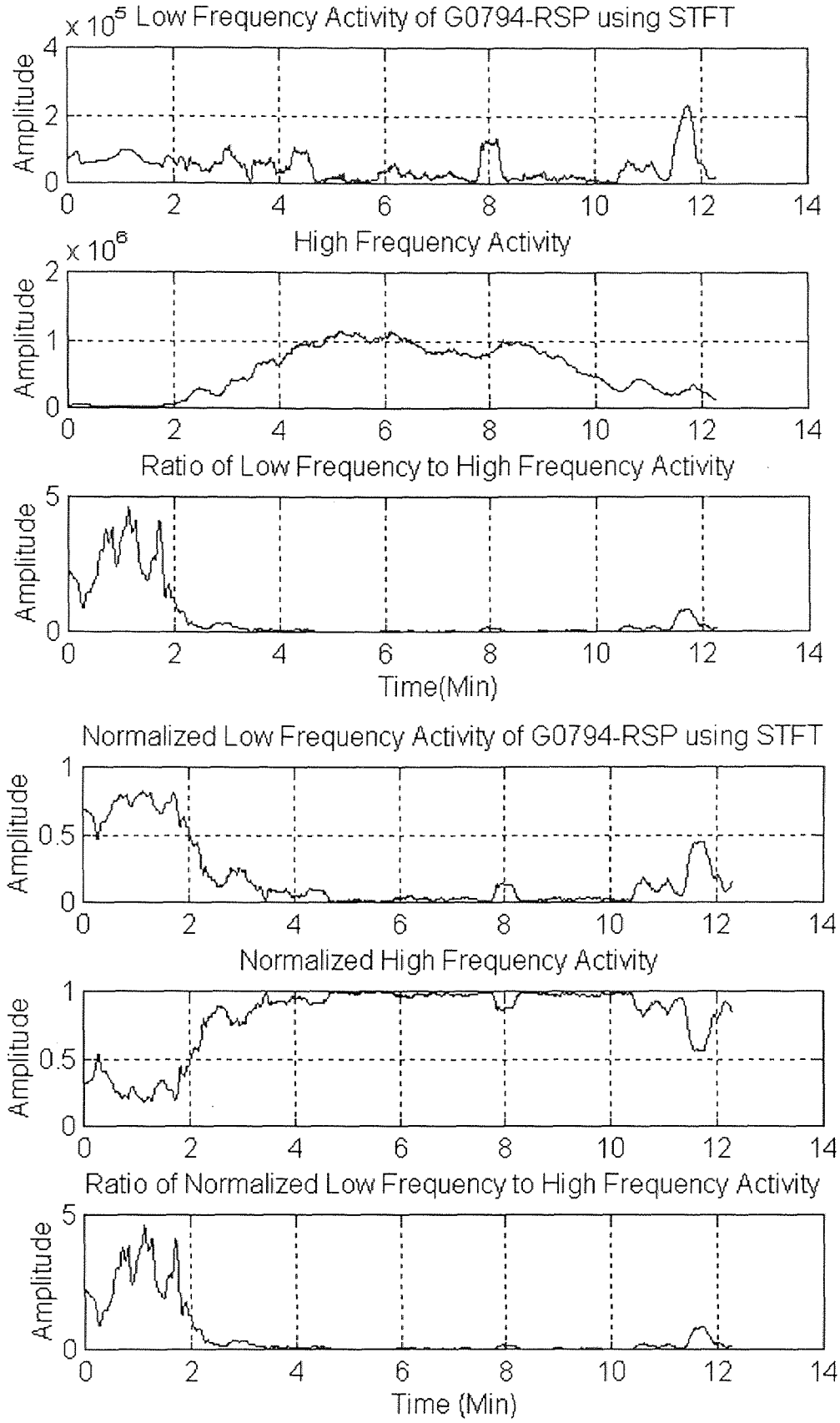

Figure 4.20 LF and HF activity of the STFT of the respiration signal (Subject G0794)

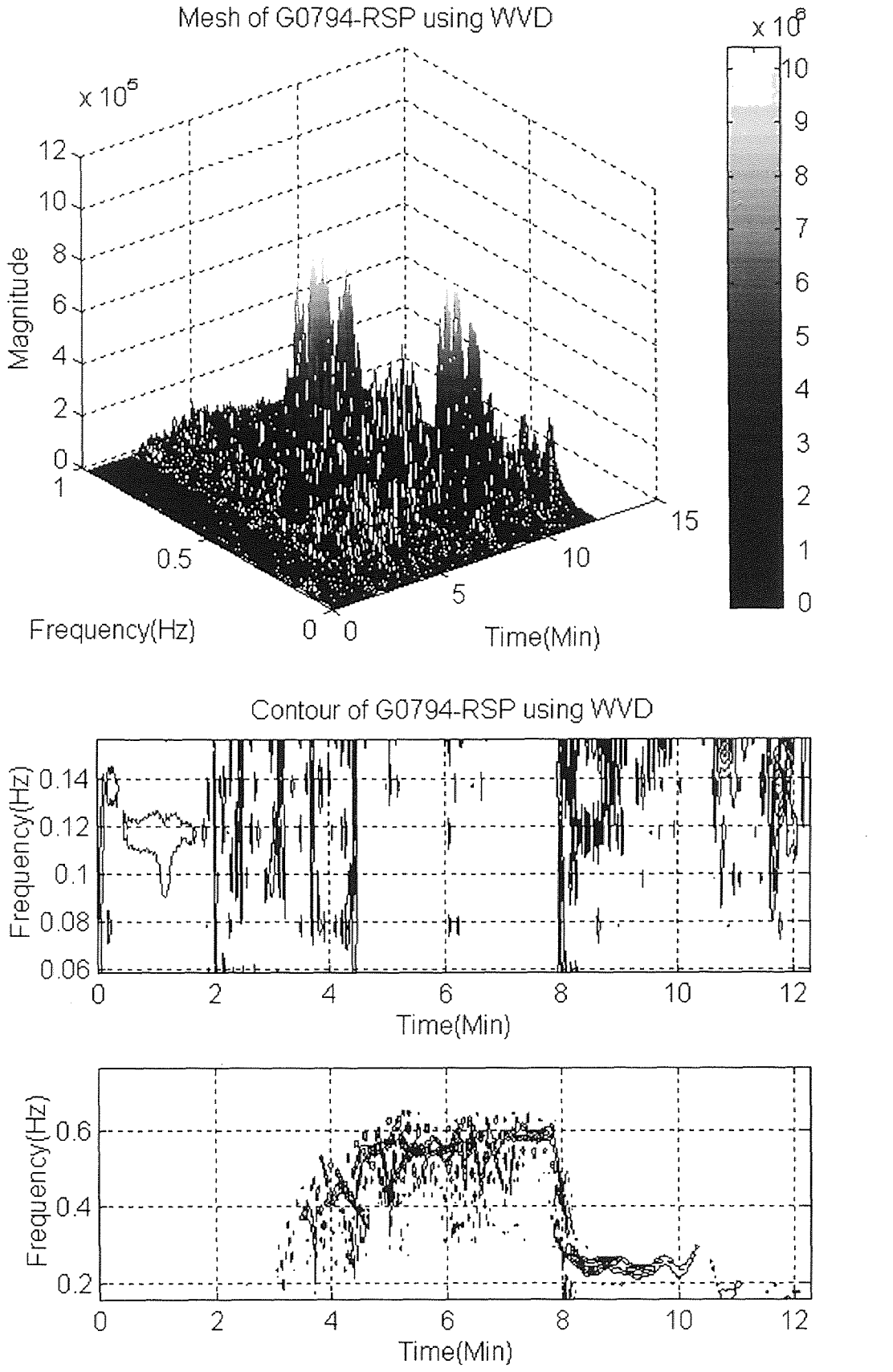

Figure 4.21 Mesh and contour of the WVD of the respiration signal (Subject G0794)

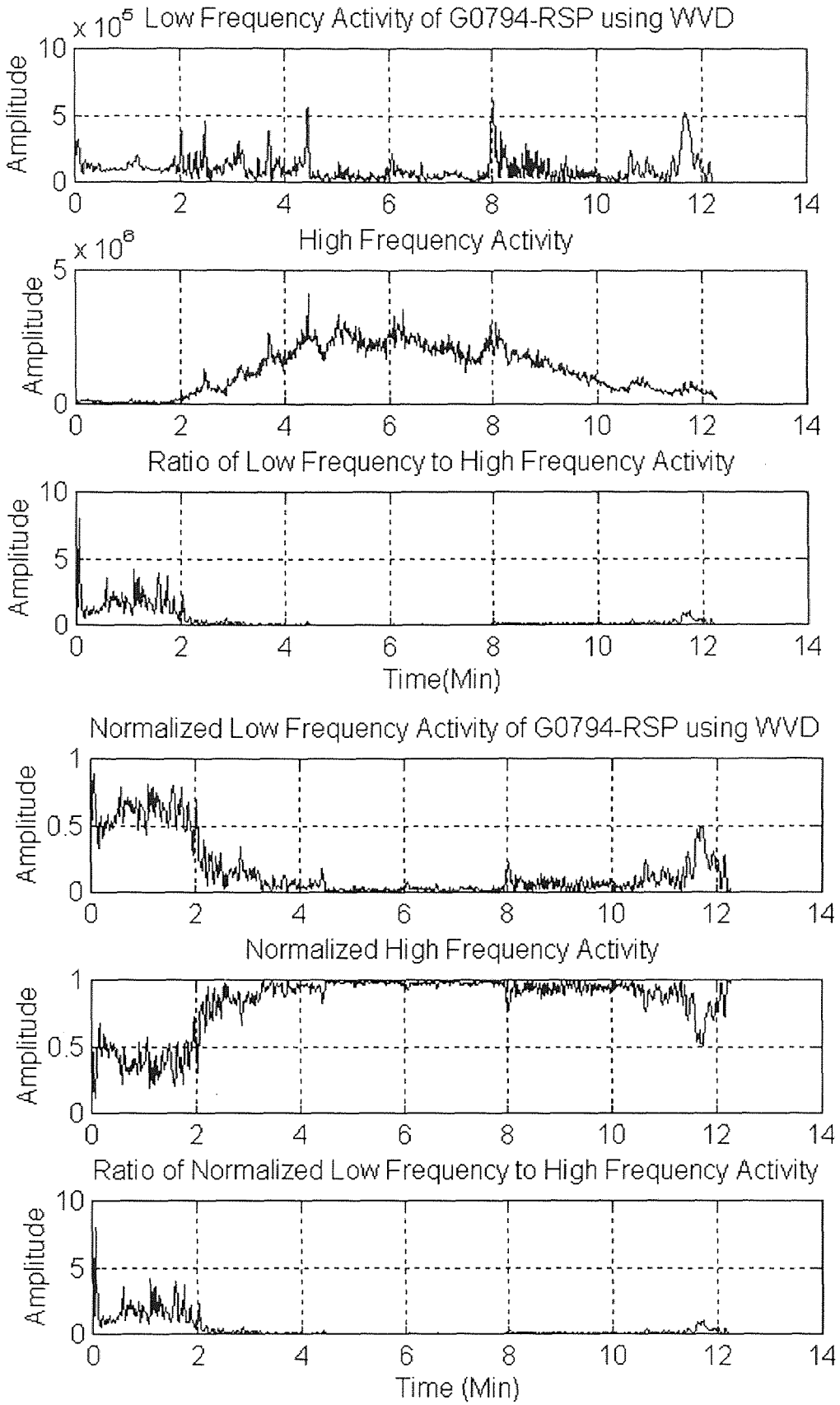

Figure 4.22 LF and HF activity of the WVD of the respiration signal (Subject G0794)

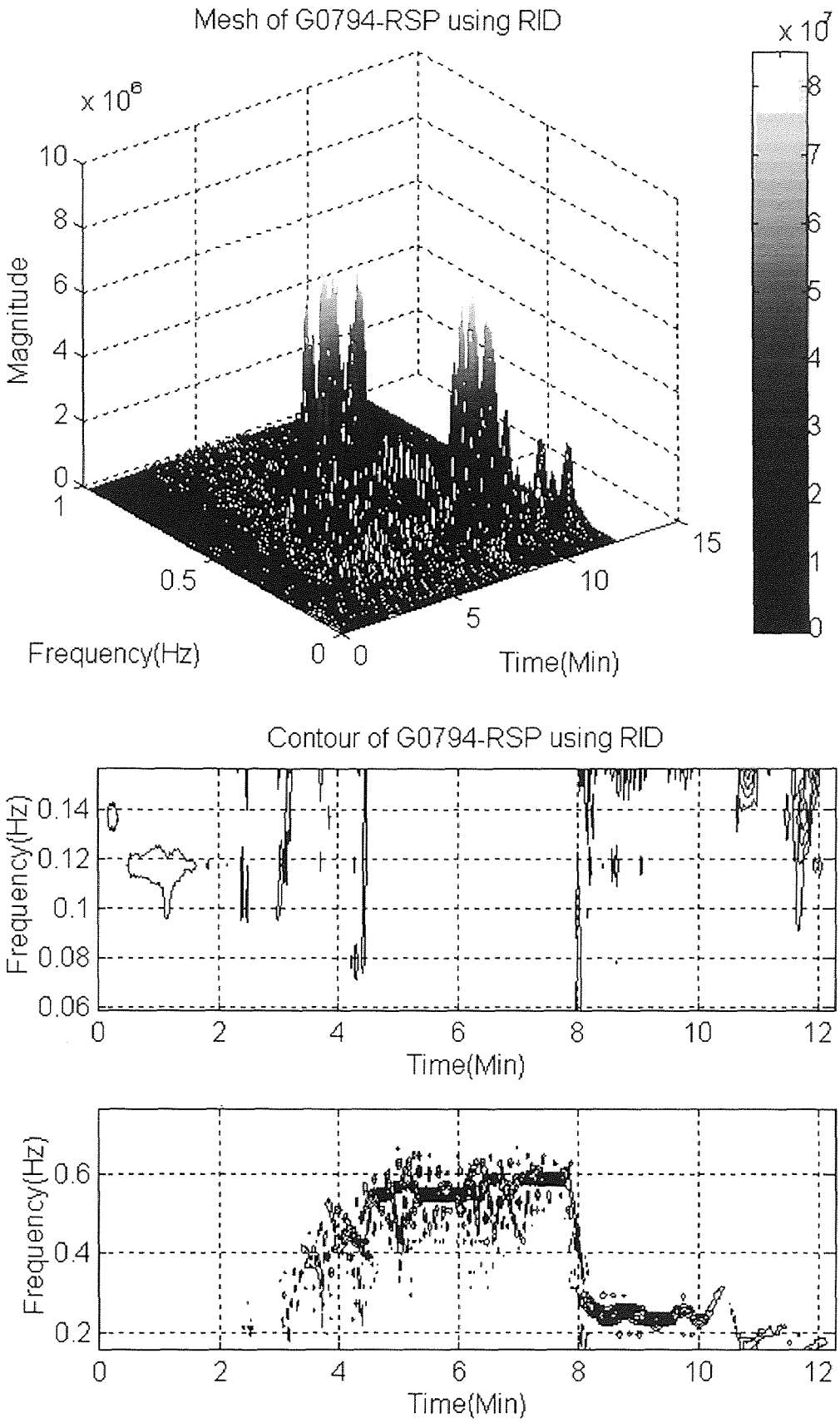

Figure 4.23 Mesh and contour of the RID of the respiration signal (Subject G0794)

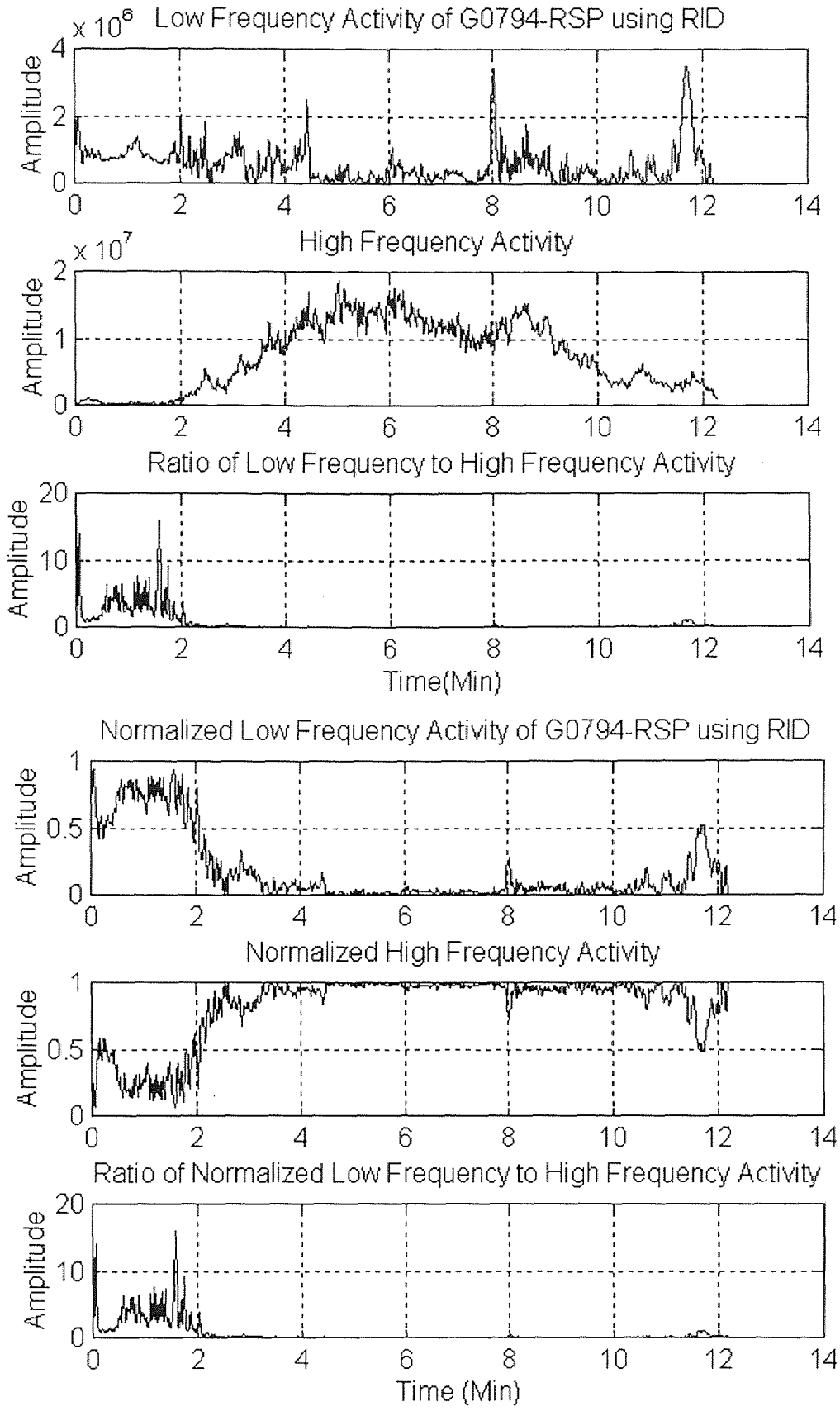

Figure 4.24 LF and HF activity of the RID of the respiration signal (Subject G0794)

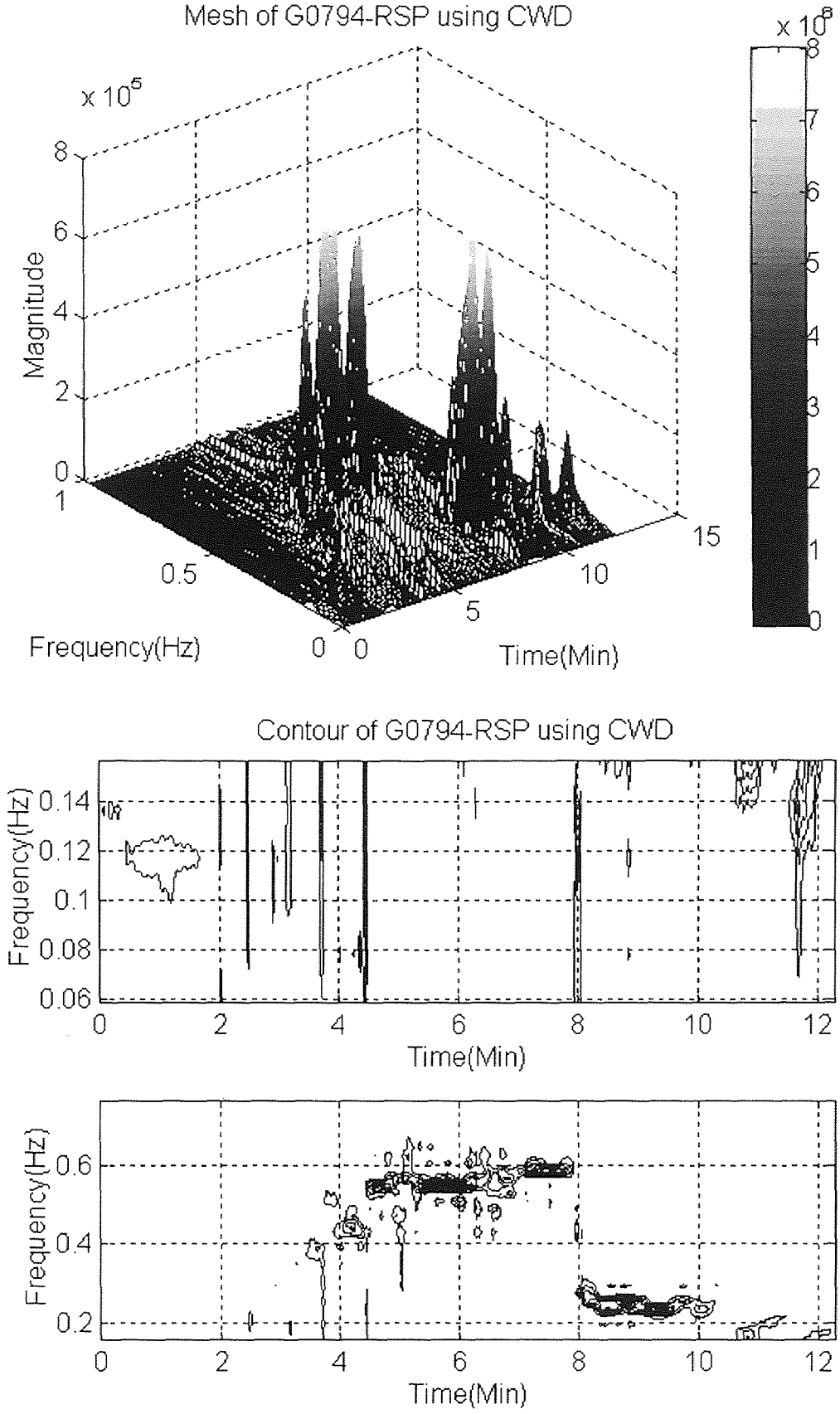

Figure 4.25 Mesh and contour of the CWD of the respiration signal (Subject G0794)

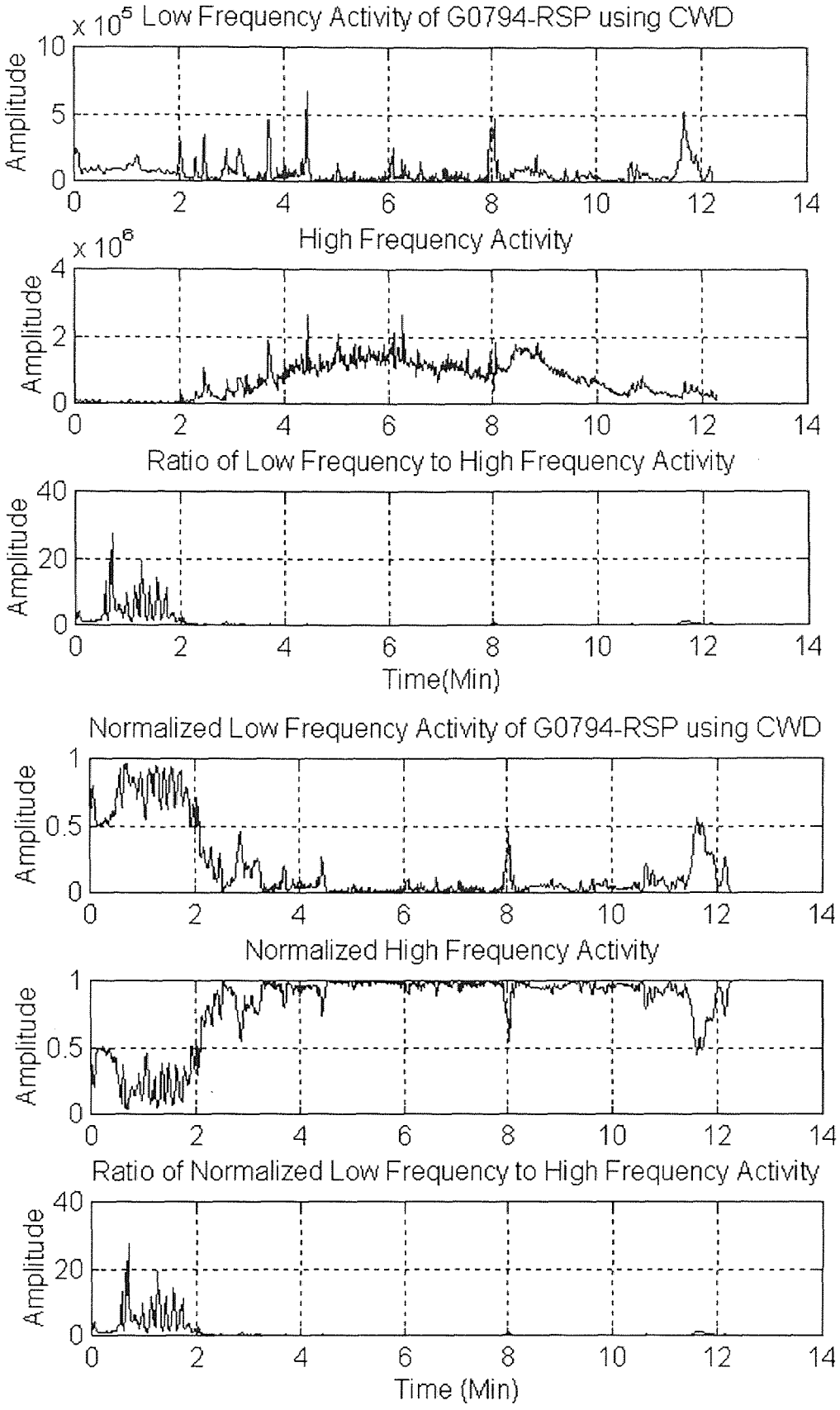

Figure 4.26 LF and HF activity of the CWD of the respiration signal (Subject G0794)

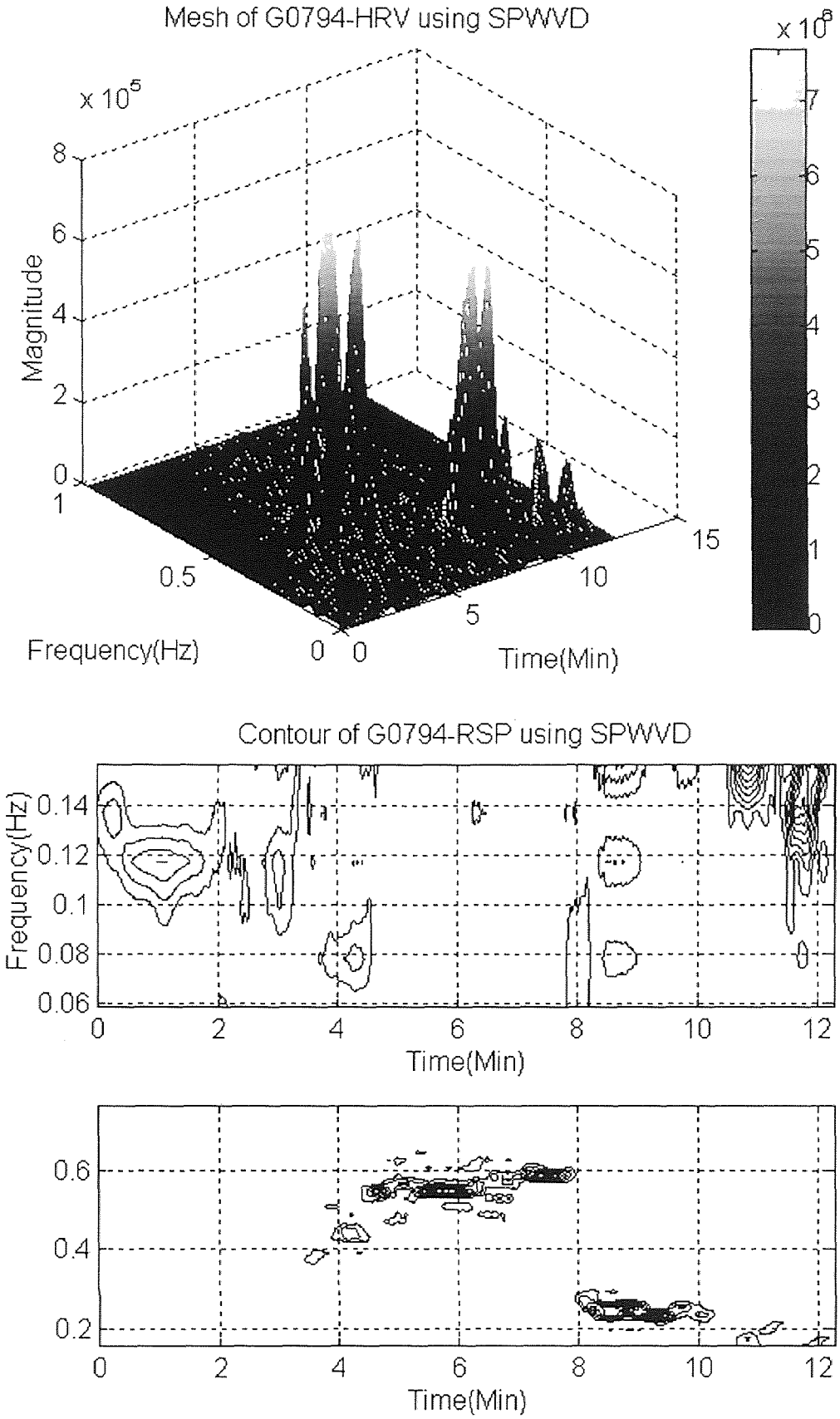

Figure 4.27 Mesh and contour of the SPWVD of the respiration signal (Subject G0794)

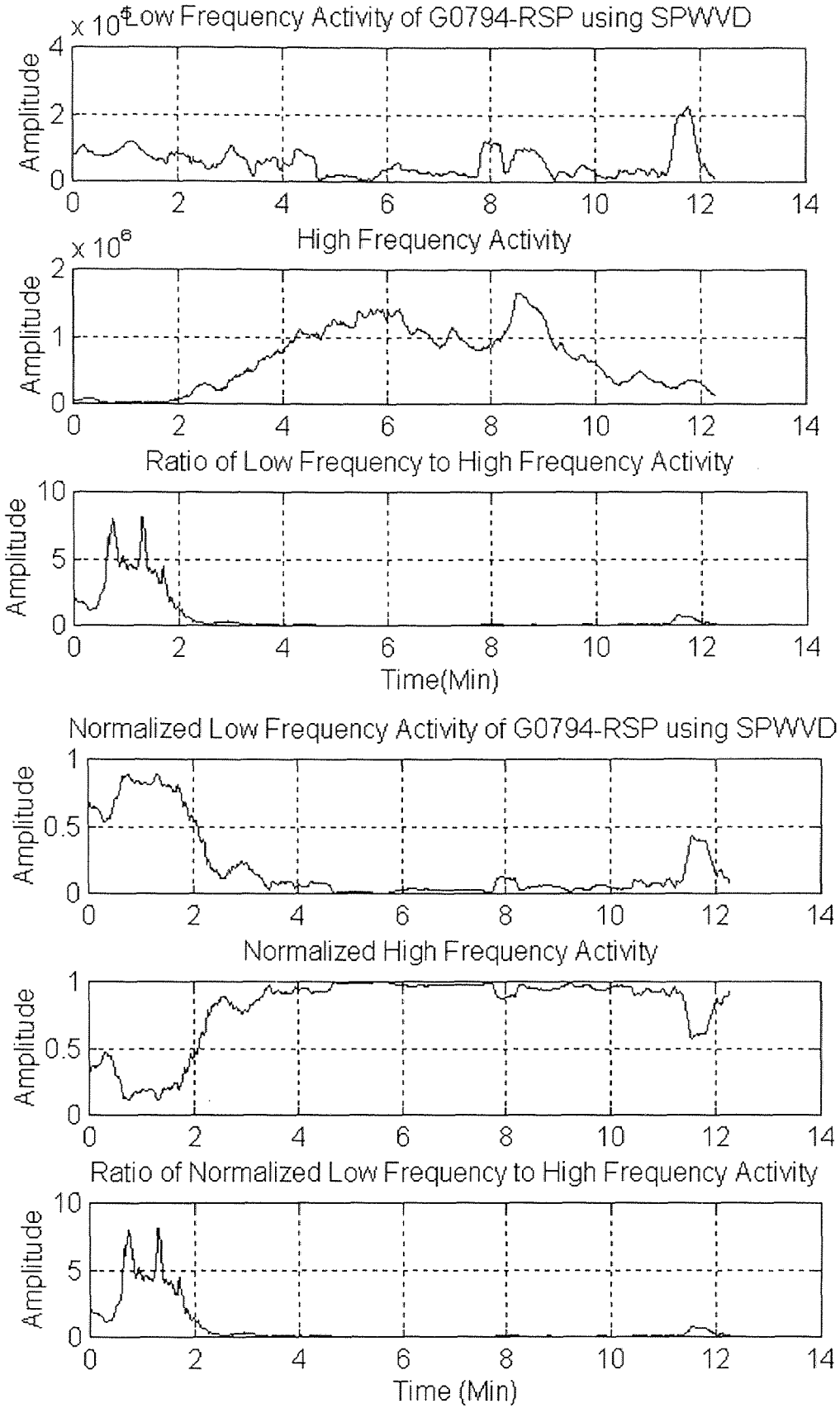

Figure 4.28 LF and HF activity of SPWVD of the respiration signal (Subject G0794)

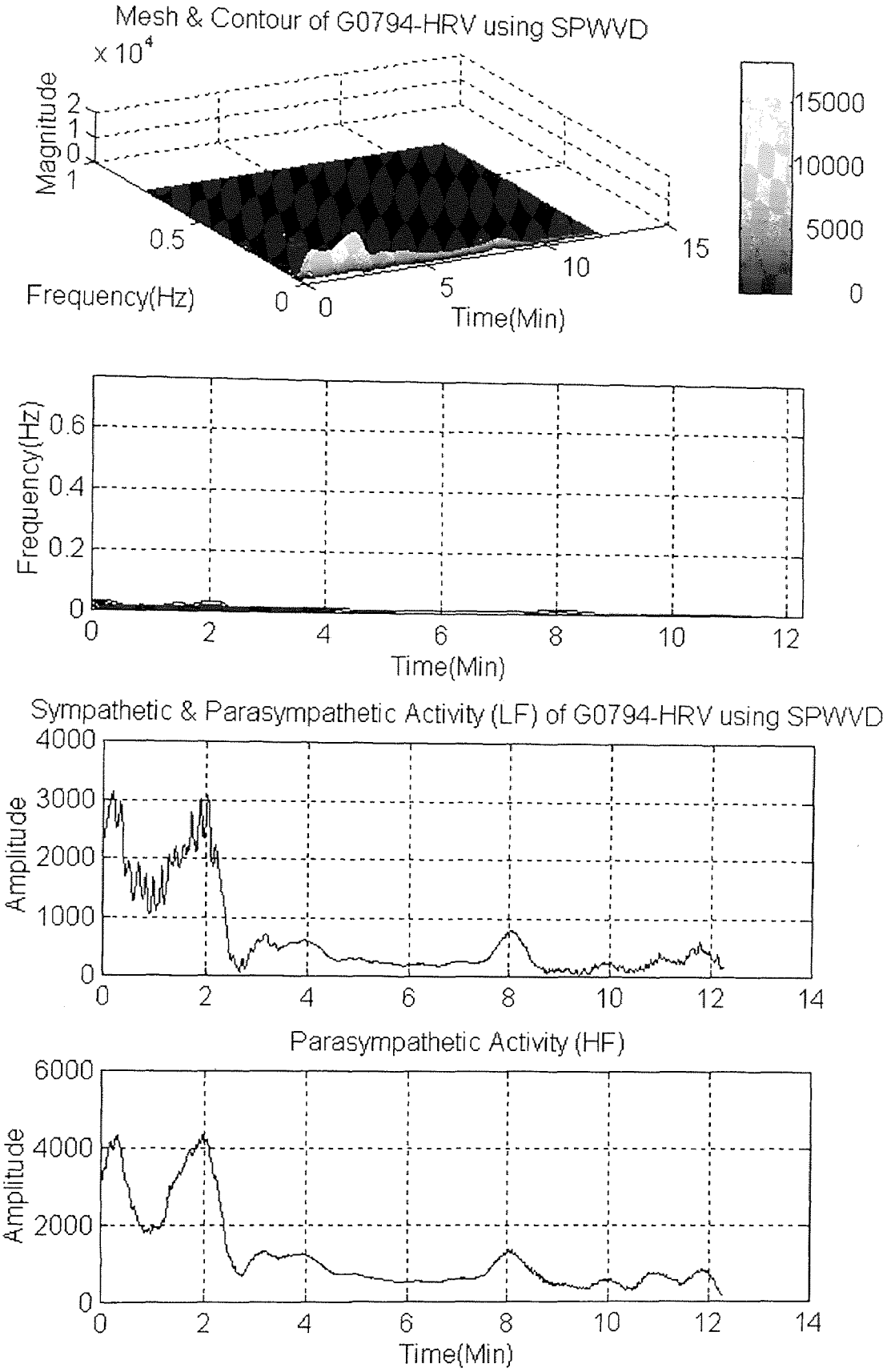

Figure 4.29 Mesh, contour, LF and HF activity of SPWVD of HRV (Subject G0794)

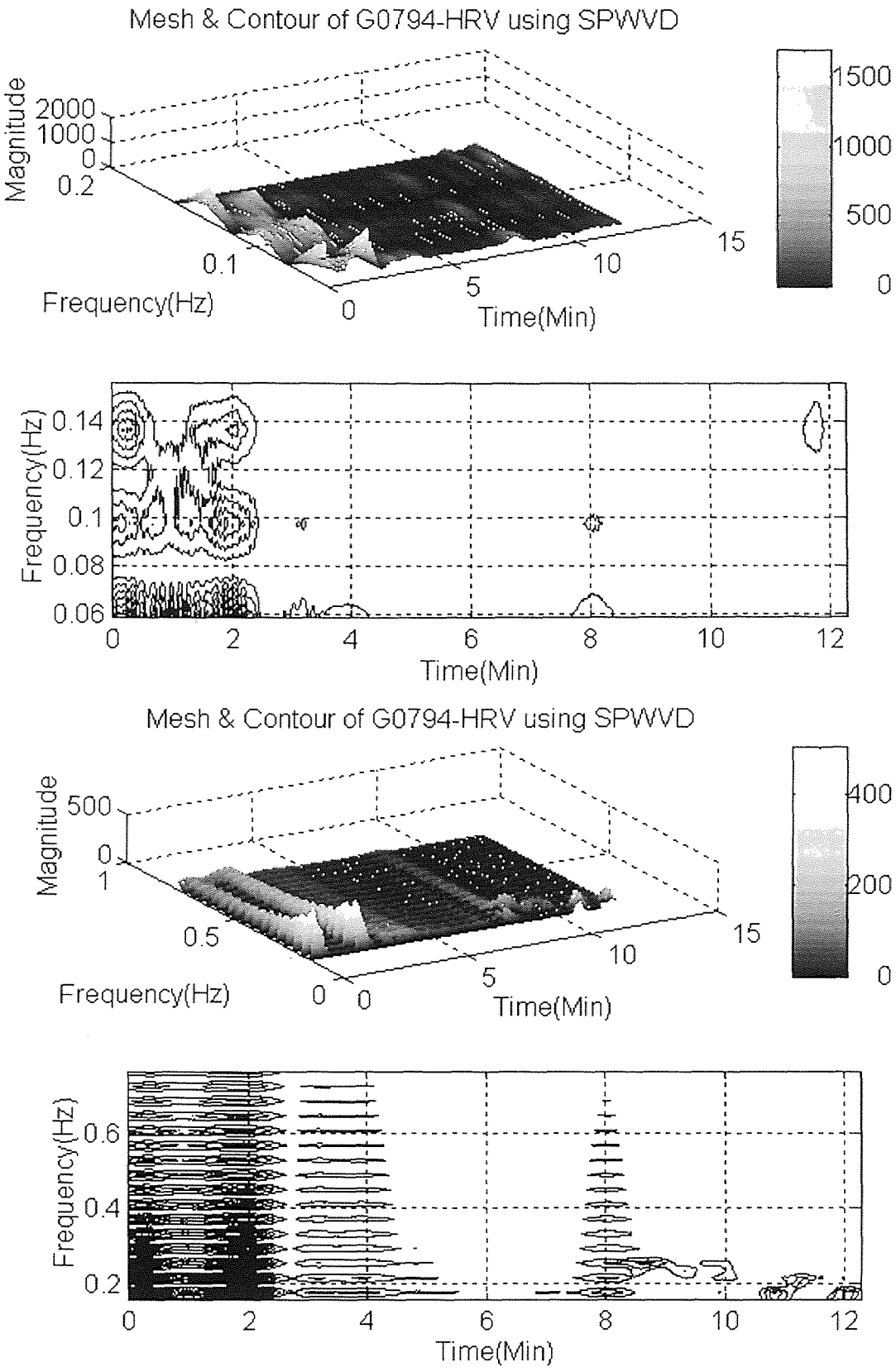

Figure 4.30 Mesh and contour of SPWVD of G0794-HRV showing LF and HF ranges

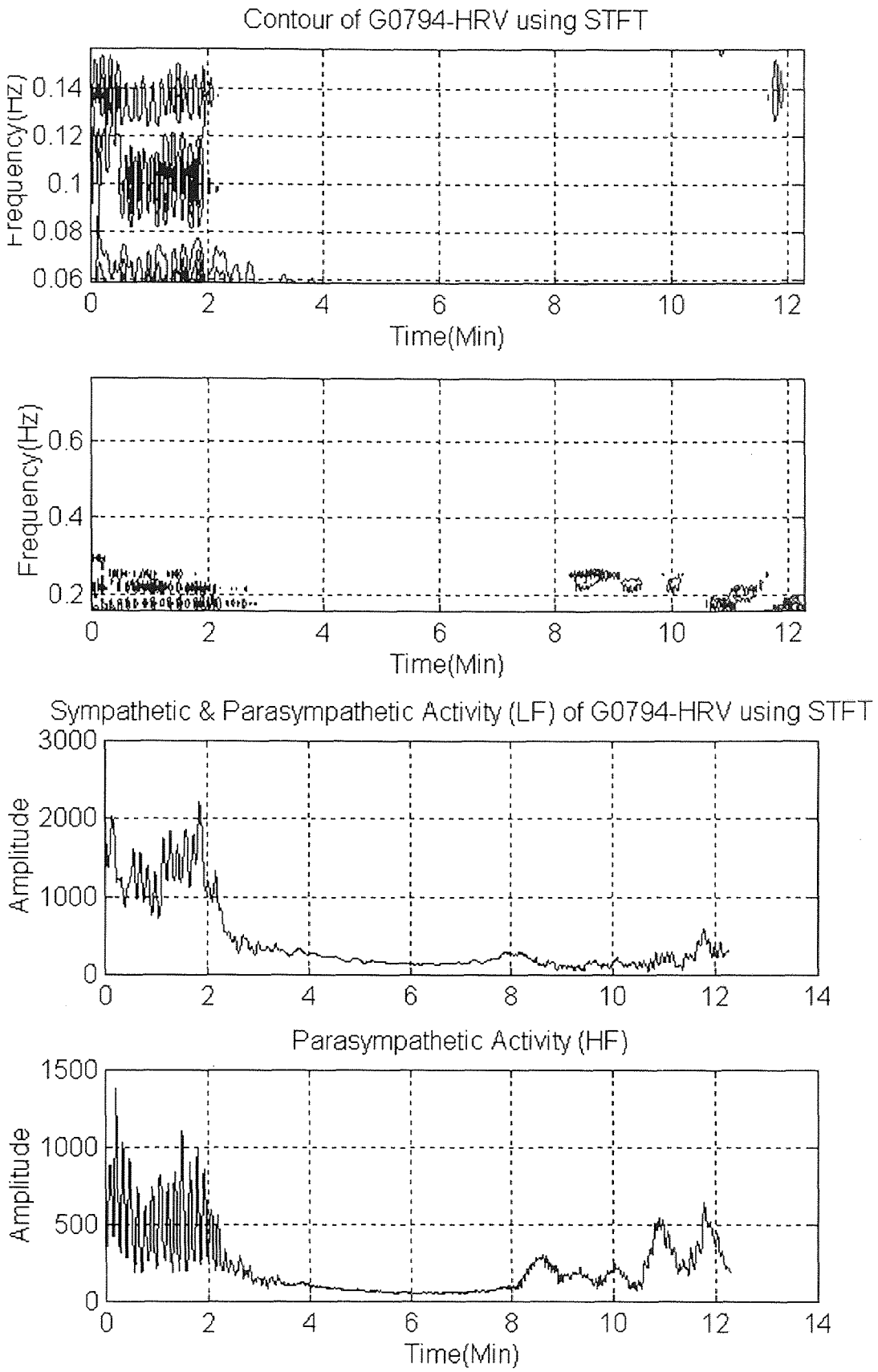

Figure 4.31 Contour, LF and HF activity of the STFT of HRV (Subject G0794)

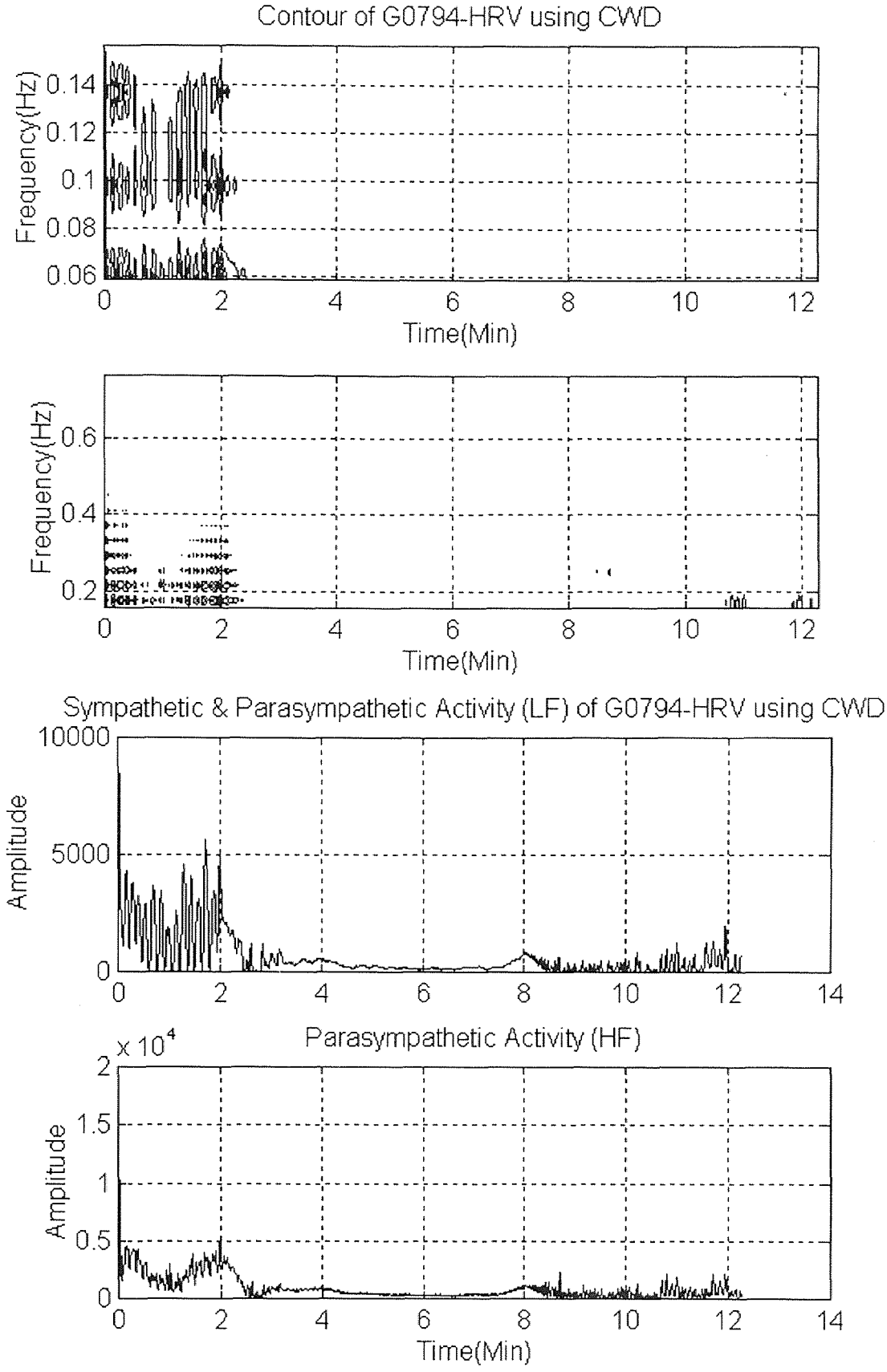

Figure 4.32 Contour, LF and HF activity of the CWD of HRV (Subject G0794)

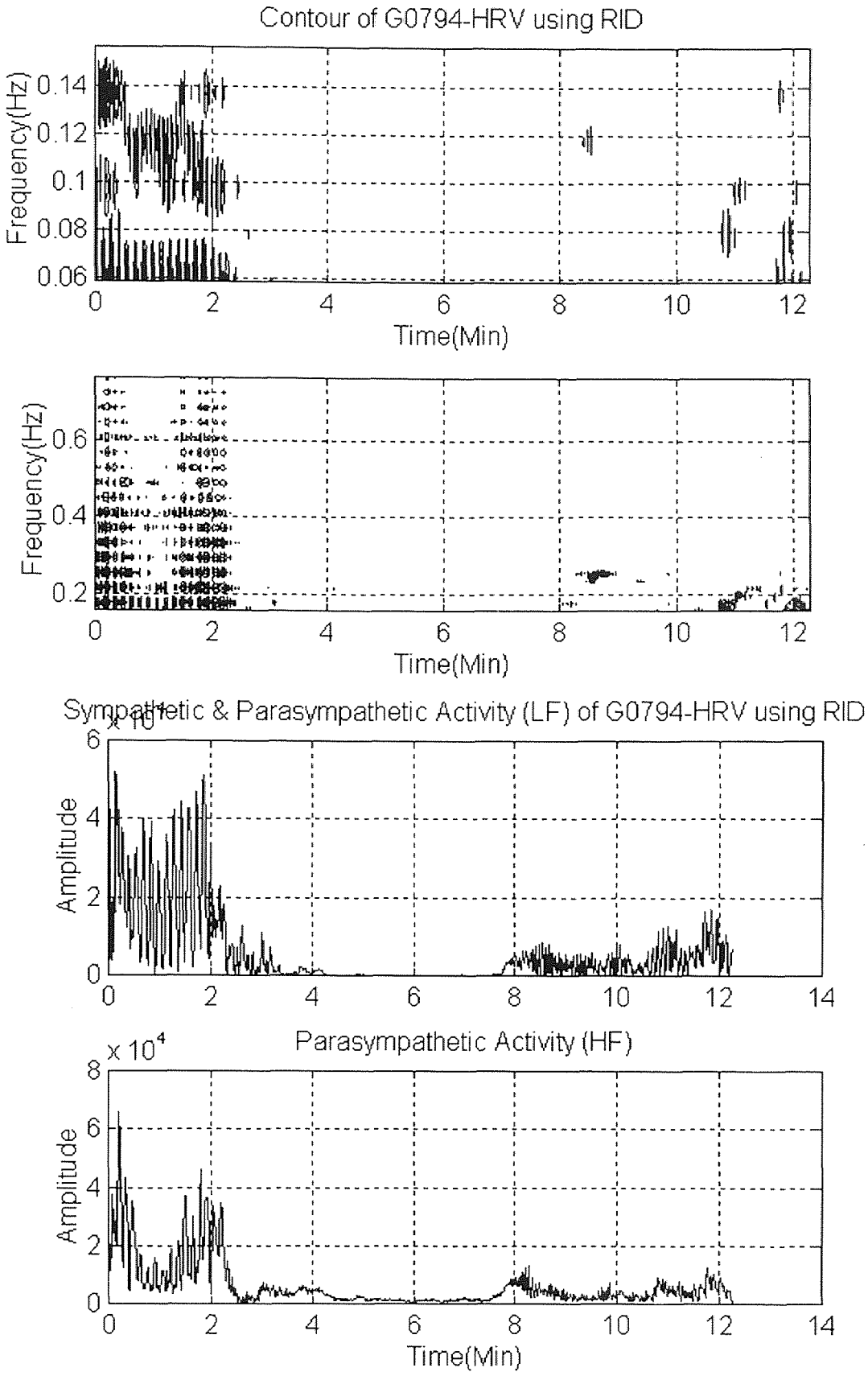

Figure 4.33 Contour, LF and HF activity of the RID of HRV (Subject G0794)

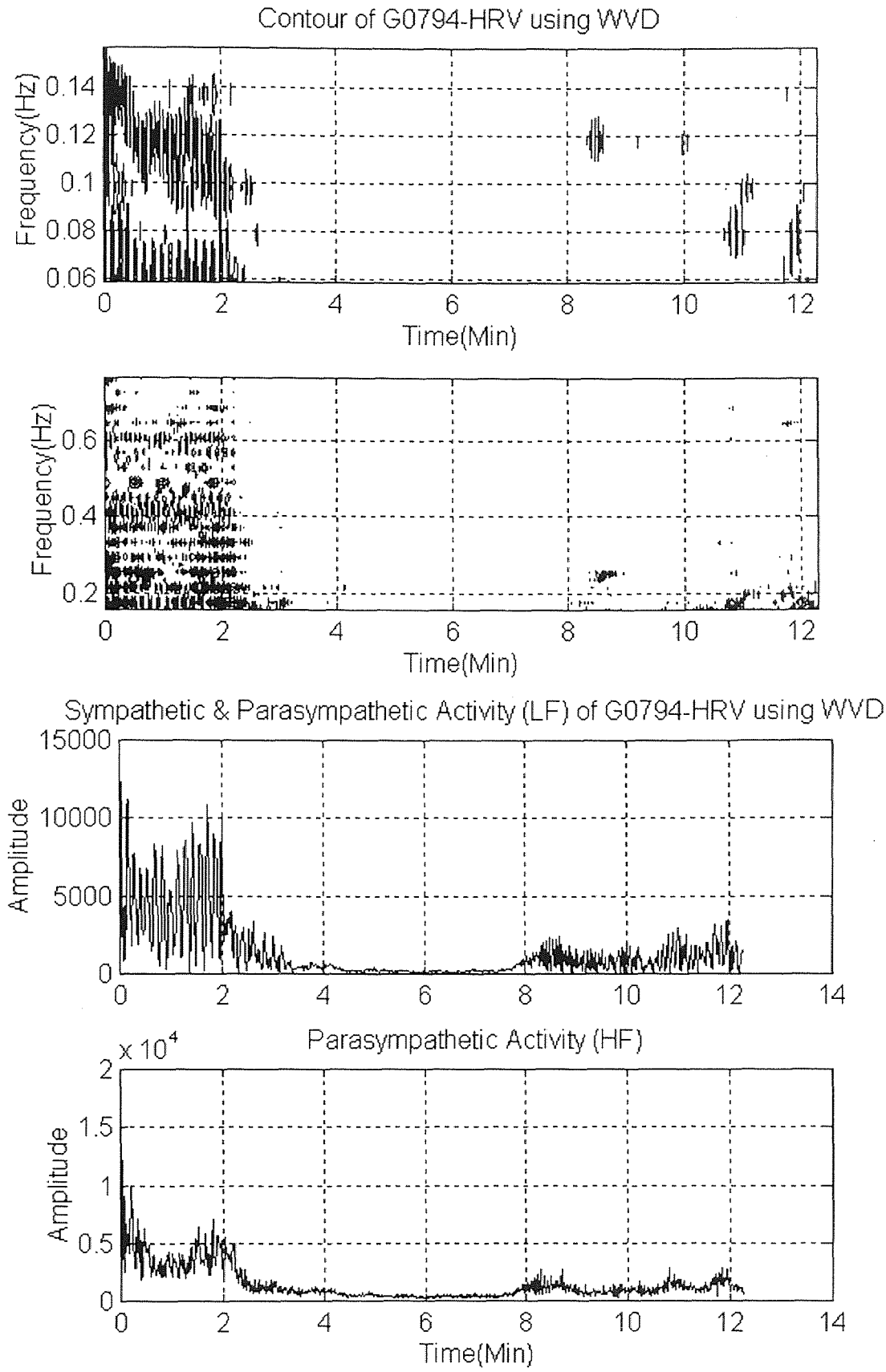

Figure 4.34 Contour, LF and HF activity of the WVD of HRV (Subject G0794)

4.3 Time-Frequency Analysis of the Anticipation Protocol

In this section, the smoothed pseudo Wigner-Ville and the Choi-Williams distributions are used to quantify the changes in the heart rate variability signal during the anticipation protocol. The choice of these distributions stems from the thorough investigation and evaluation performed on the modeled and experimental heart rate variability signals in the previous sections. The main purpose of this investigation is to test for the presence of an anticipatory component due to a stressful exercise condition as reflected in the heart rate variability signal from a change in behavior in the autonomic nervous system, specifically between minutes [15 to 16] and [16 to 17]. The aim in using such a challenging exercise level is also to test the reproducibility of the results of the preliminary study. Thus, we are reassessing whether there is a significant difference in the HRV signal produced by the stressful exercise sessions and whether the transitions between the three main states of rest, exercise and recovery are evident.

4.3.1 SPWVD of Heart Rate Variability

Although both the CWD and the SPWVD were used to analyze the four exercise protocols, this section will only illustrate the results of the SPWVD. The SPWVD has been shown to demonstrate the changes brought about in the heart rate variability signal while presenting a smoother envelope than the CWD results.

Examination of the results for these nine subjects presented a real challenge. As expected, the following study has been very involved. We basically have two unique protocols that are performed twice for each subject under different anticipatory

conditions. There are many factors that can affect the outcome of this investigation that range from the physical fitness that the subjects are in, to the mood or psychological state at the time of the experiment. It also is affected by the personality traits of these subjects, their reactivity within a certain frame of time, the environmental factors, or even the tone of voice or type of instructions the subjects are given. In order to control as many of these variables as possible, many conditions were addressed to maintain homogeneity between subjects. To ensure the severity of the exercise level, all the subjects were tested prior to the experiment and assigned a level of activity that would be tedious enough to present a real challenge but physically manageable at the same time. Also, the experimental setup was done in such a way that the subjects were always facing away from the hardware and the experimenter to eliminate any possible anticipatory affect due to distraction or what is commonly referred to as white coat syndrome. The participants were all read the same text to inform them about the nature of the experiments and time involved. Caffeine, food intake, and smoking along with other variables were also controlled. However, with all this cautionary measures taken into account, we note that not all the subjects behaved in the same manner.

Comparing the nine subjects across all protocols, we note that the most striking finding relates to a definite change at minute 16 in response to the experimenter intervention, regardless of the message relayed in the information provided. As will be demonstrated below with a typical sample response, most subjects reacted to the voice after 8 minutes of silence for most protocols. That does not indicate in any way that they all reacted in the hypothesized way. Most subjects were able to illicit the proper response

for some sessions but not consistently for all four protocols (A1 through B2). Examining the different protocols separately for the 9 subjects, we note that protocol A1 shows more than half the subjects responding in a relative increase in the normalized LF power, which is a representative of a mixture of sympathetic and parasympathetic activity, relative to the normalized HF power, which is a representative of parasympathetic activity. However, the reproducibility of this response is not as evident in the second protocol A2, under the same conditions and even for the same subject. With the introduction of exercise, two factors can play an important part in explaining the physiology of the system. There is the increase of sympathetic activity due to the stress introduced by the physical challenge, and at the same time there is an accompanied increase in the frequency of respiration which occurs in the region indicative of the parasympathetic activity. These two factor may show either an increase in the low frequency activity relative to the parasympathetic activity, or visa versa. Thus, different subjects may react differently to the same situation, or even the same subject may illicit different response at a different time or day depending on the range of factors from his state of mind to the state of physical condition at that moment. This whole interplay makes it very difficult to make a definite conclusion about the physiology of the system especially with such a small group of participants.

The same deduction can be carried through in the second set of protocols B1 and B2. Most subjects responded to the verbal intervention at eight minutes into the recovery session after the first bout of exercise, regardless of what was said. Some subjects displayed a decrease or no change in the normalized LF activity between minutes 16 and

17, relative to the parasympathetic activity. Others, or sometimes the same subject will illicit the opposite response the second time in protocol B2. Note that the majority of the subjects reported that they didn't anticipate to start exercising again in protocol B2.

Figures 4.35-4.38 display the raw and detrended heart rate variability data for one of the subjects that participated in this pilot study (S0795). Note that both protocols A1 and B1 are 24 minutes long while protocols A2 and B1 are 18 minutes as expected. Looking at the raw data itself and comparing across the same protocols, (A1 B2) and (A2 B1), we note that the signals vary slightly. However, they all validate the findings relayed in the previous section. There is a definite change in the HRV signal attributed to the tedious exercise between the three states of rest, exercise and recovery. Also, even with allowing a 10 minute resting recovery period between minutes 8 and 18, the heart rate variability signal never recovered to its original resting phase.

Figures 4.39-4.41 show the results of the application of the SPWVD to the heart rate variability for the first protocol A1. Figure 4.39 displays the mesh and contour plots for the low frequency and high frequency regions respectively. They show that most of the power in the 3-D time dependent spectra is concentrated in the first two minutes of rest and especially in the low frequency region. This is further displayed in the increased magnitude scale in the LF spectrum. Figure 4.40 shows the mesh and contour plots of the corresponding LF and HF regions for the two minutes (15-17) of interest. Note that now we can see clearly the activity in this time interval since they are displayed without the presence of the much higher first two minute magnitude. The LF activity still demonstrates a higher magnitude. Figure 4.41 presents the LF and HF activity as the

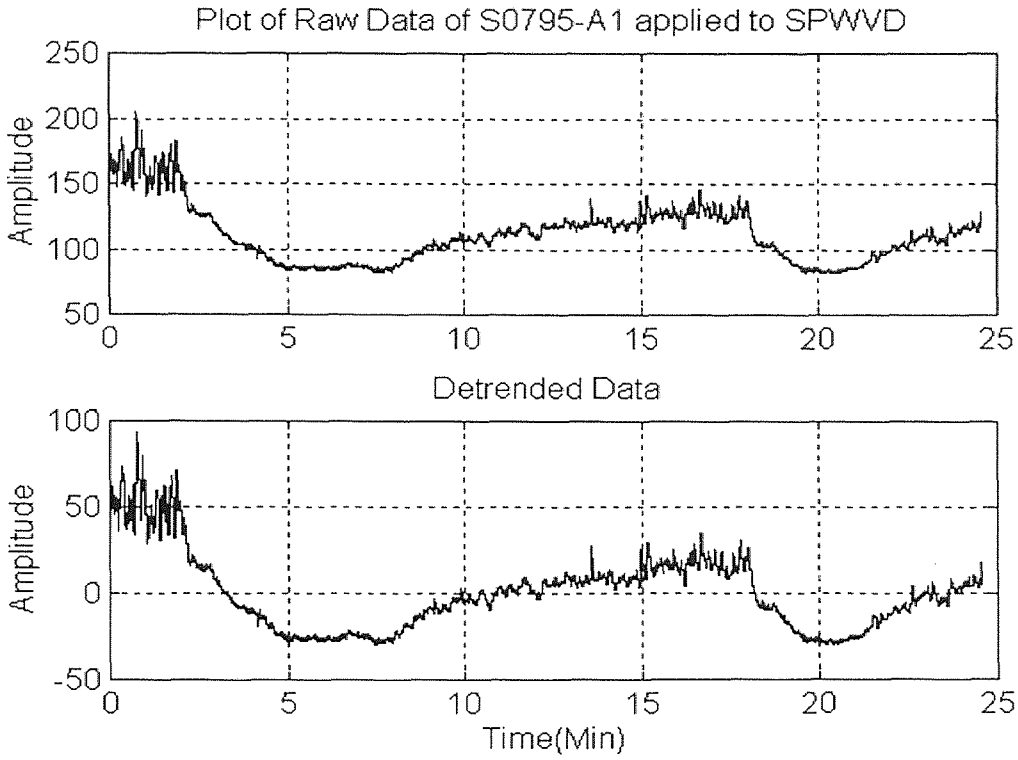

Figure 4.35 The raw and detrended HRV signal for subject S0795 protocol A1

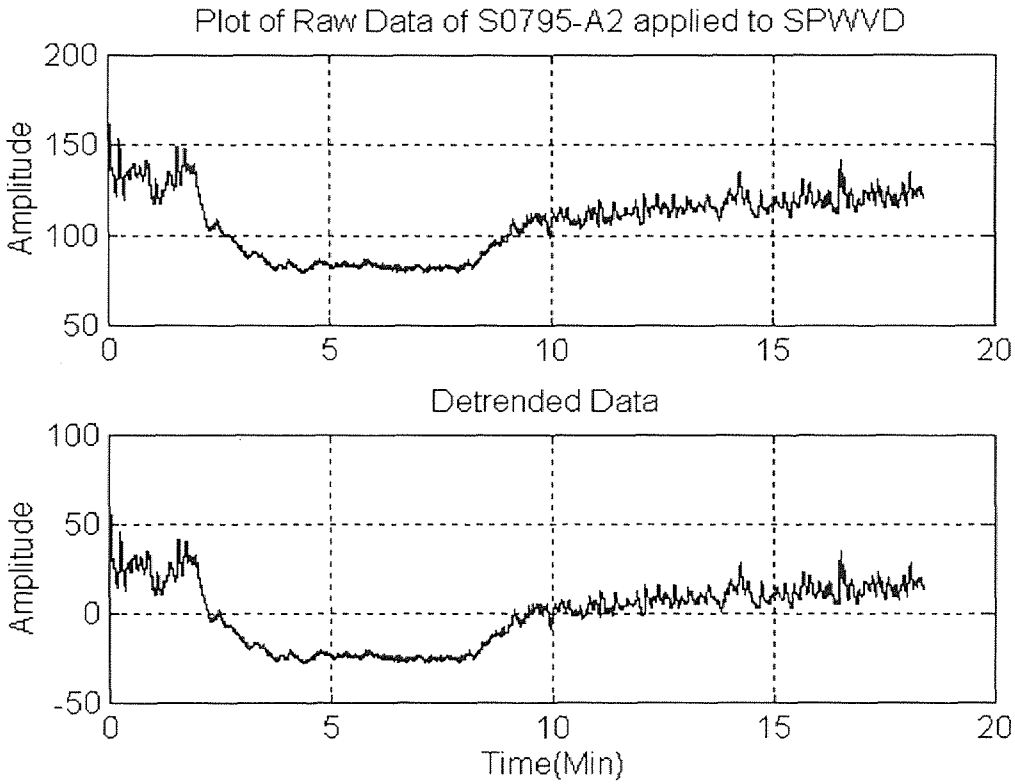

Figure 4.36 The raw and detrended HRV signal for subject S0795 protocol A2

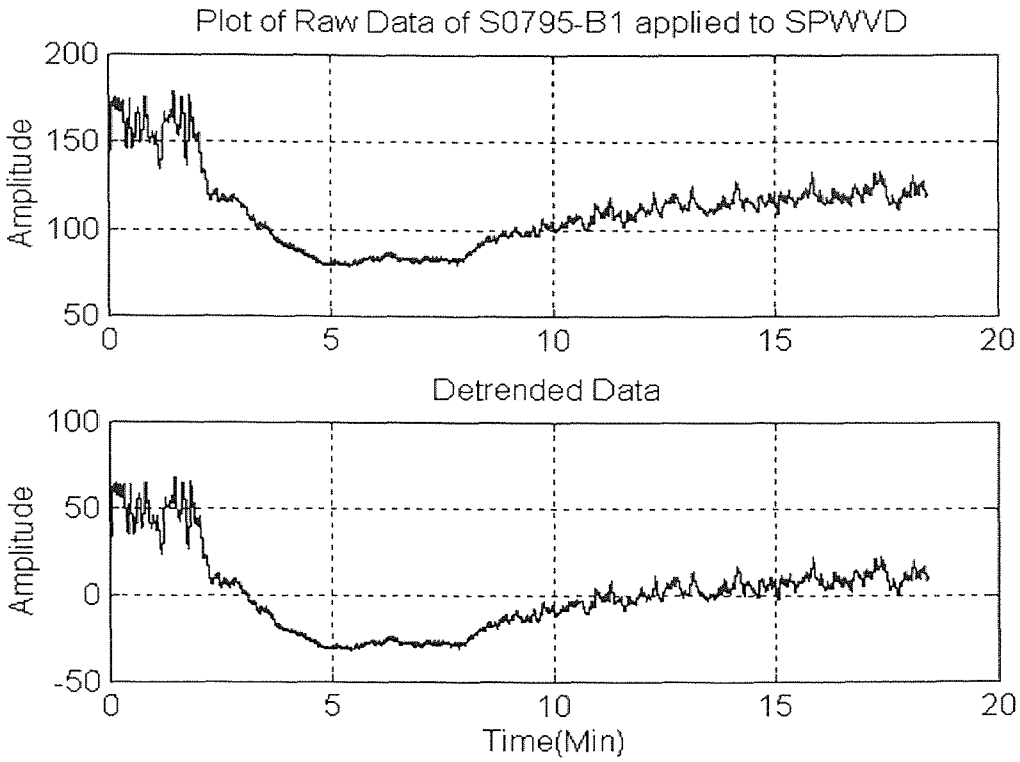

Figure 4.37 The raw and detrended HRV signal for subject S0795 protocol B1

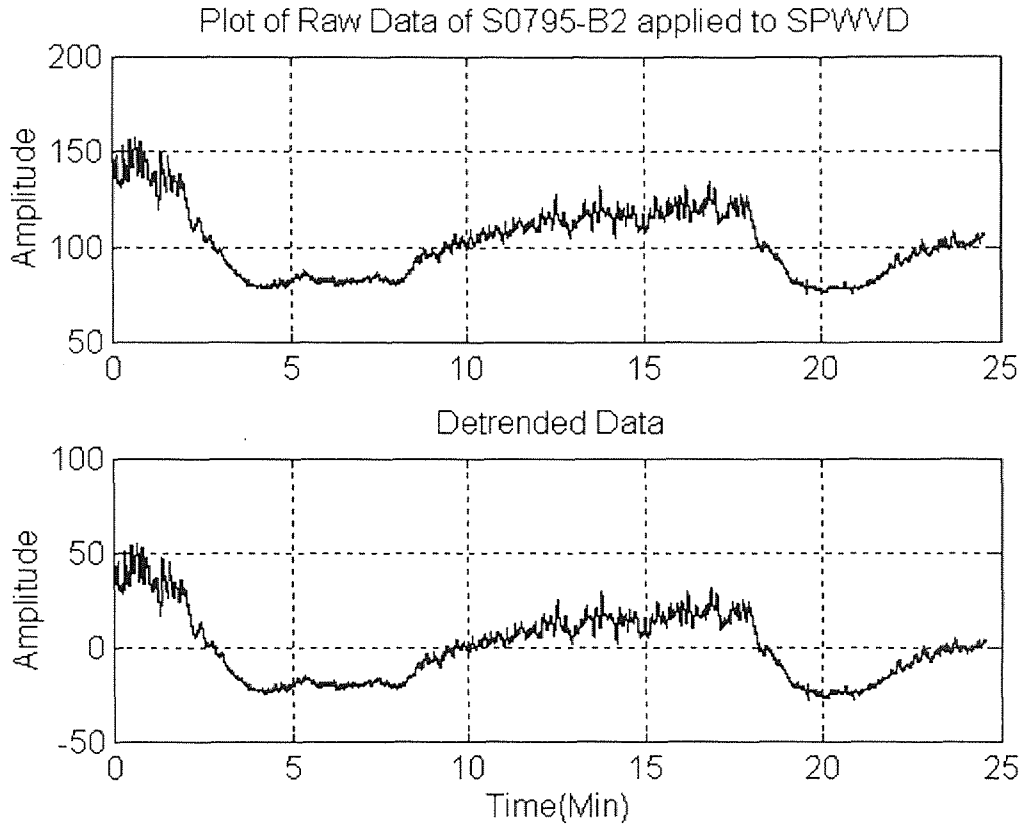

Figure 4.38 The raw and detrended HRV signal for subject S0795 protocol B2

quantitative area for the two frequency regions at each time obtained from the SPWVD spectrum. The first three plots display the results for the whole duration of the experiment while the latter three show the normalized activity for the particular area of interest. Note the increasing trend in the normalized LF activity relative to the parasympathetic (HF) activity at minute 16. The same conclusion can be deduced from looking at the sympatho-vagal balance, the ratio of the LF to HF activity, which shows an overall increase in sympathetic activity right after minute 16 when the subject was told about the second exercise session. This subject demonstrates the sympathetic anticipatory response and the reactivity to the information relayed in the message. Figures 4.42 and 4.43 reflect the same results obtained for protocol A2. Looking at Figure 4.43, we note that at minute 16, the normalized LF activity demonstrates an increase in the mixture of sympathetic and parasympathetic activity relative to the normalized parasympathetic activity (HF). The increase in sympathetic activity reflects the anticipation effect also demonstrated in the sympatho-vagal balance.

Figure 4.44 displays the mesh and contour plots of the SPWVD reflecting the LF and HF activity during minutes 15 to 17. Looking at the normalized LF and HF activity plots in Figure 4.45, we see a decreasing trend of the normalized LF activity at minute 16 relative to an increasing trend in the normalized parasympathetic activity. The sympatho-vagal balance also shows an immediate decline in the sympathetic activity right at minute 16 as reflected in the decreasing trend in the ratio. This shows that although the subject was alerted to the intervention at minute 16, he was able to react immediately to

the message relayed and was relieved to hear about the termination of the experiment, thus reflecting no anticipatory response as hypothesised. However, the same can not be said about the reactions of this subject to protocol B2. On the contrary, it reflects the case when the same subject was not able to illicit a similar response for the identical message relayed at minute 16 for the same set of experiments. This is clearly demonstrated in Figures 4.46 and 4.47. We note that in this particular subject, the normalized LF and HF activity do not change at minute 16. This indicates that the subject did not respond either way to the information announced at minute 16.

This demonstration of the results reflects the change in a particular individual that reacted , in most cases, in a manner similar to the original hypotheses. However, the same can not be exactly reproduced in the remaining eight subjects. Some of them reacted the same in one or two protocols, but not in all. This emphasizes the point that this pilot study does not show a significant change because of the small sample size.

4.3.2 Statistical Analysis of the Heart Rate Variability Signal

In order to test the presence of a change in behavior in the HRV signal due to the anticipation of the vigorous exercise, statistical analysis was also performed by comparing data from minute 16 [min 15 to 16] to that of minute 17 [min 16 to 17]. These particular time intervals were chosen because they included minute 16, the time at which the experimenter intervened to illicit a particular response from the subject. In protocol A1, the subjects were told that they would be asked to exercise for a second time after minute 18; the reminder came exactly at minute 16. The hypothesis was that, since the

exercise level was so strenuous, the subject would dread repeating it. This stress would induce an anticipatory effect that would be reflected as a change in the HRV signal, either in mean heart rate, or variability, or both. We expected a similar reaction in protocol A2, since the subject had no prior knowledge that the exercise session would not take place. In protocol B1, the subjects were told that they would perform the exercise session only once. At minute 16, they were reminded that the experiment would terminate in 2 minutes. The hypothesis was that no anticipatory effect should be detected, which would imply either no change in HRV or actually an increase in HF activity because the unpleasant stress would not be present. We expected a similar reaction to protocol B2 since the subject had no prior knowledge that he would be required to undergo a second bout of exercise starting at minute 18.

In order to perform our comparisons, the difference in average heart rates, the ratio of variations in heart rate, and the difference in slopes of a straight line fit to the heart rate were calculated for minute 16 and minute 17. For each test, 36 observations were compared for the 4 protocols across the 9 subjects. Assuming the observations for each of the 9 subjects were independent, a repeated measures analysis of variances (ANOVA) was performed. No significant differences between the mean heart rates and slopes of heart rate were found at the 5% significant level. The ratio of variances in heart rate before and after the intervention at minute 16 was not significantly different from one. A second attempt compared the difference in average heart rate and the ratio of the variability in heart rate for the 9 subjects for each protocol separately. No significant

differences from 0 or 1, reported at the 5% significance level, were found for the mean heart rate and the ratio of heart rate variation respectively.

Because the heart rate measures indicated a stochastically changing mean level, another approach was used to test for significant differences in the variability in measured heart rate from one time period to the next for each subject and protocol separately. The differences in observed heart rate variability were calculated for all the sample points between minutes [15-16] and minutes [16-17] in an attempt to remove the non-stationarity in the levels. Analysis of the sample autocorrelations of the differenced data showed no significant correlation, indicating that the differenced sample data could be considered to be independent. A test of equality of variances was performed for each of the 9 subjects for the 4 protocols separately using the sample variance of the differenced sample data at minute 16 and 17. For 28 of these experiments, a significant difference in the variability during minute 16 and minute 17 was detected. This strongly indicates that the intervention at minute 16 produced a definite change in most subjects for most protocols. Five of the trials for which no reaction was detected were for protocols B1 and B2, when no change was expected.

These results indicate that subjects responded to the intervention at minute 16. However, along with the time-frequency findings, it suggests further that it didn't matter in most cases words were used. The mere fact that the experimenter gave instructions after eight minutes of silence was enough to illicit a reaction in the majority of the cases. The reactivity to the information carried in these words was then an after effect in most cases.

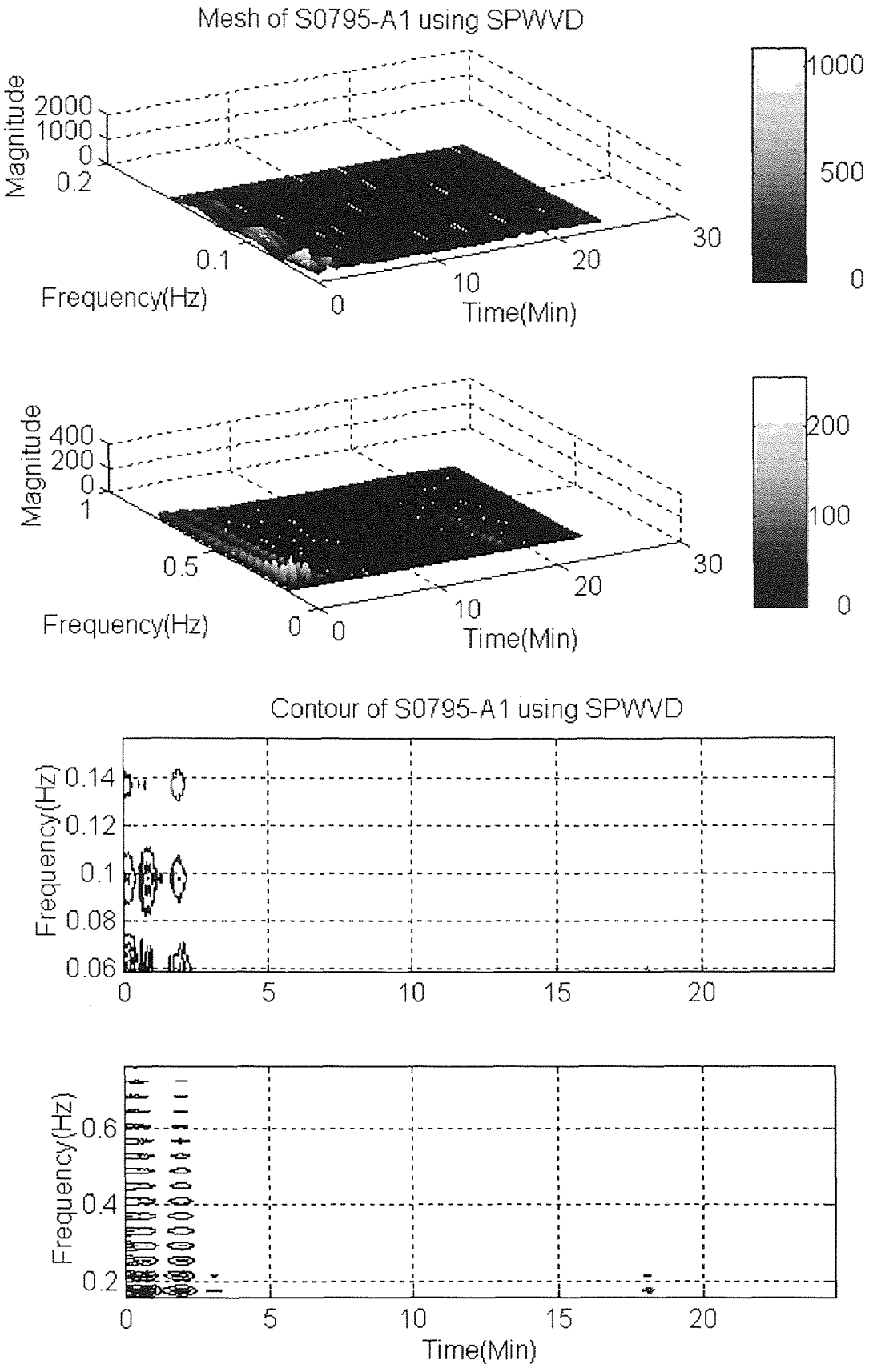

Figure 4.39 Mesh and contour of SPWVD of HRV of subject S0795 protocol A1

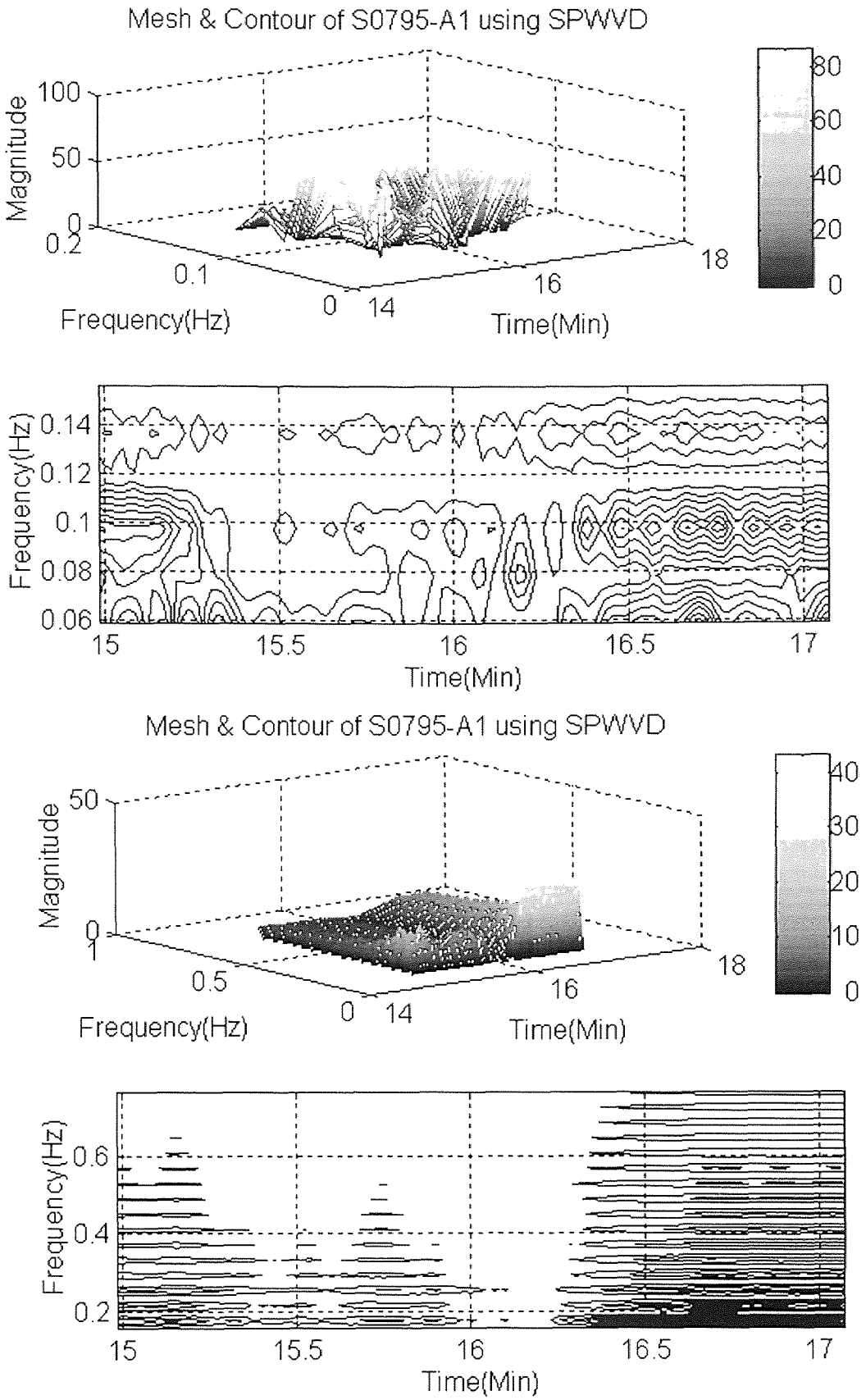

Figure 4.40 Mesh and contour of SPWVD (min15-17) of subject S0795 protocol A1

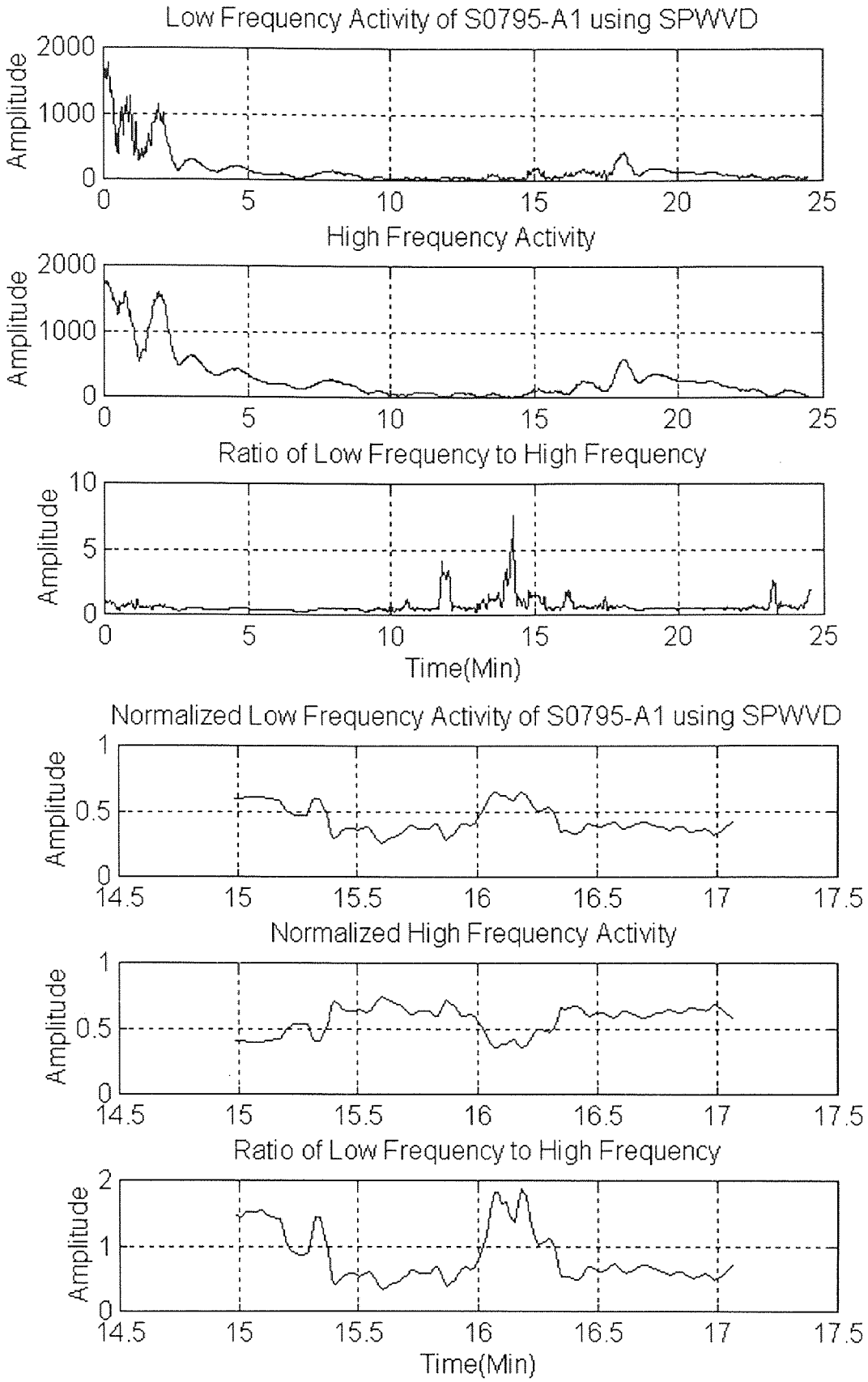

Figure 4.41 LF and HF activity of SPWVD of HRV of subject S0795 protocol A1

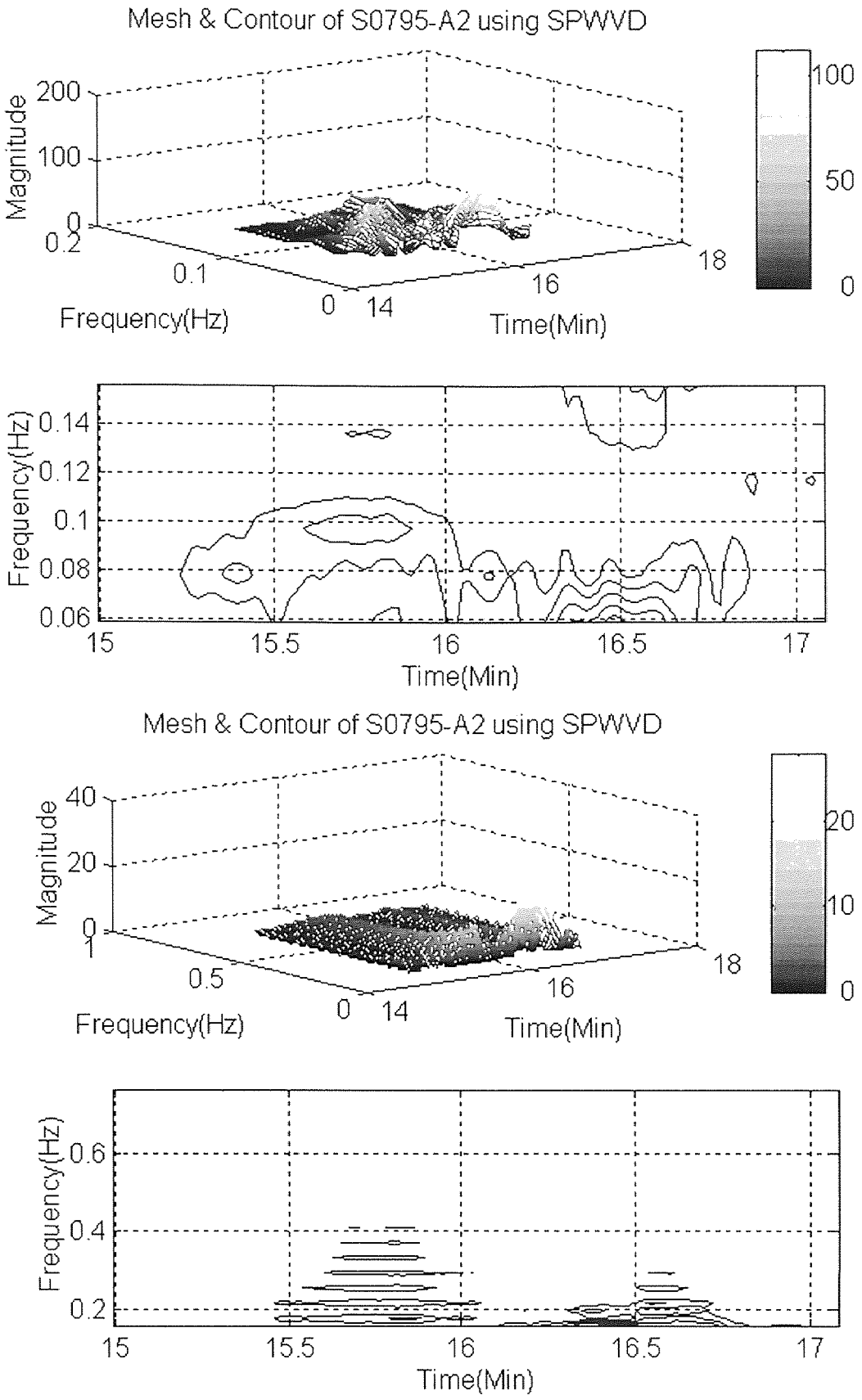

Figure 4.42 Mesh and contour of SPWVD (min15-17) of subject S0795 protocol A2

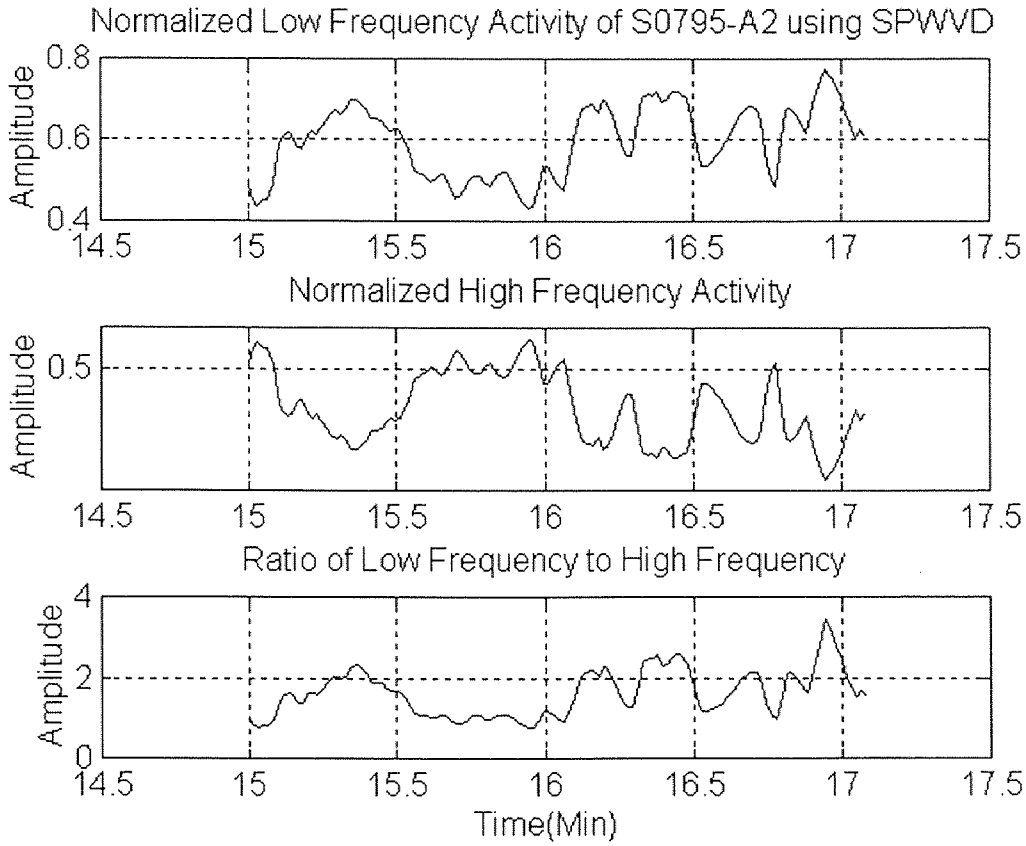

Figure 4.43 LF and HF activity of SPWVD of HRV of subject S0795 protocol A2

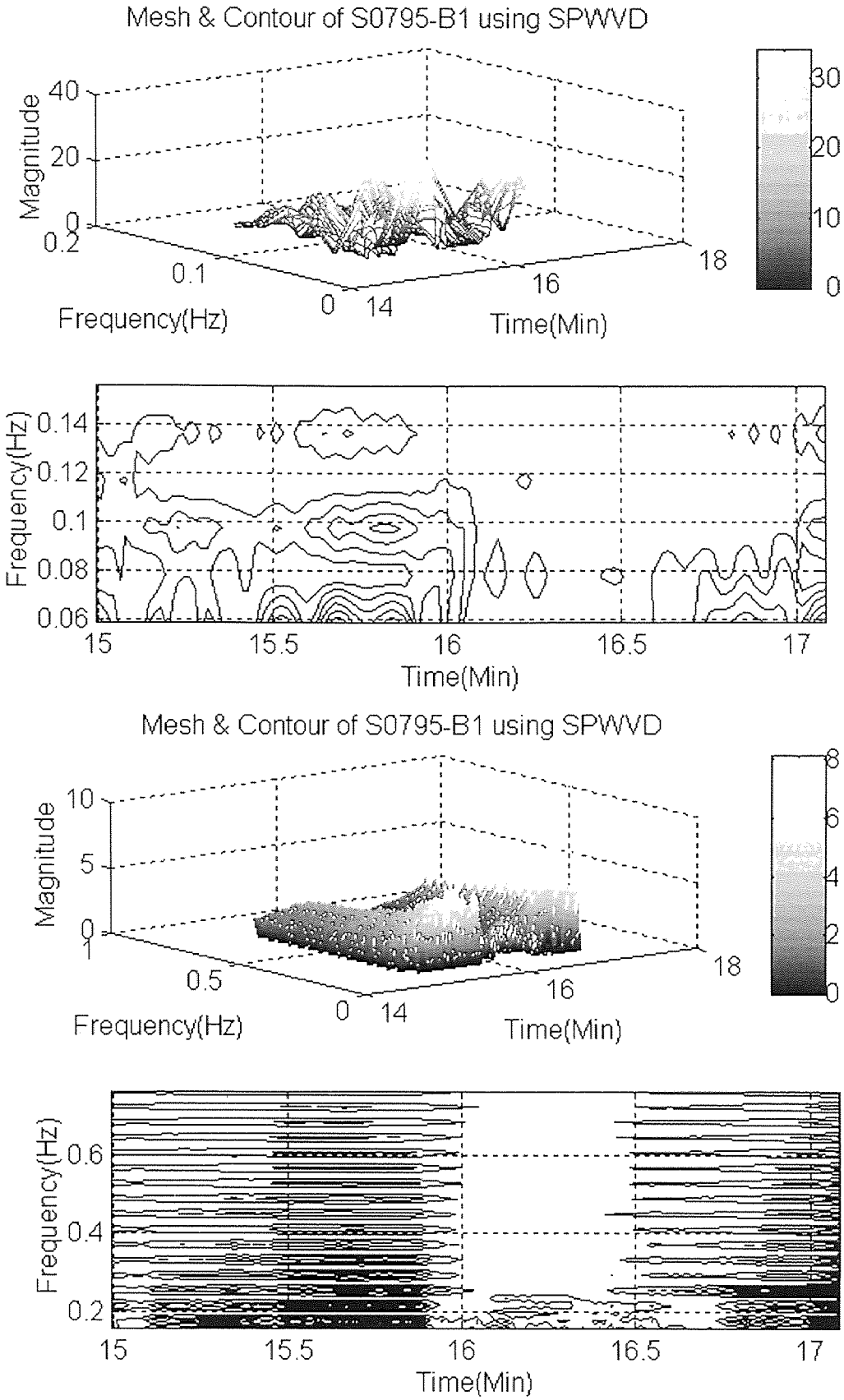

Figure 4.44 Mesh and contour of SPWVD (min15-17) of subject S0795 protocol B1

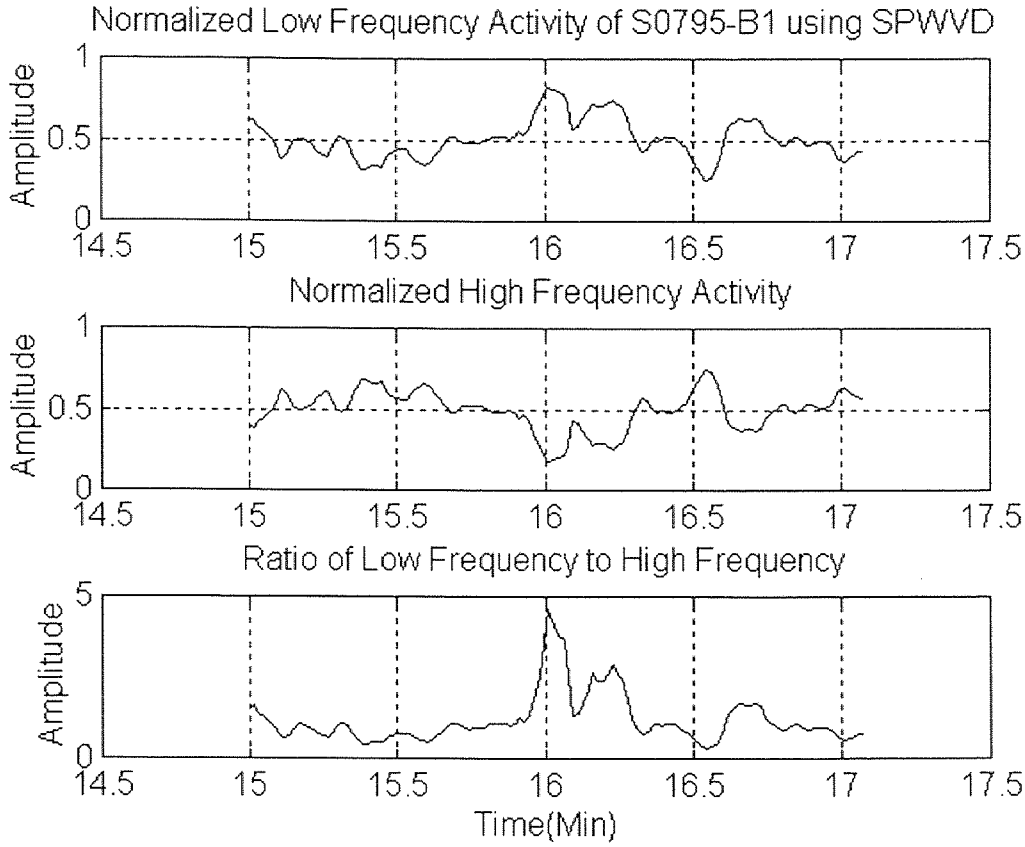

Figure 4.45 LF and HF activity of SPWVD of HRV of subject S0795 protocol B1

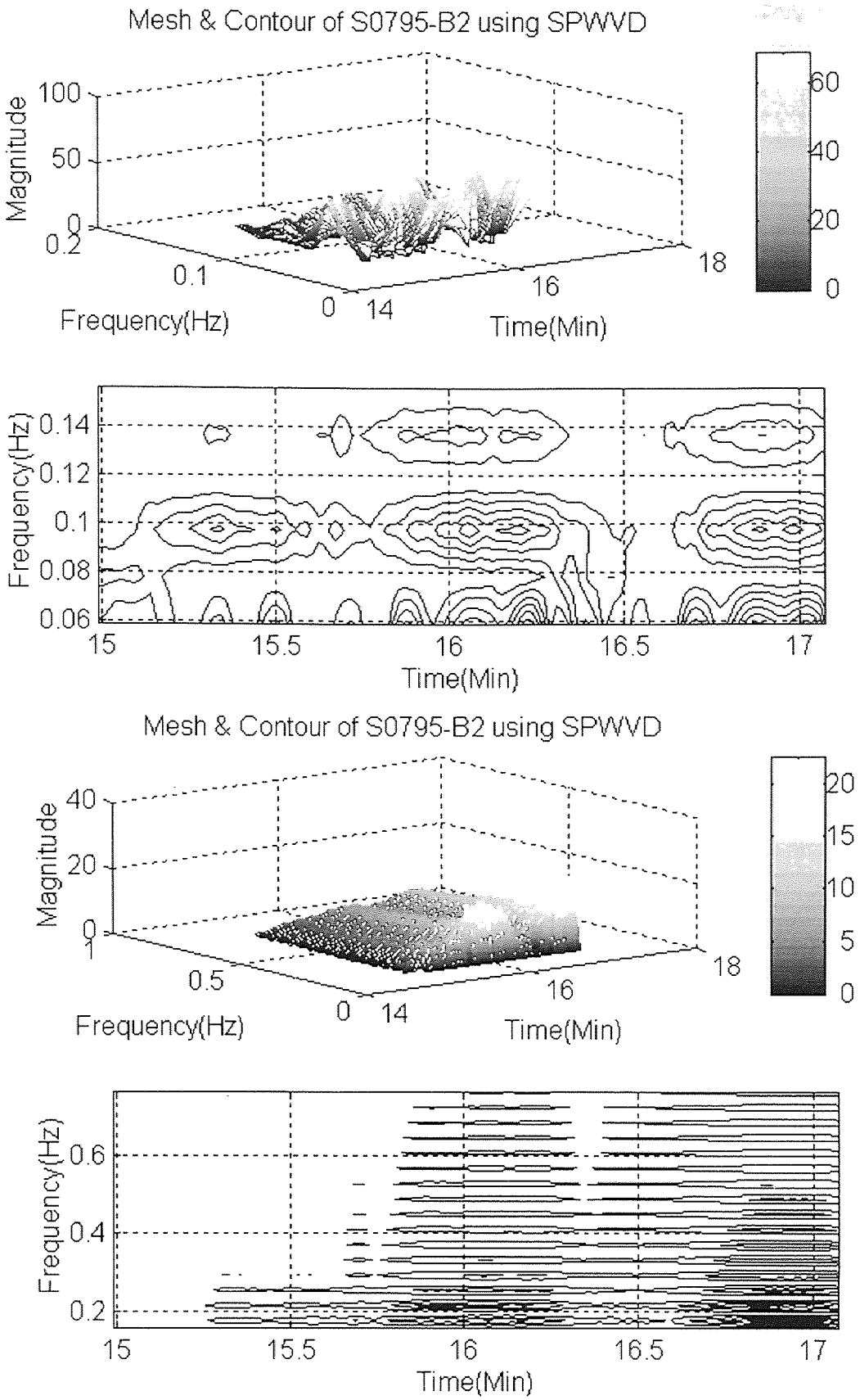

Figure 4.46 Mesh and contour of SPWVD (min15-17) of subject S0795 protocol B2

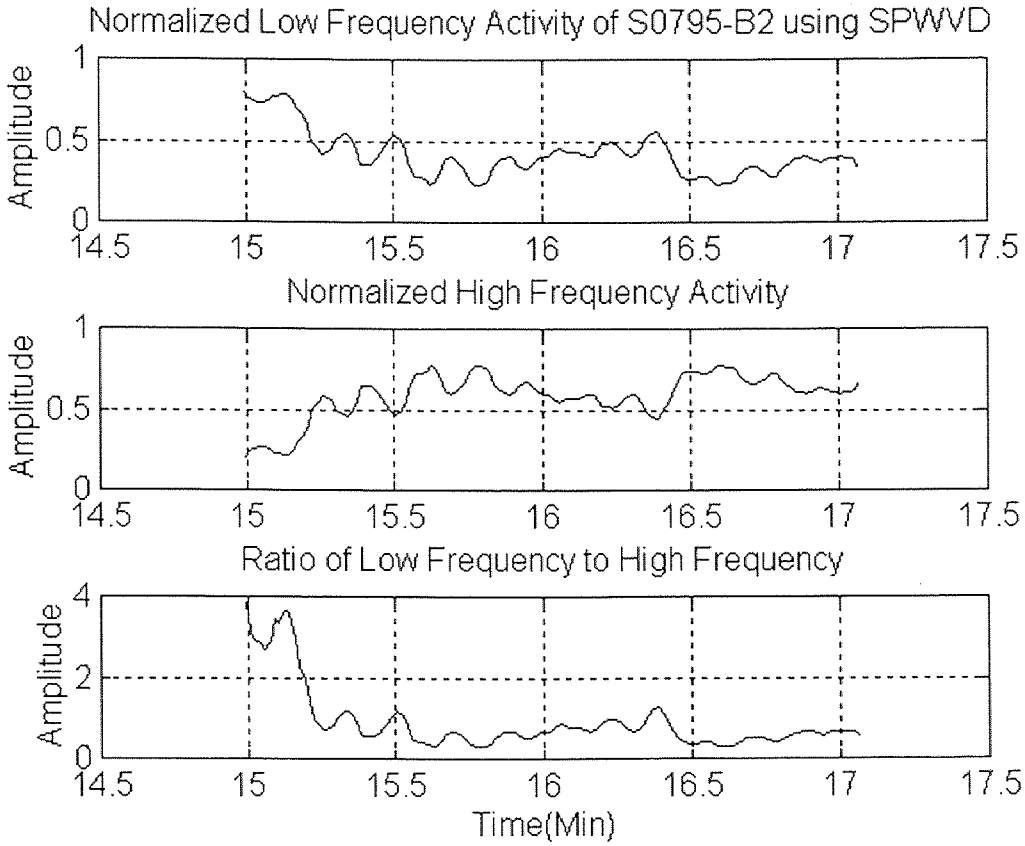

Figure 4.47 LF and HF activity of SPWVD of HRV of subject S0795 protocol B2

4.4 Adaptive Time-Frequency Analysis of Heart Rate Variability

Time-frequency signal representations characterize signals over a time-frequency plane. They combine time and frequency information to yield a potentially more revealing picture of the temporal localization of a signal spectrum. Time-frequency representations have been applied to analyze non-stationary or time-varying signals. Hence, TF representations provide excellent platforms for biological signals because of their high non-stationarity. In reality, signals may have unknown spectral components . In that case, TF representations may suffer significantly from cross-terms of these spectral components. This problem may be partially overcome by designing specific kernels for the signal at hand. A thorough evaluation of five kernels in the previous sections has shown that the Choi-Williams and the smoothed pseudo Wigner-Ville distributions overcome this drawback while presenting a high resolution spectra.

In the following sections, we present an alternative method to overcome this problem [51]. The new methodology adaptively uncovers the region of parasympathetic activity. First, the heart rate variability signal is analyzed with the existence of the respiration signal as a reference. Then, HRV is spectrally tailored to yield the high frequency activity. Finally, an STFT is utilized on the processed data in order to obtain a TF representation.

4.4.1 Adaptive TF Analysis of HRV using Respiration Reference

Our motivation in this development is to uncover the region of parasympathetic activity. It is well known that parasympathetic activity is highly correlated with the respiration

frequency. An adaptive analysis method that traces the respiration frequency and extracts the corresponding parasympathetic activity from the HRV signal is proposed in this section.

In particular, the parasympathetic activity can be precisely extracted from the HRV signal by using a sliding frequency window with an adaptive bandwidth. A cosine-modulated binomial-Gaussian function will be excellent match for this purpose because of its simplicity, smooth frequency response and excellent frequency localization[51]. The block diagram of the adaptive time-frequency analysis method is shown in Figure 4.48.

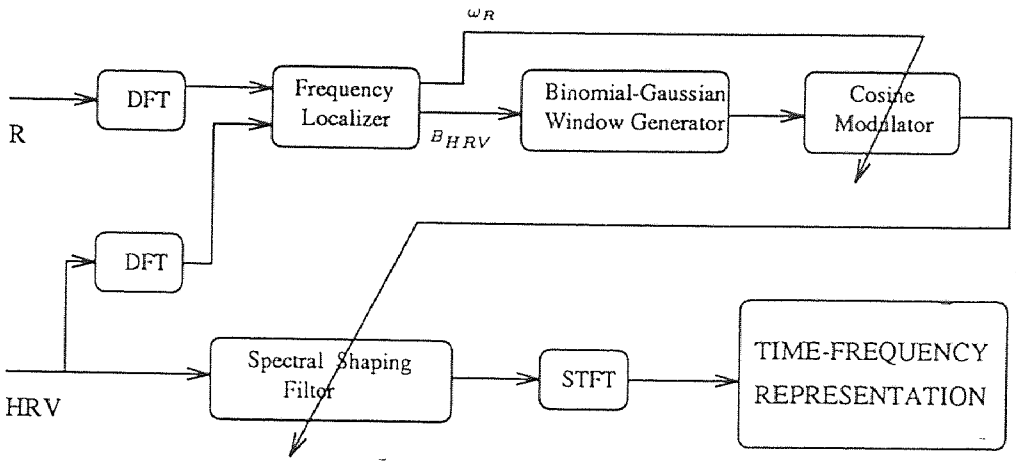

Figure 4.48 The generic block diagram of adaptive time-frequency analysis

The method proceeds as follows:

I) First, the respiration and HRV signal are broken into overlapping time windows to reflect the temporal changes of vagal activity over time and frequency. For a

typical subject, the window length is chosen as 256 samples (12.8 secs), where each successive window is shifted by 64 samples (3.2 secs) from the previous one. These particular values are chosen such that the temporal changes can be closely monitored during the analysis.

I I) Second, a smart frequency localizer examines the peak frequency of the respiration (w_R). Also, the frequency localizer detects the half-power bandwidth of the respiration peak in the HRV (B_{HRV}) in that particular time window.

I I I) The binomial-Gaussian generator produces an M-tap, low-pass prototype ($\underline{f}_P$), with the given approximate bandwidth (B_{HRV}).

I V) The low-pass prototype is modulated to the respiration peak frequency by means of cosine modulation, as :

$$f(k) = f_P(k).\cos[w_r(k - \frac{N-1}{2})] \qquad (4.1)$$

V) The HRV data segment is filtered or shaped with the bandpass filter given in equation 4.1

V I) The STFT is applied on the filtered HRV signal, and TF plots ale finally obtained.

V I I) The window is shifted through the HRV and respiration signals. The procedures (through VII) are repeated until the end of the data files.

Figure 4.49 displays a normalized power spectrum of a typical subject's HRV on the time-frequency plane without any processing. As seen from the figure, the desired information is smeared with the undesired information. After adaptive tailoring of the

HRV by binomial-Gaussian filtering, however, the desired parasympathetic activity becomes clearly visible, as shown in Figure 4.50. The advantage of this method is also demonstrated in Figure 4.51 and Figure 4.52 for another subject.

Although the proposed method is a non-parametric analysis, the time-frequency properties of the analyzed signals are closely monitored and utilized in TF analysis. The Binomial-Gaussian window used here is by no means optimal, but it does provide precise results. Also the STFT may not be the only alternative for the TF representation. Other TF-representations such as smoothed pseudo Wigner-Ville or Choi-Williams are also expected to yield good results after adaptive treatment of the HRV signal. Note that the signal is almost tailored to a single component so that the effect of cross-terms would naturally be minimal. For example, the TF-representation of a chirp signal is perfect since it is a single component signal with time-varying frequency. In conclusion a TF representation would benefit greatly if the biological signal can be tailored before any TF operation.

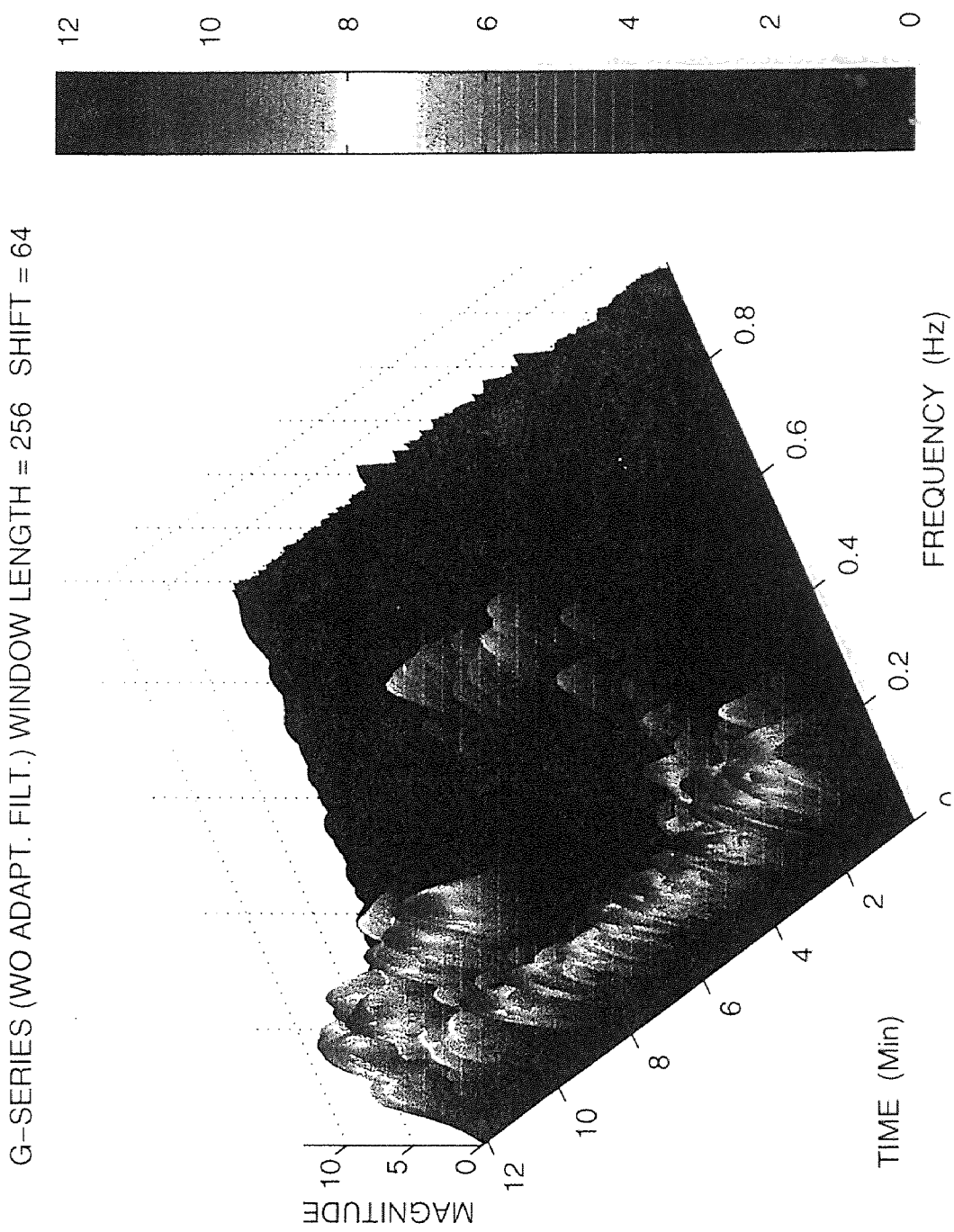

Figure 4.49 TF representation of HRV without adaptive analysis (Subject: G0719)

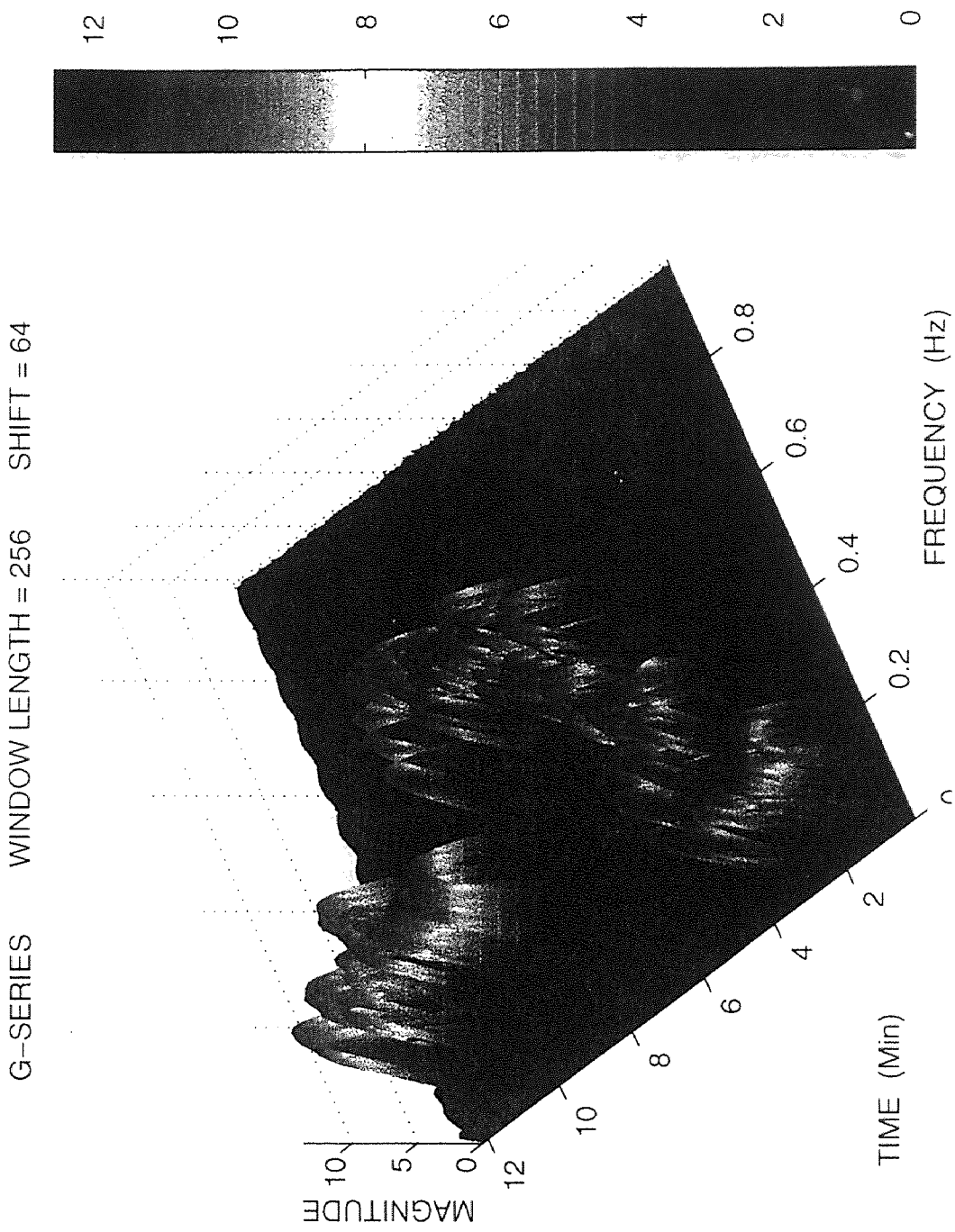

Figure 4.50 TF representation of HRV with adaptive analysis (Subject: G0719)

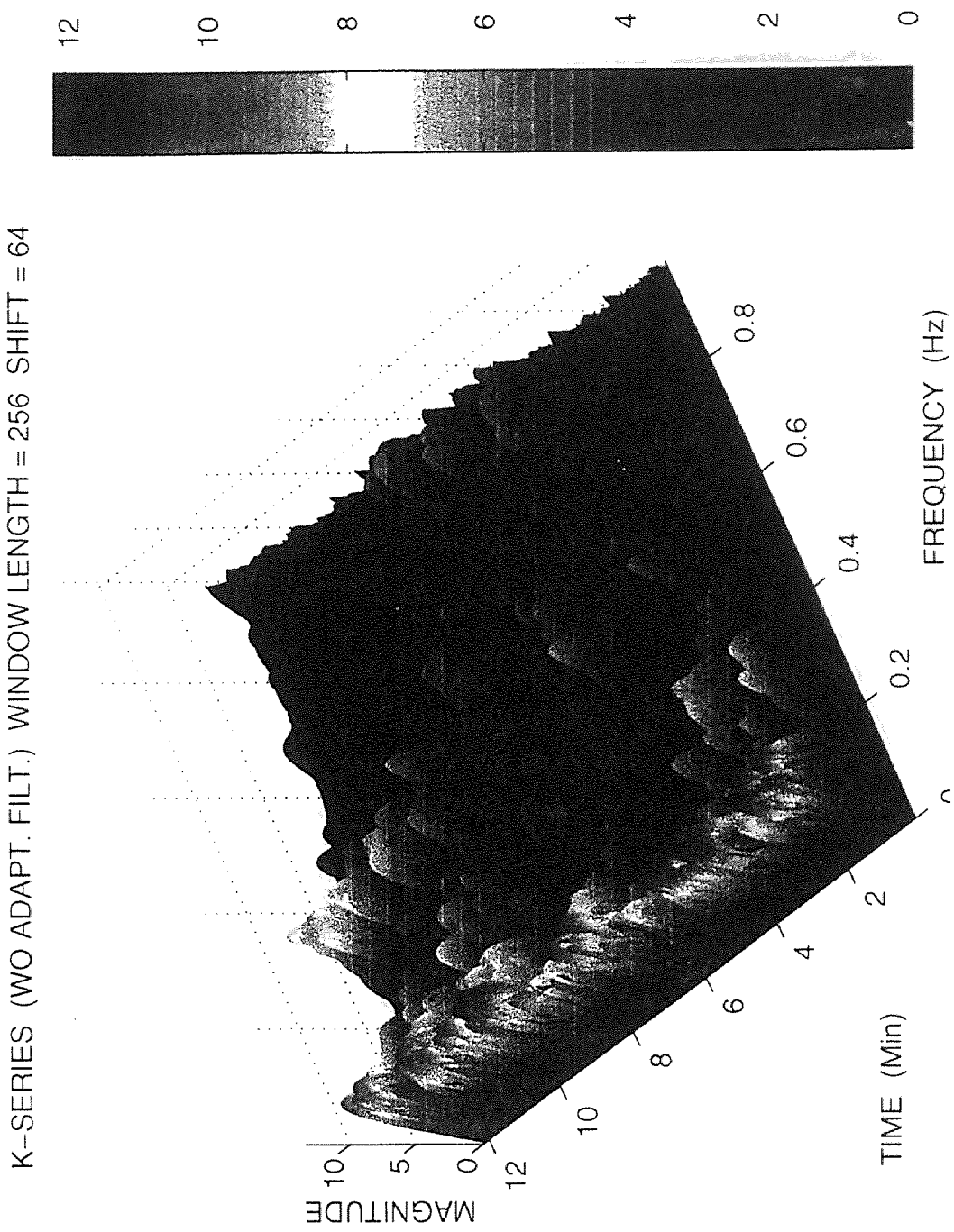

Figure 4.51 TF representation of HRV without adaptive analysis (Subject: K0719)

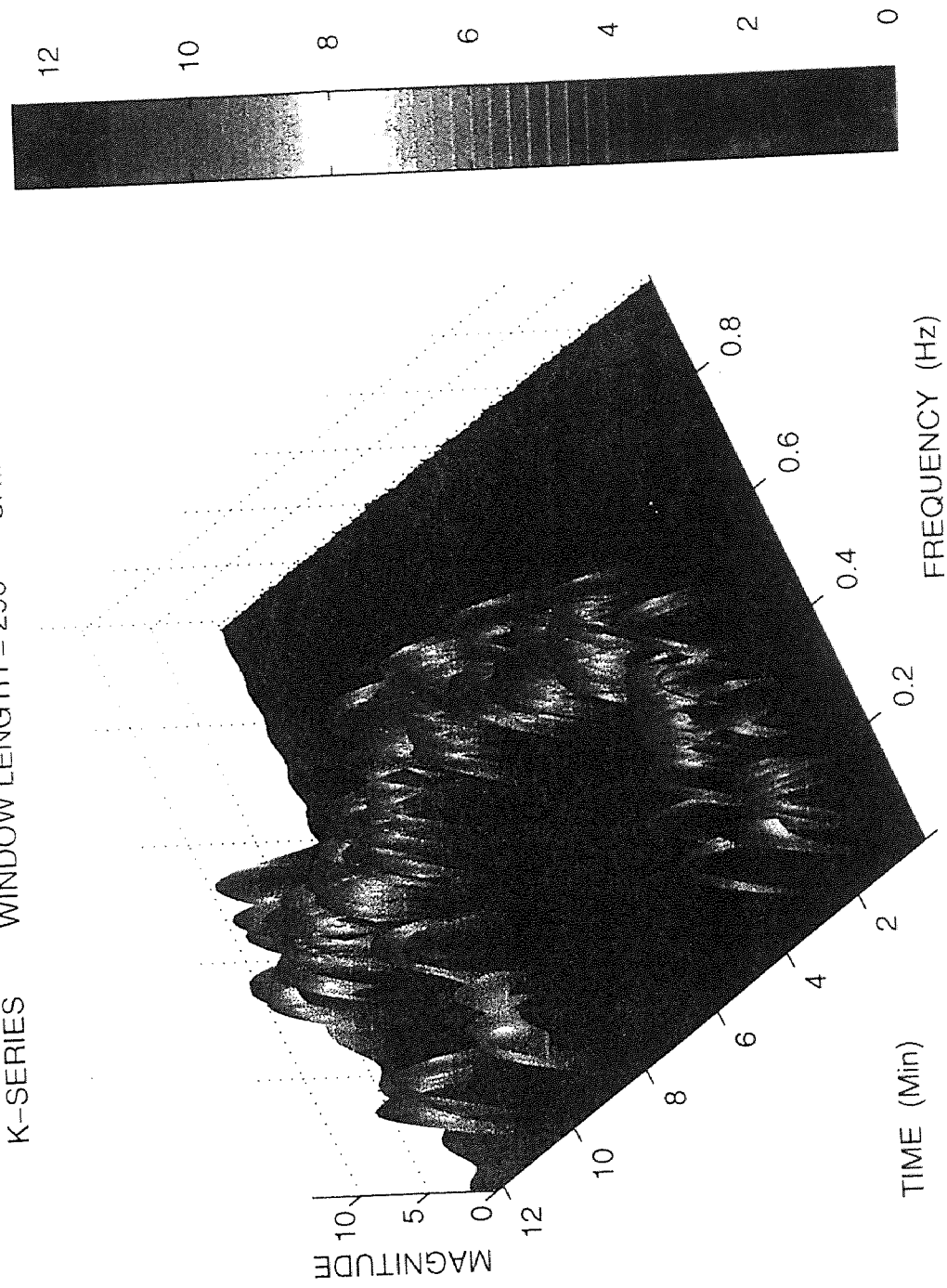

Figure 4.52 TF representation of HRV with adaptive analysis (Subject: K0719)

CHAPTER 5

CONCLUSIONS

Recently, joint time-frequency signal representation has received considerable attention as a powerful tool for analyzing a variety of signals and systems of biological origin which do not comply with the stationarity assumptions The time-frequency representations of signals can be classified as linear and quadratic. The linear TF representations might be the short-time Fourier transform (STFT) and the wavelet transform. All linear TF representations satisfy the superposition or linearity principle. On the other hand, the quadratic TF representations provide a time-frequency energy distribution or instantaneous power spectrum[44]. They are called quadratic since the energy is a quadratic signal representation. An energy distribution-based TF representation combines the instantaneous power and the spectral energy density. The temporal and spectral correlations can also be combined as an alternative quadratic representation[44]. In reality signals may have unknown spectral components. In that case, TF representations may suffer significantly from cross-terms of these spectral components. This problem may be partially overcome by designing specific kernels for the signal at hand. In this dissertation, we explored the possibility of better representation of two particular biological signals, namely heart rate variability and respiration. We evaluated the use of time-frequency analysis to investigate the physical and anticipatory effects attributed to stress.

In the first phase of this work, the application of five different bilinear representations on modeled HRV test signals, and experimental HRV and respiration

signals of the preliminary protocol were evaluated. Each distribution: the short time Fourier transform (STFT), the pseudo Wigner-Ville (WVD), the smoothed pseudo Wigner-Ville (SPWVD), The Choi-Williams (CWD), and the Born-Jordan-Cohen (RID) has unique characteristics which was shown to affect the amount of smoothing and the generation of cross-terms differently . The difficulty with TF analysis was the ability to extract the relevant information. The resulting 3-D time dependent spectra contained a lot of information and knowing how to extract it was crucial to the interpretation of the physiology. By expanding the concept of spectral analysis of heart rate variability (HRV) into time-frequency analysis, we were able to quantitatively assess the parasympathetic (HF) and sympatho-vagal balance (LF:HF) changes as a function of time. As a result, the assessment of the autonomic nervous system during rapid changes was made. The results demonstrated that TF analysis provided temporal and spectral localization that could not be revealed by the use of standard spectral methods. The CWD and the SPWVD were chosen for further application because of overcoming the drawbacks of the other distributions by providing higher resolution in time and frequency while suppressing interferences between the signal components. The respiration analysis validated the physiological states the subjects were in. With rest and relaxation, the breathing rate decreased producing a low respiration frequency. With exercise and exertion, the breathing rate increased to supply the body with more oxygen and remove more carbon dioxide, thus shifting the frequency of respiration into higher ranges that could reach as high as 0.75 Hz. The HRV analysis showed that with rest the average heart rate slows down while the variability in the heart rate increases. On the other hand, with exercise,

the average heart rate speeds up while the variability in the heart rate decreases. Both the TF and statistical analysis of the HRV signals showed that a stressful exercise level drastically changed the HRV signal, and that there was a significant difference between the three states of rest, exercise, and recovery. More importantly, there was a significant difference between rest and recovery which indicated that four minutes of recovery was not enough for the heart rate to reach its normal resting state.

In the second phase of this research, the SPWVD and CWD were used to investigate the presence of an anticipatory component due to the stressful exercise condition as reflected in the HRV signal from a change in behavior in the autonomic nervous system. Although both the CWD and the SPWVD were used to analyze the four exercise protocols, the SPWVD was shown to present a smoothed envelope of the CWD results. Examination of the results for the nine subjects presented a real challenge. Comparing the nine subjects for all protocols, we noted that the most striking finding related to a definite change at minute 16 in response to the experimenter intervention, regardless of the message relayed in the information provided. Most subjects reacted to the verbal intervention after 8 minutes of silence for most protocols. They were also able to illicit the proper response for some sessions but not consistently for all four protocols (A1 through B2). Examining the different protocols separately for the 9 subjects, we noted that protocol A1 showed more than half the subjects anticipating the stressful exercise by a relative increase in the normalized LF power, which is a representative of a mixture of sympathetic and parasympathetic activity, relative to the normalized HF power, which is a representative of parasympathetic activity. However, the

reproducibility of this response was not as evident in the second protocol A2, under the same conditions and even for the same subject. With the introduction of exercise, time-frequency analysis revealed two factors that could play an important part in explaining the physiology of the system. There was the increase of sympathetic activity due to the stress introduced by the physical challenge, and at the same time there was an accompanied increase in the frequency of respiration which occurred in the region indicative of the parasympathetic activity. These two factors might show either an increase in the low frequency activity relative to the parasympathetic activity, or visa versa. Thus, different subjects might react differently to the same situation, or even the same subject might illicit different response at a different time or day depending on the range of factors from his state of mind to his physical condition at that moment. This whole interplay made it very difficult to assess a definite conclusion about the physiology of the system especially with such a small group of participants. The same deduction could be carried through in the second set of protocols B1 and B2. Most subjects responded to the voice intervention at eight minutes into the recovery session after the first bout of exercise, regardless of what was said. Some subjects displayed a decrease or no change in the normalized LF activity between minutes 16 and 17, relative to the parasympathetic activity. Others, or sometimes the same subject would illicit the opposite response the second time in protocol B2. These results indicated that subjects responded to the intervention at minute 16. However, along with the statistical findings, it suggested further that it didn't matter in most cases what words were used. The mere fact that the experimenter gave instructions after eight minutes of silence was enough to illicit a reaction in the majority

of the cases. The reactivity to the information carried in these words was then an after effect in most cases.

In the last phase, a new methodology was proposed that adaptively uncovered the region of parasympathetic activity. It is well known that parasympathetic activity is highly correlated with the respiration frequency. This technique traced the respiration frequency and extracted the corresponding parasympathetic activity from the heart rate variability signal by adaptive filtering. Although the proposed method was a non-parametric analysis, the time-frequency properties of the analyzed signals were closely monitored and utilized in TF analysis. The Binomial-Gaussian window used was by no means optimal, but it provided precise results. Also, as demonstrated in the previous comparisons, the STFT should not be the only alternative for the TF representation. Other TF-representations such as the smoothed pseudo Wigner-Ville or Choi-Williams are also expected to yield good results after adaptive treatment of the HRV signal. The signal was almost tailored to a single component so that the effect of cross-terms would naturally be minimal. In conclusion we found that TF representation would benefit greatly when extracting a certain response if the biological signal could be tailored before any TF operation.

5.1 Future Work

The utilization of time-frequency analysis is vast. This research provided more insight on the wide clinical application of this emerging technique to quantify rapid changes in biological signals. One application may be the assessment of manual manipulation of the

skull to induce an increase in parasympathetic activity. It may also be used to study electromyographic changes during various conditions or to assess autonomic nervous system damage. A future project may be the assessment of the autonomic nervous system in spinal cord injury patients. Comparison of the rate of change of the vagal tone during a provocation of healthy subjects to spinal cord injured subjects may allow us to categorize the severity of the injury as well as increase our understanding of the nervous system dysfunction in spinal cord injured people.

Although as many conditions as possible were controlled to maintain homogeneity between the subjects, psychological evaluation proved hard to assess. There were two interesting observations unveiled from the data and the experimental setup of the anticipation protocol. The first was the interplay of the two opposing physiological factors that were simultaneously revealed in the time-frequency analysis of the heart rate variability signal during stressful exercise conditions. The second was the definite reaction due to the verbal intervention after eight minutes of silence no matter what was said. These two findings should be studied further and accounted for in future research. A study of the effects of heart rate reactivity is suggested as a possible variable to clarify the different reactions to stress between subjects. A thorough study of different interventions that avoid the drawback of the verbal shock might also help refine the techniques to better illicit the anticipatory component. Other helpful insights that might affect the variability in the data are the gender, smoking, and fitness conditions. With such a small sample of participants (nine), these conditions should be limited to one

gender and one fitness level, with no smoking to assess better the findings in a specified population.

REFERENCES

[1] A.J. Vander, J.H. Sherman, and D.S. Luciano. *Human Physiology*. New York: McGraw-Hill Publishing Company. Sixth Edition. 1994.

[2] A.C. Guyton. *Textbook of Medical Physiology*. Philadelphia: W.B. Saunders Company. Eighth Edition. 1991.

[3] M.D. Kamath and E.L. Fallen, "Power spectral analysis of heart rate variability: A noninvasive signature of cardiac autonomic function," *Crit. Rev. in Biomed. Eng.*, vol. 21, no. 3, pp. 245-311, 1993.

[4] G.G. Berntwon, J.T. Cacioppo, and K.S. Quigley, "Respiratory sinus arrhythmia: Autonomic origins, physiological mechanisms, and psychophysiological implications," *Psychophysiology*, vol. 30, pp. 183-196, 1993.

[5] S.J. Shin, W.N. Tapp, S.S. Reisman, and B.H. Natelson, "Assessment of autonomic regulation of heart rate variability by the method of complex demodulation," *IEEE Trans. on Biomed. Eng.*, vol. 36, no. 2, pp. 274-282, 1989.

[6] R. Saliba, S. Fernando, and S.S. Reisman, "Autonomic nervous system evaluation using instantaneous frequency," *Proceedings of the 21st IEEE Annual Northeast Bioengineering Conference*, Maine, 1994.

[7] M. Pagani, F. Lombardi, S. Guzzetti, O. Rimoldi, R. Furlan, P. Pizzinelli, G. Sandrone, G. Malfatto, S. Del' Orto, E. Piccaluga, M. Turiel, G. Baselli, S. Cerutti, and A. Malliani, "Power spectral analysis of heart rate and arterial pressure variabilities as a marker of sympatho-vagal interaction in man and conscious dog," *Circulation Res.*, vol. 59, pp. 178-93, 1986.

[8] P. Novak and V. Novak, "Time/frequency mapping of the heart rate, blood pressure and respiratory signals," *Medical & Biological Engineering & Computing*, vol. 31, pp. 103-110, 1993.

[9] L. R. Rabiner and R. W. Schafer. *Digital Processing of Speech Signals*. Englewood Cliffs, NJ: Prentice-Hall, 1978.

[10] A.S. Gevins, "Analysis of the electromagnetic signals of the human brain: Milestones, obstacles and goals," *IEEE Tans. on Biomed. Eng.*, vol. 33, pp. 833-850, 1984.

[11] L. G. Durand, A. P. Yoganathan, E. C. Harrison, and W. H. Corcoran, "A quantitative method for the in vitro study of sounds produced by prosthetic aortic

heart valves," Parts 1-3. *Medical & Biological Engineering & Computing*, vol. 22, pp. 32-54, 1984.

[12] S. H. Nawab and T. F. Quatieri, "Short-time Fourier transform," in *Advanced Topics in Signal Processing*, J. S. Lim and A. V. Oppenheim, Eds. Englewood Cliffs, NJ: Prentice-Hall, pp. 289-337, 1988.

[13] E. Wigner, "On the quantum correction for thermodynamic equilibrium," *Phys. Rev.*, vol. 40, pp. 749-759, 1932.

[14] J. Ville, "Theorie et applications de la notion de signal analytique," *Cables Transmiss.*, vol. 20A, pp. 61-74, 1948.

[15] W. Martin and P. Flandrin, "Wigner-Ville detection of changes of signal structure by using Wigner-Ville spectrum," Sig. Proc., vol. 8, pp. 215-233, 1985.

[16] R. M. S. S. Abeysekera, , R. J. Bolton, L. C. Westphal, and B. Boashash, "Patterns in Hilbert Transforms and Wigner-Ville distributions of electrocardiogram data," *Proc. IEEE ICASSP*, Tokyo, vol. 34, pp. 1793-1796, 1986.

[17] R. I. Kitney and H. Talhami, "The zoom Wigner transform and its application to the analysis of blood velocity waveforms," *J. Theoret. Biol.*, vol. 129, pp. 395-409, 1987.

[18] K. Kaluzynski, "Selection of a spectral analysis method for the assessment of velocity distribution based on the spectral distribution of ultrasonic Doppler signals," *Medical & Biological Engineering & Computing*, vol. 27, pp. 463-469, 1989.

[19] J. J. Eggermont and G. M. Smith, "Characterising auditory neurons using the Wigner and Rihacek distribution: a comparison," *J. Acoust. Soc. Am.*, vol. 87, pp. 246-259, 1990.

[20] D. T. Barry and N. M. Cole, "Muscle sounds are emitted at the resonant frequencies of skeletal muscle," *IEEE Trans. on BME*, vol. 37, pp. 525-531, 1990.

[21] L. Cohen, "Time-Frequency Distributions - A Review," *Proceedings of the IEEE*, vol. 77, no. 7, July 1989.

[22] B. Boashash. *Time-Frequency Signal Analysis Methods and Applications* , Wiley Halsted Press, 1992.

[23] T.A.C.M. Classen and W.F.G. Mecklenbrauker. "The Wigner Distribution-a Tool for Time-Frequency Signal Analysis", Philips J. Res. 35, Part I, 217-250; Part II, 276-300; Part III, 372-389, 1980.

[24] H. I. Choi and W. J. Williams, "Improved time-frequency representation of multicomponent signals using exponential kernels," *IEEE Trans. Acoust., Speech, Signal Processing*, vol. 37, no. 6, pp. 862-871, 1989.

[25] C. Zheng, A. Tornow, R. Kushwaha, and J. C. Sackellares, "Time-frequency analysis of EEG recordings with the reduced interference distribution," *Proc. 12th annu. Int. Conf. IEEE EMBS*, vol. 12, pp. 857, 1990.

[26] H. P. Zaveri, W. J. Williams, and J. C. Sackellares, "Cross time-frequency representation of electrocorticograms in temporal lobe epilepsy," *Proc. 13th annu. Int. Conf. IEEE EMBS*, vol. 13, pp. 437-438, 1991.

[27] C. Zheng, S. E. Widmalm, and W. J. Williams, "New time-frequency analyses of EMG and TMJ sound signals," *Proc. 11th annu. Int. Conf. IEEE EMBS*, vol. 11, pp. 741-742, 1989.

[28] B. Sahiner and A. E. Yagle, "Application of time-frequency distributions to magnetic imaging of non-constant flow," *Proc. IEEE ICASSP*, pp. 1865-1868, 1990.

[29] J. Jeong and W. J. Williams. "Kernel design for reduced interference distributions", *IEEE Transactions on Signal Processing*, vol. 40, no. 2, February 1992.

[30] W. J. Williams, H. P. Zaveri, and J. C. Sackellares, "Time-frequency of electrophysiology signals in epilepsy," *IEEE Engineering in Medicine & Biology*, pp. 133-143, March/April 1995.

[31] J. C. Wood and D. T. Barry, "Time-frequency analysis of the first heart sound," *IEEE Engineering in Medicine & Biology*, pp. 144-151, March/April 1995.

[32] R. F. Rushmer, "Structure and function of the cardiovascular system," in *Handbook of research methods in cardiovascular behavioral medicine*, N. Schneiderman, S. M. Weiss, and P. G. Kaufmann, NY: Plenum Press, pp. 5-22, 1989.

[33] D. S. Krantz and J. Ratliff-Crain, "The social context of stress and behavioral medicine research," in *Handbook of research methods in cardiovascular behavioral medicine*, N. Schneiderman, S. M. Weiss, and P. G. Kaufmann, NY: Plenum Press, pp. 383-392, 1989.

[34] J. Mason, "Re-evaluation of the concept of non-specificity in stress theory," *Journal of Psychiatric Research*, vol. 8, pp. 323-333, 1971.

[35] G. R. Elliott and C. Eisdorfer. *Stress and human health*, Berlin: Springer, 1982.

[36] F. Cohen, M. Horowitz, R. Lazarus, R. Moos, L. Robins, R. Rose, and N. Rutter, "Panel report on psychosocial assets and modifiers of stress," in *Stress and human health*, G. Elliott and C. Eisdorfer, Berlin: Springer, pp. 147-288, 1982.

[37] R. S. Lazarus. *Psychological stress and the coping process*, NY: McGraw-Hill, 1966.

[38] P. A. Obrist, C. J. Gaebelein, E. S. Teller, A. W. Langer, A. Grignolo, K. C. Light, and J. A. McCubbin, "The relationship among heart rate, carotid dP/dt and blood pressure in humans as a function of the type of stress," *Psychophysiology*, vol. 15, pp. 102-115, 1978.

[39] S. B. Manuck, C. D. Corse, and P. A. Winkelmen, "Behavioral correlates of individual differences in blood pressure reactivity," *Journal of Psychosomatic Research*, vol. 23, pp. 281-288, 1979.

[40] T. M. Dembroski, J. M. MacDougall, J. A. Herd, and J. C. Shields, "Effects of level of challenge on pressor and heart rate responses in type A and B subjects," *Journal of Applied Social Psychology*, vol. 9, pp. 209-228, 1979.

[41] D. C. Glass, L. R. Krakoff, R. Contrada, W. F. Hilton, K. Kehoe, E. G. Mannucci, C. Collins, B. Snow, and E. Elting, "Effect of harassment and competition upon cardiovascular and plasma catecholamine responses in Type A and Type B individuals," *Psychophysiology*, vol. 17, pp. 453-463, 1980.

[42] A. Szabo, F. Péronnet, G. Boudreau, L. Côté, L. Gauvin, and P. Seraganian, "Psychophysiological profiles in response to various challenges during recovery from acute aerobic exercise," *International Journal of Psychophysiology*, vol. 14, pp. 285-292, 1993.

[43] S. Fernando, "Autonomic nervous system evaluation using time-frequency analysis," *NJIT, MS. Thesis*, October 1994.

[44] F. Hlawatsch and G. F. Boudreaux-Bartels. "Linear and Quadratic Time-Frequency Signal Representations", *IEEE Signal Processing Magazine*, pp. 21-67, April 1992.

[45] R. Ziemer, W. Tranter, and R. Fannin. *Signals and Systems: Continuous and Discrete*. New York: Macmillan Publishing Company. Second Edition. 1989.

[46] R. E. Ziemer and W. H. Tranter. Principles of Communications. Houghton Mifflin Company. Third Edition, 19-119, 1990.

[47] M. Amin, L. Cohen and W.J. Williams, "Methods and Applications for Time-Frequency Analysis" *Conference Notes*, University of Michigan, 1993.

[48] D. L. Jones and T. W. Parks, "A Resolution Comparison of Several Time-Frequency Representations", *IEEE Transactions on Signal Processing*, vol. 40, no. 2, February 1992.

[49] P. V. O'Neil. *Advanced Engineering Mathematics*, Wadsworth Publishing Company. Second Edition. 575-585,1987.

[50] M. Adib, "Implementation of time-frequency distribution software and its use to study biological signals," *NJIT, MS. Thesis*, January 1995.

[51] M.V. Tazebay, R.T. Saliba and S.S. Reisman, "Adaptive Time-Frequency Analysis of Autonomic Nervous System," *Proceedings of the 17th IEEE Annual International Conference of the Engineering in medicine and Biology Society,* Montréal, Canada, 1995.